Destruction of selected pharmaceuticals by ozonation and heterogeneous catalysis

Soudabeh Saeid

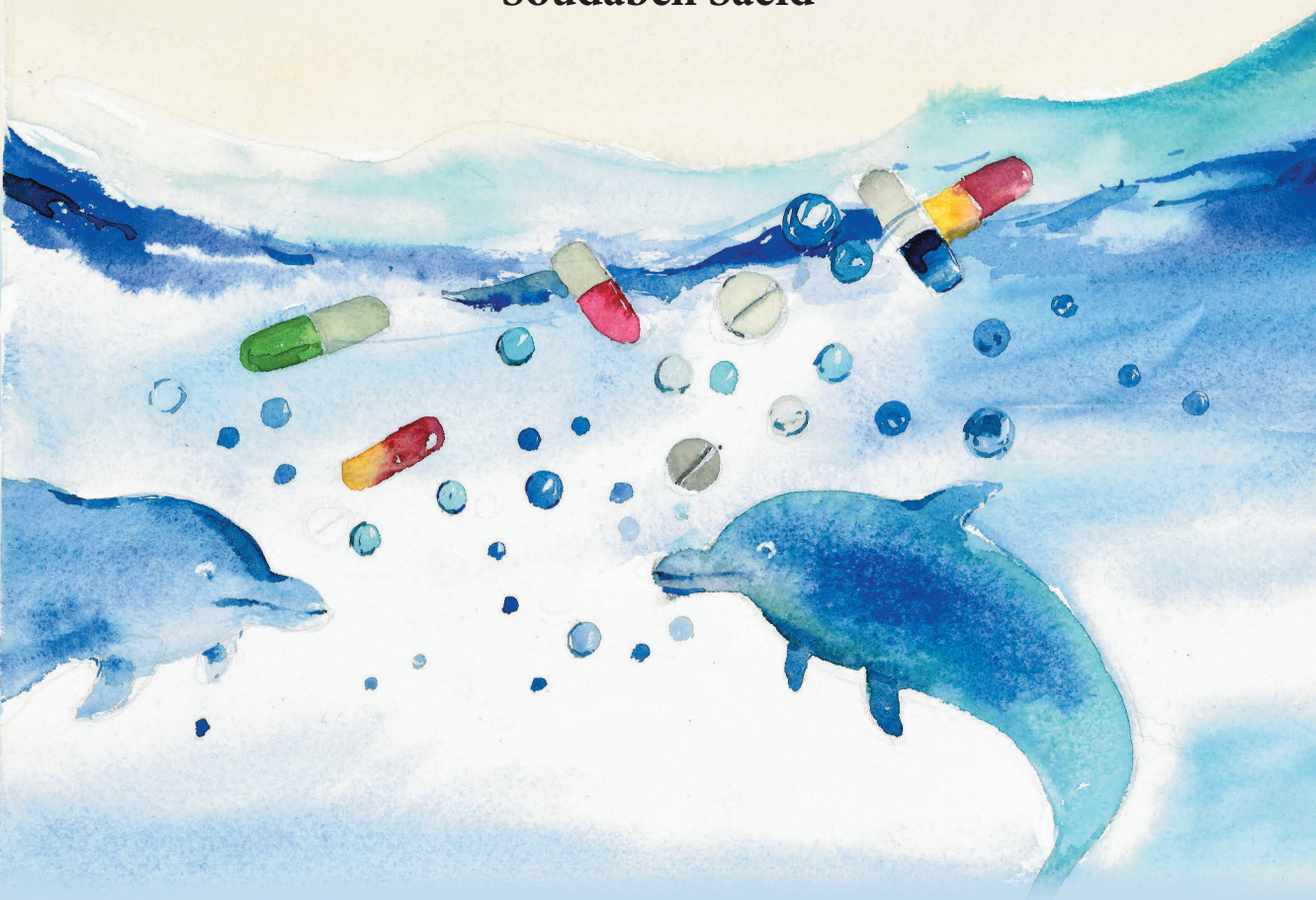

Laboratory of Industrial Chemistry and Reaction Engineering
Faculty of Science and Engineering /Chemical Engineering
Åbo Akademi University
Turku/Åbo 2020

Soudabeh Saeid

b. 1990 in Tabriz, Iran
M.Sc., Applied Chemistry, 2014
Department of Chemistry, Tabriz Branch, Islamic Azad University, Tabriz, Iran (IAUT)

Destruction of selected pharmaceuticals by ozonation and heterogeneous catalysis

Soudabeh Saeid

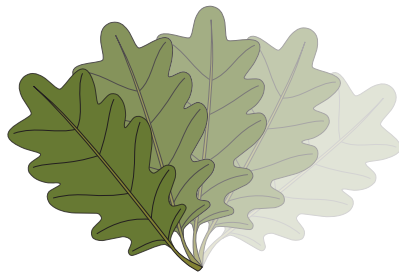

Laboratory of Industrial Chemistry and Reaction Engineering
Johan Gadolin Process Chemistry Centre
Faculty of Science and Engineering / Chemical Engineering
Åbo Akademi University

2020

Supervised by

Academy Professor Dr Tapio Salmi
Docent Dr Pasi Tolvanen
Docent Dr Narendra Kumar

Laboratory of Industrial Chemistry and Reaction Engineering
Faculty of Science and Engineering /Chemical Engineering
Johan Gadolin Process Chemistry Centre
Åbo Akademi University
Turku/Åbo, Finland

Reviewers

Professor Dr, Dr habil. Rüdiger Lange
Chemische Verfahrenstechnik
Technische Universität Dresden (TUD)
Dresden, Germany

Professor Dr Albin Pintar
Kemijski inštitut
Ljubljana, Slovenia

Faculty Opponent

Professor Dr, Dr habil. Rüdiger Lange
Chemische Verfahrenstechnik
Technische Universität Dresden (TUD)
Dresden, Germany

Cover image credit: Zhila Esmkhani Jam (watercolor paint)

ISBN 978-952-12-3911-3 (printed version)/ ISBN 978-952-12-3912-0 (electronic version)
ISSN 2669-8315 2670-0638 (*Acta technologiae chemicae Aboensia* 2020 A/1)
Painosalama Oy Turku/Åbo 2020

Təqdim olunur mehrəban Ata və Ana'ma

"*You are not a drop in the ocean. You are the entire ocean, in a drop.*"

Rumi

Preface

This work was carried out between 2015 and 2020 at the Laboratory of Industrial Chemistry and Reaction Engineering, Faculty of Science and Engineering, Åbo Akademi University. The doctoral studies were a part of the activities at Johan Gadolin Process Chemistry Centre (PCC), a centre of excellence financed by Åbo Akademi. Financial support received from Svenska Litteratursällskapet (SLS), Centre for International Mobility (CIMO), Tekniikan Edistämissäätiö (TES) and Graduate School of Chemical Engineering (GSCE) Åbo Akademi is gratefully acknowledged.

I would like to acknowledge Academy Professor Tapio Salmi, Docent Pasi Tolvanen and Docent Narendra Kumar for supervision of my doctoral studies and deep scientific discussions. I would like to express my deepest gratitude to Academy Professor Tapio Salmi for giving me the opportunity to work and study at laboratory, thank you for your guidance, advices, discussions, kindness and support. It has been a biggest honour in my life to be your student. I sincerely thank you for bringing inspiration, and for sharing knowledge and experience with me. Docent Pasi Tolvanen is acknowledged for his "always open door" concept, helps, advices and encouragements. Thanks Pasi for being so kind and supportive, the completion of my PhD would not have been possible without your help. I am deeply grateful for your willingness to help not only on my professional development, but also on the personal level. I am sincerely grateful to Docent Narendra Kumar for his help and guidance with catalyst synthesis, characterization and being so kind. I would like to express appreciation to Docent Kari Eranen for his support with the instrumentation and analysis. Professor Vincenzo Russo is acknowledged for the modelling effort and simulations. It has been a priviledge to learn and work with such a high-level scientist. I am very grateful to Professor Dmitry Murzin for scientific advice and great lectures. I would like to tank Docent Päivi Mäki-Arvela for scientific advice and support.

I am very grateful to my colleagues from the Laboratory of Organic Chemistry; the project was a successful collaboration. M.Sc.Matilda Kråkström is gratefully acknowledged for identification, structure determination and quantification of samples. Professor Leif Kronberg and Docent Patrik Eklund are acknowledged for valuable scientific discussions. Atte Aho, Janne Peltonen, Markus Peurla, Andrey Shchukarev are acknowledged for catalyst characterisation.

I feel very lucky to be surrounded by good friends. I deeply appreciate their care, support and motivation. Pasi, Mojde, Imane, Erfan, Atte , Cesar, Cai, Lu, Lidia, Ole, Ekaterina, Zuzana, Nemanja, Jussi, Ananias, Sanaz, Pegah, Behnoush, Shema, Paula, Shuyana, Maria, Ricardo, Stephanie, Andrea, Andreas, Sebastian, Matias, Ramakrishna, Carmen, Karolina, Masoumeh, sweetheart Adriana and researchers from Laboratory of Industrial Chemistry and Reaction Engineering, thank you for being around and making the life better.

Ailəmin dəstəyinə görə təşəkkür edirəm. Təşəkkür edirəm, əziz ana, ömrümün ən çətin vaxtlarında mənimlə olduğunuz və məni irəliyə itələdiyinə görə. Və bütün dəstəklərə və qeydşərtsiz sevgiyə görə əziz atama təşəkkür edirəm. sevimli bacım bütün dəstəyinizə görə təşəkkür edirəm.

Abstract

Destruction of selected pharmaceuticals by ozonation and heterogeneous catalysis

Soudabeh Saeid

Doctoral Thesis, Laboratory of Industrial Chemistry and Reaction Engineering, Johan Gadolin Process Chemistry Centre, Faculty of Science and Engineering, Åbo Akademi University, 2020.

The availability and quality of clean and safe water supplies is directly connected to the modality of wastewater treatment. Municipal wastewater treatment processes are designed to purify and degrade polluting components from water, most of these technologies are not capable to eliminate organic micro-pollutants entirely but might even increase the toxicity of the treated water compared to untreated water by transforming these contaminants to more toxic components. Among these organic pollutants, the frequently occurrence of pharmaceuticals in surface waters has attracted a significant concern due to their non-biodegradability, chemical resistance, and toxicity impact on the aquatic life. These contaminants and the by-products of their degradation continuously discharge to surface waters and maintain their chemical structure, and therapeutic efficiency for a long period of time.

The degradation of four frequently detected pharmaceutical molecules in the Baltic Sea region, ibuprofen, carbamazepine, diclofenac and sulfadiazine by catalytic and non-catalytic ozonation was studied in this work. The purpose of the research was to synthesize active and durable heterogeneous catalysts that, combined with an ozonation process could eliminate these contaminants without toxic by-products.

All these components were pharmaceutical destroyed within one hour by ozonation in a laboratory scale semi-batch reactor, however, the ozonation process produced several long-lasting degradation by-products. The kinetics of the pharmaceuticals degradation and formation of by-products were investigated in detail. Twenty-four heterogeneous catalysts were screened in the presence of ozone to optimize the destruction process. For a better mass transfer between the phases and easier separation of catalysts, the catalysts were immobilized inside the Spinchem™ Stirrer. The catalytic ozonation technology allowed the enhancement of the degradation rate of pharmaceuticals and the suppression the formation of by-products. The catalytic and non-catalytic ozonation screening revealed the reaction kinetics of the pharmaceuticals and their transformed intermediates during the ozonation experiments. Later on, based these results, a kinetic model for the ibuprofen ozonation was derived. The model exhibited a good correspondence with experimental data.

The heterogeneous catalysts were synthesized by several methods and screened in the ozonation process to reveal the impact of various catalyst preparation techniques, type of metals, loading of metals on the catalysts, amounts of Lewis and Brønsted acid sites, type of supports, on the elimination of pharmaceuticals as well as the transformation and degradation of by-products. All-important characterization devices were employed to understand the performance of the catalysts (X-ray powder diffraction, transmission electron microscopy,

nitrogen physisorption, scanning electron microscopy, energy dispersive X-ray micro-analyses, pyridine adsorption-desorption with FTIR spectroscopy, X-ray photoelectron spectroscopy). Evaluation of the catalytic activity showed that some of the employed catalysts have the higher influence on the elimination of the pharmaceuticals such as Fe-H-Beta-25-EIM catalysts. Higher specific area, metal concentration and Brønsted acidity are some of the characteristics which made these catalysts valuable for the ozonation process.

Referat

Nedbrytning av valda farmaceutiska produkter med hjälp av ozonering och heterogen katalys

Soudabeh Saeid

Doktorsavhandling, Laboratoriet för teknisk kemi och reaktionsteknik, Johan Gadolin Processkemiska Centret, Fakulteten för naturvetenskaper och teknik, Åbo Akademi, 2020

Tillgången och kvaliteten av rena och säkra vattenkällor är direkt kopplat till kvaliteten på behandlingen av avfallsvatten. Kommunala vattenreningsprocesser har utvecklats för att eliminera organiska mikroföroreningar men de nuvarande processerna kan t.o.m. öka giftigheten av det renade vattnet genom att kontaminerande substanser förvandlas till giftigare komponenter. Bland dessa organiska föroreningar har rikligt förekommande farmaceutiska produkter väckt speciellt mycket oro p.g.a. deras bristande bionedbrytbarhet, kemisk motståndsförmåga och giftighet mot levande organismer i vattendrag. Dessa kontaminerande substanser och deras biprodukter läcks ut kontinuerligt till ytvatten samtidigt som de bibehåller sin kemiska struktur och sin terapeutiska effekt för långa tidsperioder.

Nedbrytning av fyra rikligt förekommande farmaceutiska molekyler i Östersjöområdet, nämligen ibuprofen, carbazepin, diclofenac och sulfadiazin studerades genom att tillämpa både katalytisk och icke-katalytisk ozonering i detta doktorsarbete. Målet med forskningen var att preparera aktiva och beständiga heterogena katalysatorer som kombinerade med en ozoneringsprocess kunde eliminera dessa kontaminerande komponenter utan att toxiska mellanprodukter bildas.

Alla dessa komponenter var farmaceutiska preparat som nedbröts inom en timme i en halvkontinuerlig reaktor i laboratorieskala. Ozoneringsprocessen alstrade dock flera stabila biprodukter. Kinetiken för nedbrytningen av de farmaceutiska produkterna samt bildningen av biprodukter studerades i detalj. Tjugofem heterogena katalysatorer kartlades i närvaro av ozon för att optimera destruktionsprocessen. För att förbättra massöverföringen mellan faserna och underlätta separeringen av katalysatorerna immobiliserades katalysatorpartiklarna inne i ett Spinchem^{TM}–omrörarsystem. Den kombinerade katalytiska ozoneringsteknologin gjorde det möjligt att påskynda nedbrytningshastigheten av de farmaceutiska produkterna och minimera bildningen av biprodukter. Undersökningen av den katalytiska och icke-katalytiska ozoneringen gav information om de farmaceutiska produkternas och mellanprodukternas reaktionskinetik under ozoneringens gång. Senare utvecklades även en kinetisk modell för ozonering av ibuprofen. Denna modell för ozonering av ibuprofen visade en god överensstämmelse med experimentella data.

De heterogena katalysatorerna syntetiseras med hjälp av flera metoder och användes i ozoneringsprocessen för att få fram effekten av katalysatorprepareringsmetoder, typ av metall, metallmängd på katalysatorna, mängden Lewis- and Brønstedsura säten, typ av bärarmaterial

på elimering av de farmaceutiska preparat samt omvandling och sönderfall av biprodukterna. De mest relevanta karakteriseringsmetoderna användes för att förstå och förklara katalysatorernas prestanda (röntgendiffraktion, transmissionselektronmikroskopi, fysisorption av kväve, svepelektronmikroskopi, energidispersiv röntgenmikroanalys, adsorptions- och desorptionsstudier av pyridin med hjälp av Fouriertransformerad infrarödspektroskopi, röntgenfotoelektronspektroskopi). Evaluering av den katalytiska aktiviteten visade att vissa katalysatorer såsom Fe-H-Beta-25-EIM hade en större effekt på nedbrytning av de farmaceutiska produkterna. En högre ytarea, metallkoncentration och Brønstedsurhet är några av de karakteristiska egenskaperna som gjorde dessa katalysatorer värdefulla för ozoneringsprocessen.

List of the abbreviations

2-AP	2-aminopyridine
AOP	advanced oxidation process
BQD	1-(2-benzaldehyde)-(1H,3H)-quinazoline-2,4-dione
BQM	1-(2-benzaldehyde)-4-hydro-(1H,3H)-quinazoline-2-one
CBZ	carbamazepine
DCF	diclofenac
ESI	electrospray ionization
GC	gas chromatography
H_2O_2	hydrogen peroxide
HRMS	high resolution mass spectrometry
IBU	ibuprofen
IBUNa	ibuprofen sodium salt
LC	liquid chromatography
MRM	multiple reaction monitoring
MS	mass spectrometry
NMR	nuclear magnetic resonance
NSAID	Non-steroidal anti-inflammatory drug
·OH	hydroxyl radical
SDZ	sulfadiazine
TP	transformation product
UV	ultraviolet
WWTP	wastewater treatment plant
DPD	dipropyl-p-phenylenediamine

List of publications

I. **S. Saeid**, P. Tolvanen, N. Kumar, K. Eränen, J. Peltonen, M. Peurla, J.P. Mikkola, A. Franz & T. Salmi, Advanced oxidation process for the removal of ibuprofen from aqueous solution: A non-catalytic and catalytic ozonation study in a semi-batch reactor, Appl. Catal. B Environ. 230 (2018) 77–90. doi:10.1016/j.apcatb.2018.02.021.

II. **S. Saeid**, M. Kråkström, P. Tolvanen, N. Kumar, K. Eränen, J. Peltonen, M. Peurla, J.P. Mikkola, L. Maël, L. Kronberg, P. Eklund & T. Salmi, Removal of ibuprofen from aqueous solution using a combination of heterogeneous catalysts and ozone: Effect of catalyst synthesis, metal particle size, acid sites and support structure, (submitted)

III. **S. Saeid**, M. Kråkström, P. Tolvanen, N. Kumar, K. Eränen, J.P. Mikkola, L. Kronberg, P. Eklund, M. Peurla, A. Aho & T. Salmi, Advanced oxidation process for degradation of carbamazepine from aqueous solution: Influence of metal modified microporous, mesoporous catalysts on the ozonation process, Catalysts 2020, 10(1), 90. doi.org/10.3390/catal10010090

IV. M. Kråkström, **S. Saeid**, P. Tolvanen, N. Kumar, T. Salmi, L. Kronberg & P. Eklund, Ozonation of carbamazepine: product determination and reaction mechanisms, (submitted)

V. **S. Saeid**, M. Kråkström, P. Tolvanen, N. Kumar, K. Eränen, J.P. Mikkola, L. Kronberg, P. Eklund, A. Aho, H. Palonen, A. Shchukarev & T. Salmi, Pt modified heterogeneous catalysts combined with ozonation for the removal of Diclofenac from aqueous solutions and the fate of by-products**,** (submitted)

VI. M. Kråkström, **S. Saeid**, P. Tolvanen, N. Kumar, T. Salmi, L. Kronberg & P. Eklund, Identification and quantification of transformation products formed during the ozonation of the non-steroidal anti-inflammatory pharmaceuticals ibuprofen and diclofenac, (submitted)

VII. M. Kråkström, **S. Saeid**, P. Tolvanen, T. Salmi, L. Kronberg & P. Eklund, Catalytic ozonation of the antibiotic sulfadiazine: Reaction kinetics and transformation mechanisms, Chemosphere. 247 (2020) 1-12. doi.org/10.1016/j.chemosphere.2020. 125853

Related publication

VIII. **S. Saeid**, M. A. Behnajadya, P. Tolvanen & T. Salmi, Optimization of photooxidative removal of phenazopyridine from water, Russ. J. Phys. Chem. (2018), https://doi.org/10.1134/S0036024418050266

List of related contributions

1. **S. Saeid,** V. Russo, P. Tolvanen, N. Kumar, K. Eränen & T. Salmi, **"**Development of combined ozonation and catalytic technology for elimination of pharmaceuticals from wastewaters", 24th International Congress of Chemical and Process Engineering *(CHISA August 2020), Prague (Czech Republic)*, (Oral presentation)

2. **S. Saeid**, P. Tolvanen, M. Kråkström, N. Kumar, K. Eränen, J.P. Mikkola & T. Salmi,, "Development of new technology for the destruction of pharmaceuticals: heterogeneous catalyst and ozonation", First International Conference on Unconventional Catalysis, Reactors and Applications (*UCRA October 2019), Zaragoza (Spain)*, (Oral presentation)

3. **S. Saeid**, V. Russo, P. Tolvanen, N. Kumar, K. Eränen, J. P. Mikkola & T. Salmi, "Kinetic and modeling of ibuprofen removal in the absence and presence of heterogeneous catalysts", the 12th European Congress of Chemical Engineering (*ECCE 12 September 2019*), *Florence (Italy)*, (Poster presentation)

4. **S. Saeid**, P. Tolvanen, M. Kråkström, N. Kumar, K. Eränen, J. P. Mikkola & T. Salmi,, "Towards a new technology: Ozonation of pharmaceuticals and their by-products in the presence of heterogeneous catalysts", 17th International Conference on Chemistry and the Environment *(ICCE June 2019), Thessaloniki (Greece)*, (Oral presentation)

5. **S. Saeid**, P. Tolvanen, M. Kråkström, N. Kumar, K. Eränen, J.P. Mikkola, L. Kronberg, P. Eklund & T. Salmi, "Combined technology for removal of pharmaceuticals: Catalytic ozonation of ibuprofen and diclofenac", 6th International Congress on Green Process Engineering (*GPE June 2018), Toulouse (France),* (Oral presentation)

6. **S. Saeid**, P. Tolvanen, N. Kumar, Matilda Kråkström, K. Eränen, J.P.Mikkola & T. Salmi, "The effect of catalyst synthesis methods on the degradation of pharmaceutical compounds ibuprofen and diclofenac", 12th International Symposium on the "Scientific Bases for the Preparation of Heterogeneous Catalysts", *(PREPA July 2018), Louvain-La-Neuve (Belgium)*, (Poster presentation)

7. **S. Saeid**, P. Tolvanen, M. Kråkström, K. Eränen, N. Kumar, J.P.Mikkola & T. Salmi, **"**Degradation of pharmaceutical waste from water by the combination of heterogeneous catalyst and ozonation", 23rd International Congress of Chemical and Process Engineering *(CHISA August 2018), Prague (Czech Republic)*, (Oral presentation)

8. **S. Saeid**, P. Tolvanen, M. Kråkström, K. Eränen, N. Kumar, J.P.Mikkola & T. Salmi, "Evaluation of the byproduct formation in the catalytic ozonation of residual pharmaceutical compounds in wastewater", 10th World Congress of Chemical Engineering *(WCCE October 2017), Barcelona (Spain)*, (Oral presentation)

9. **S. Saeid**, P. Tolvanen, M. Kråkström, K. Eränen, N. Kumar, J.P.Mikkola & T. Salmi, "Development of Three-Phase Catalytic Ozonation Technology for Treating Pharmaceutical Compounds in Waste Water" 10th International Symposium on Catalysis in Multiphase Reactors *(CAMURE-10 July 2017), Qingdao (China),* (Poster presentation)

10. **S.Saeid**, P.Tolvanen, K. Eränen, N. Kumar J.P.Mikkola & T. Salmi, "Degradation of pharmaceutical compounds by Catalytic ozonation promoted with zeolite-based catalysts", 7th FEZA Conference, The Zeolites- Materials with Engineered Properties *(July 2017), Sofia (Bulgaria),* (Oral presentation)

11. **S. Saeid**, P.Tolvanen, K. Eränen, N. Kumar J.P.Mikkola & T. Salmi, "Catalytic Degradation of Pharmaceuticals by Ozonation", 17th Nordic Symposium on Catalysis *(NSC17 June 2016), Lund (Sweden)*, (Oral presentation)

12. P. Tolvanen**, S**. **Saeid,** A, Franz, K. Eranen, N. Kumar & T. Salmi, "Catalyst screening and reaction kinetics in the degradation of pharmaceuticals by ozonation", 22nd International Congress of Chemical and Process Engineering *(CHISA August 2016), Prague (Czech Republic)*, (Oral presentation)

Table of contents

1. Introduction

1. Introduction

1.1. The appearance and toxicity of pharmaceutical compounds in aquatic environment

Pharmaceutical products are complex molecules, ordinarily named medicines or drugs, mainly organic compounds which possess a wide range of several physicochemical and therapeutic characteristics [1][2]. Nowadays, enormous quantities of pharmaceuticals are consumed by humans which leads to a growing and continuous release of harmful components into the environment. Moreover, most of these molecules persistent in the aquatic environment and can therefore be classified as contaminants [3], which implies that the occurrence and sources of pharmaceutical compounds in the environment become a global growing awareness [4]. Recently, several studies have been conducted regarding the existence and ecological hazard of the pharmaceuticals and personal care products discharged into the surface waters [5][6][7][8]. The appearance of these components and their metabolites in a considerable quantity in the aquatic environment is due to the fact that conventional wastewater treatments plant cannot degrade them efficiently enough due to their chemical stability. Existing conventional water treatment plans are designed mainly for eliminating biodegradable organics and nutrients [5][9][10]. Various paths for pharmaceuticals excite to penetrate to the aquatic and terrestrial ecosystems from excrement of humans and animals. The reasons originate from the effluent of the water treatment process and discharges from hospitals and household pharmaceuticals [11]. These pollutants are toxic to aquatic animals, microorganisms and conceivably human beings at very low concentration levels because they have been designed to have a powerful biological activity at low doses to promote particular mechanisms in the human and animal bodies [12][13].

Common pharmaceuticals are highly prescribed and consequently, enter the wastewater at large amounts. Therefore, some of these pharmaceuticals have been quantified in the rivers, lakes and seas at high concentrations [14]. In Finland, at 2014, the consumption of Ibuprofen (IBU), Carbamazepine (CBZ), Diclofenac (DCF) and Naproxen were respectively 119, 3.4, 0.9, and 6.1 tons per year was reported by the Finnish Medicine Agency Fimea. Likewise, the consumption of IBU and DCF were reported to equal 345 and 86 tons per year in Germany in 2001, and 162 and 26 tons per year in England at 2000 [15]. In an investigation performed by United Nations Educational, Scientific and Cultural Organization (UNESCO) on the pharmaceutical discovery at the aquatic environment of Baltic Sea region revealed that generally the elimination rate of pharmaceuticals in municipal wastewater treatment plants were low for the majority of the pharmaceuticals studied. The most commonly detected anti-inflammatory and analgesics medicine in this area were DCF and IBU, whereas the most commonly detected antimicrobial medicines were paracetamol, sulfamethoxazole, and the most frequently found central nervous system (CNS) drugs were CBZ and primidone, respectively. Hormones such as a estradiol (1.1 ng/l) were also observed in a some samples [16].

1.1.1. Ibuprofen

IBU [2-(4-isobutyl phenyl) propionic acid] is a pharmaceutical belonging to the group of a non-steroidal anti-inflammatory drugs (NSAID). The structural formula of IBU is given in Fig.1. This medicine is typicaly prescribed for treating pain, inflamation, migraine and fever [17][18]. IBU is vividely used worldwide in several formulations and is generally sold in 400 to 600 mg tablets. This medication is one of the main pharmaceuticals in the list of essential drug compiled by the World Health Organization (WHO) [19][20]. Commonly, IBU is mixed with other medicines, including antihistamines and decongestants and it can be obtained over-the-counter [21]. It is the most used pharmaceutical in Finland and as a consequence, it is one of the pharmaceuticals with the highest concentration in the raw sewage. This compound almost always detected in a broad range of concentrations in aquatic environments in Finland and worldwide mostly at the discharge points of the water treatment plan effluents due to an inadequate elimination in conventional wastewater treatment plan [22][23][24]. A number of studies have reported the detection of IBU in the rivers such as a Aura river, Turku, Finland around 20 μg/L, River Aire and Calder catchment, UK around 4.8 μg/L [25][26][27]. This medicine is a hazard to aquatic organisms. Consequently, the accumulation of IBU in the food chain has many toxic impacts on the human health as well. For instance, the harmfull effect of IBU on fish species has been noticed, i.e. the reproduction of Japanese rice fish *(Oryzias latipes)* at quite low concentration (0.1 μg/L), and health effects in freshwater fish *(Rhamdia quelen)*, and damaging influences to the kidney, and endocrine disruption in zebrafish [28][20][29]. IBU has a 49.5% risk characterization ratio (RCR) in the rivers of UK, which can be classified as an unacceptable environmental risk [30]. Another study revealed that two of the compounds that were determined in larger concentrations in the effluent than the influent were metabolited of IBU (IBU-OH and IBU-COOH) which are produced through the biological degradation of the parent compound in the manciple wastewater treatment [16]. Several treatments have been proposed for the elimination of IBU, for example a Fe^{II}-NTA complex-activated persulfate combined by hydroxylamine, while hydroxylamine is harmful itself, UV combined with chlorine, this method resulted in toxic chlorinated by-products and the abiotic treatment also possess the toxic by-products [31][32]. Consequently, it is highly desirable to find a technologically reliable treatment method for eliminating IBU leading to no or at least lower amount of toxic by-products.

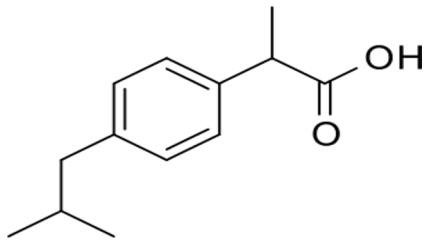

Fig. 1. Structural formula of ibuprofen (IBU).

1.1.2. Carbamazepine

CBZ [5H-dibenzo(b,f)azepine-5-carboxamide] is a pharmaceutical belonging to the group of central nervous system agents (psychiatric). Fig.2 displayes the structural formula of CBZ. This medicine is prescribed for treatment of epilepsy, bipolar disorder, chronic nerve and trigeminal neuralgia, a chronic pain disorder [33][34]. CBZ is one of the essential medications for basic health care reported by WHO in 2017 (it is a member of anticonvulsant and antiepileptic medicines) [35]. This medicine is used widely and the global consumption is nearby 1014 tons per year [36]. Upon consumption, the human body metabolizes only 28% of CBZ, while the rest is enzymatically transformed to CBZ intermediates which are excreted by urination. These intermediates are transformed via hydrolysis into CBZ-diOH, and it was one of the most detected CBZ compound in surface waters [37]. CBZ has become one of the most detected pharmaceuticals in the effluent and water bodies due to its low degradation rate, resistance against biodegradation and high persistence [10][38]. In municipal wastewaters, the average removal amount of CBZ was -86%. This is owing to the discharge of parent compounds from β-glucuronated CBZ from the disposal of human or in activated sludge, *E. coli secrete* the β-glucuronidase enzyme, can deconjugate glucuronated metabolites and discharge the active CBZ inside the treated wastewater [16]. This medicine can be found almost everywhere in the surface waters of the Baltic Sea region with a very long half–life time of approximately 3.5 years, which has resulted in the accumulation of over 55 tons of CBZ in the Baltic Sea. The elimination efficiency of CBZ in Finland is -41% [39]. Detection of CBZ and its metabolites has been reported in several surface waters, for example in Milan, Italy, the surface water contains up to 0.1 μg/l, whereas in Germany and Portugal, the amount is much higher, around 5 μg/l. It is one of the most frequent medicine detected in Serbian and Spanish rivers. The reason is that these compounds are not eliminated by conventional treatment methods [40][13][41][42]. CBZ, human metabolites of CBZ, and CBZ transformation by-products have been detected everywhere inside surface waters in Germany wherein they are potentially dangerous to mammalians and humans [43]. The threat of CBZ to the marine life and human body (induces chromosomal damage) have resulted to that many studies try to eliminate this compound from water [44][45], For example, by adsorption[46], using membrane [47], radiation activation of peroxymonosulfate [48], chlorination, chloro-amination and ozonation [49], CBZ residues have genotoxicity after most of these treatments. However, it is proposed that one of the most efficient way to remove CBZ is by ozonation. Nevertheless, by-products are formed via the ozonation of CBZ, such as 1-(2-benzaldehyde)-4-hydro-(1H,3H)-quinazoline-2-one (BQM) and 1-(2-benzaldehyde)-(1H,3H)-quinazoline-2,4-dione (BQD), which are stable and have a high cytotoxicity and genotoxicity with a chromosomal damage impact. Most of the proposed treatments for CBZ have a low degradation rate or they lead to high amounts of toxic by-products.

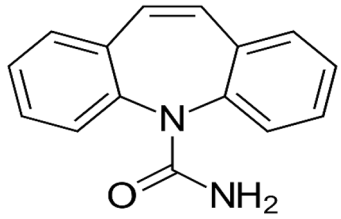

Fig.2. Structural formula of carbamazepine (CBZ).

1.1.3. Diclofenac

DCF (2-(2-(2,6-dichlorophenylamino) phenyl) acetic acid) is a pharmaceutical belonging to the group of non-steroidal anti-inflammatory drugs (NSAID). Fig.3 reperesents the structural formula of DCF. This medicine is prescribed for migraine headache, osteoarthritis, rheumatoid arthritis, and menstrual cramps [50][51]. The biodegradation and conventional wastewater treatment cannot eliminate DCF effectively [52]. Therefore, this medicine has been discovered in several surface waters worldwide, and moreover it can be found in freshwaters at ecotoxicological levels [53]. For instance, in Pakistan rivers, DCF and two of its transformation by-products (4-hydroxydiclofenac, and 5-hydroxydiclofenac) had concentrations of 85 μg/L, 18 μg/L, and 3 μg/L, respectively [6]. In the wastewater effluents in Colombia, DCF concentration was detected with a concentration of 0.34 μg/L [54], and in the surface waters of Milan to the concentration was 0.1 μg/L [13] In Eastern Finland, the surface waters had a daily accumulation of 10000 mg/day of DCF, depending on the season [26]. This medicine has a potentially adverse impact on the marine life and by accumulation in the food chain to human health. For instance, it has toxic effects on the kidney of fishes [55][56][57]. This medicine can interact with other organic and inorganic contaminants via wastewater treatment process, it leads to production of other pollution in water [58]. Several methods have been published for the degradation of DCF from water, for example treatment utilizing sludge [50], microorganisms[59], adsorption [60] and photocatalysis [61]. However, most of the technologies published for the elimination of DCF do not have completely degradation, and they are costly, long-duration processes. There is also a the lack of analyzing the transformation products of the treatments [60].

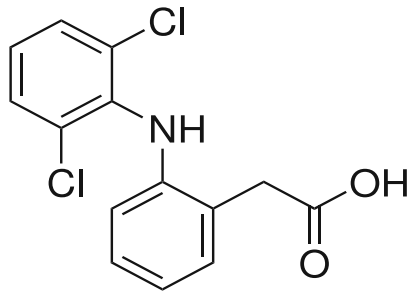

Fig.3. Structural formula of diclofenac (DCF).

1.1.4. Sulfadiazine

Sulfadiazine (SDZ) 4-amino-N-pyrimidin- 2-yl-benzenesulfonamide is one the most beneficial antibiotics used for treat toxoplasmosis. Fig.4 displayes the structural formula of SDZ [62][63]. SDZ has been utilized broadly in the clinic, veterinary medicine, and furthermore in aquaculture. However, this medicine has some adverse impacts, for instance, allergies, methemoglobinemia, immune complex formation. Due to the long half-life of SDZ, it can simply remain in the bodies of animals and via the food chain, SDZ ultimately accumulates in the human body. This pharmaceutical compounds has even at low concentrations the potential to pose serious threats to human health and ecosystems. For instance, it has a toxic effect on *Sparus aurata* fish [64][65][66]. SDZ is a very mobile and easily passage into the water due to its high solubility of about 77mg/L in water [67]. This medicine has been detected in several surface waters such as a in the Chinese Beiyun river 0.16 μg/l [68], 0.147 μg/l in the Soeste River of Germany [69], and in the group of antimicrobial and antidote pharmaceuticals sulfadiazine detected in rivers in Baltic Sea countries at the highest maximum concentration (19 μg/l) [16]. The elimination of sulfadiazine has been studied by several methods such as oxidation, adsorption [70], membrane [71] and oxidation by permanganate [72], but most of these treatments cannot degrade sulfadiazine entirely or they lead to the formation of by-products which may more toxic than the parent medicine.

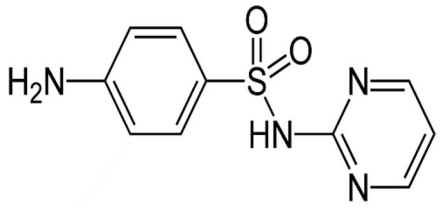

Fig. 4. Structural formula of sulfadiazine (SDZ).

1.2. Advanced oxidation process

Pharmaceutical residues are not easily eliminated nor mineralized by biodegradation and conventional water treatment methods, which leads to a partial removal efficiency only as well as accumulation of toxic by-products. Advanced oxidation processes (AOPs) provide a promising path to achieve entirely degradation of these contaminants and suppression of toxicity [73][74]. In AOPs, oxidizing species such as hydroxyl radicals, hydrogen peroxide and ozone attack organic components, for which these species are sensitive, non-selective and highly reactive [75][73]. Several studies have applied AOPs for the removal of pharmaceuticals, for example ozonation [76], electrochemical oxidation [77], and photocatalytic degradation [78].

1.2.1. Ozone

Ozone is a highly reactive oxygen species and ozonation is broadly applied in the wastewater treatment due to the ozone strong oxidizing properties, disinfection potential, and low selectivity of ozone. This treatment could substitute environmentally harmful chlorination. Ozone under the conditions of water treatment can generate hydroxyls radicals which are extremely reactive spices [79][80][81]. Ozone can react directly with an organic compound or produce hydroxyl radicals which can react with organic compounds. These two reaction routes can lead to various oxidation products and they are controlled via a large variety of reaction mechanisms (Fig.5) [81].

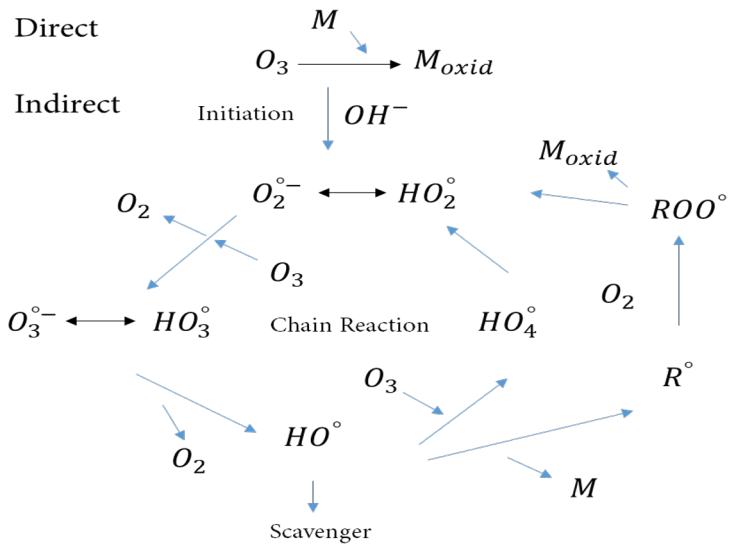

Fig. 5. Overview of ozonation reaction with micropollutant in direct and indirect pathway, R present reaction product and M present micropollutant [81].

Ozonation is a well-known chemical treatment for the elimination of pharmaceuticals due to the ability of ozone to attack aromatic molecules and unsaturated bonds [82][83]. Ozone treatment is well-known and it has been utilized for the elimination of pharmaceuticals in hospitals and other wastewaters [84][82]. In pharmaceutical ozonation, for example, 99% of DCF has been removed, still only 24% mineralized and toxicity was slightly reduced [85].

Ozonation treatment has been proved to be an efficient pathway for the removal of pharmaceuticals but there is a potential of the formation of toxic by-products due to its deficiency in reacting with some organic and inorganic compounds (e.g. saturated aliphatic acid and NH_4^+), therefore, the oxidation processes are sometimes slow or incomplete. Moreover, ozone has a low solubility and stability in water. To improve ozonation treatment with high mineralization, low toxic transformed by-products, and higher reaction rate, it can be applied with a combination of other AOP treatments, for instance O_3/H_2O_2, O_3/UV, O_3/UV/H_2O_2 as well as catalytic ozonation [86][87][88].

1.2.2. Catalytic ozonation

The application of the ozone-based process for water treatment is so beneficial because it can produce hydroxyl radicals in ambient temperatures and pressures. One of the highly recommended ozone-based processes for wastewater treatment is a combination of ozone and heterogeneous catalyst. This method has the potential to mineralize organic pollutions [79][89]. The catalytic ozonation can be utilized for the removal of a wide range of pollutants such as industrial organic pollutants, pharmaceuticals, and personal care products in wastewater. This treatment is consist of two parts, namely homogeneously catalyzed and heterogeneously catalyzed ozonation. In the homogeneous systems, ozone can be activated through metal ions (catalyst) existing in water and in the heterogeneous system, ozone can be activated via metal oxides upon the support [90][91]. Several studies have been utilized and proposed the heterogeneously catalyzed ozonation for the elimination of organic pollutants, particularly pharmaceuticals from wastewaters because it is an easier application and catalyst separation from water is straightforward [90][92][93]. Zeolites have excellent chemical stabilities in the presence of ozone which makes them more attractive heterogeneous catalysts for long-term ozonation processes [94].

1.3. Scope of the research

The approach of our research was to study the elimination of pharmaceuticals from water by non-catalytic and heterogeneously catalyzed ozonation. Initially, the gas-liquid semi-batch reactor was designed and the operation parameters; temperature, type and position of the stirrer, initial concentration of IBU, pH, and gas flow rate has been studied in the ozonation of IBU. Later on H- and Fe-modified Beta zeolite catalysts H-Beta-25, Fe-H-Beta-25-EIM and Fe-H-Beta-150-SSIE) were applied on the combination of ozonation (**Publication I)**. To achieve total decomposition of IBU in a shorter time of ozonation, new reactor vessel with glass baffles was implemented, different nitrogen concentrations were used in inlet gas of ozonator, and nine different catalysts (Cu-H-Beta-25-IE, Cu-H-Beta-150-IE, Cu-H-Beta-300, Cu-H-Beta-150-EIM, Cu-H-Beta-150-DP, Cu-Na-Mordenite-12.8-IE, Pd-H-MCM-41-EIM, Fe-SiO2-DP, and Ni-H-Beta-25-EIM) were used for the degradation of IBU. The by-products formed in these experiments were studied and identified by liquid chromatography-mass spectrometry (LC-MS/MS) **(Publication II)**.

In **Publication III,** the removal of CBZ and its by-products in aqueous solutions was investigated. The task is challenging because the degradation rates of the by-products are relatively low. A high concentration of CBZ (30 mg/L) was selected to study the degradation kinetics of the by-products of the degradation. For this purpose, the main products were isolated and their concentrations were monitored with high performance liquid chromatography (HPLC). In order to optimize the degradation of the by-products, the catalysts Pt-MCM-41-IS, Ru-MCM-41-IS, Pd-H-Y-12-EIM, Pt-H-Y-12-EIM, Pd-H-Beta-300-EIM and Cu-MCM-41-A-EIM where used, at two different reaction temperatures. The

detailed by-product identification and the transfromation pathway of the ozonation of CBZ are presented in **Publication IV**.

In **Publication V** the removal of DCF and the evolution of by-products were reported. Pt-modified catalysts were synthesized (H-MCM-22-100, 1%wt Pt-MCM-22-100-EIM, 2%wt Pt-MCM-22-100-EIM, 5%wt Pt-MCM-22-100-EIM, Pt-H-Y-12-IE, Pt-γ-Al2O3 (UOP)-EIM) and applied on ozonation. The effect of the Pt loading the catalysts, the catalyst concentration and catalyst structures in the transformation of DCF and its degradation by-products were studied in detail. The by-product classification and the transformation pathway of the ozonation of IBU and DCF are reported in **Publication VI.**

The removal and transformation of SDZ was investigated in **Publication VII.**

The heterogeneous catalysts were characterized by several physical and chemical methods to explain their activities in the ozonation experiments.

2. Experimental

2. Experimental

2.1. Chemicals

IBU ($C_{13}H_{18}O_2$, MW:206.28 g/mol, CAS number:15687-27-1,>98% purity) was provided in solid state by Sigma Life Science (China). Ethanol (C_2H_6O, MW: 46.06 g/mol, CAS number: 64-17-5,>96% purity) was provided by Altia (Finland). CBZ ($C_{15}H_{12}N_2O$, MW: 236.269 g/mol, CAS number: 298-46-4) was purchased from Sigma Life Science. The CBZ was in crystal powder form, therefore it was first dissolved in methanol. BQM and BQD were prepared from ozonation following to the procedure Kråkström *et al.* **(IV)** Stock solutions of BQM and BQD were prepared in acetonitrile. DCF ($C_{14}H_{11}Cl_2NO_2$, MW: 296.148 g/mol, CAS number: 15307-86-5, >98% purity) was purchased from Sigma Aldrich. The internal standard, SDZ-D4 ($C_{10}H_{10}N_4O_2S$, MW: 250.278 g/mol, CAS number: 68-35-9) was purchased from Toronto Research Chemicals, North York, ON, Canada. Analytical standard of sulfadiazine was purchased from Sigma-Aldrich, St. Louis, MO, USA.

HPLC grade methanol (H_3COH, MW:32.04 g/mol, CAS number:67-56-1) provided Vwr Prolabo Chemicals (France) and orto-phosphoric acid 85% (H3PO4, MW:98 g/mol, CAS:7664-38-2) were used. For the analysis of the concentration of ozone in the aqueous samples, potassium indigo tri-sulfonate ($C_{16}H_7K_3N_2O_{11}S_3$, MW:616.72 g/mol, CAS number:67627-18-3) obtained from Sigma-Aldrich (USA), sodium phosphate monobasic (H2NaO4P, MW: 119.98 g/mol, CAS number:7558-80-7) provided from Sigma life science (Germany) and orto-phosphoric acid were used and dipropyl-p-phenylenediamine (DPD) provided from Merck KGaA (Germany). For the determination of ozone in gas phase, potassium iodide (KI, MW:166 g/mol, CAS number:7681-11-0) was provided from Merck KGaA (Germany), disodium hydrogen phosphate (Na_2HPO_4*$2H_2O$, MW:177.99 g/mol, CAS number:10028-24-7) obtained from Sigma-Aldrich (Germany), potassium dihydrogen phosphate (H_2KO_4P, MW:136.09 g mol−1, CAS number:7778-77-0) was provided from Fluka (Switzerland).The water used in the LC-MS analysis was purified using a Millipore Simplicity 185 system (Millipore S.A.S., Molsheim, France). The acetonitrile used in the LC-MS analysis was of LC-MS grade and was obtained from Fisher Scientific and formic acid was obtained from Sigma-aldrich.

2.2. Catalyst preparation

Originate zeolites were provided by Zeolyst International. The H-Beta-25 catalyst was obtained using a step calcination procedure of NH_4-Beta-25 zeolite. The calcination was carried out in a muffle oven at 450 ^{0}C for 240 min. The methods used for the synthesis of the metal modified (Cu-, Fe-, Pd-, Ni-, Pt-, Ru-) catalysts were: evaporation impregnation (EIM), solid-state ion exchange method (SSIE), solution ion exchange (IE) and deposition-precipitation (DP), in-situ (IS)(Table 1).

Table 1. Catalysts preparation method studied in this Thesis.

Method	Synthesized procedure	Catalyst
evaporation impregnation (EIM)	For example, the Fe-H-Beta-25-EIM synthesis was done by stirring the mixture of ferric nitrate solution and H-Beta-25 zeolite in a rotavapor at 60˚C [95]. It was rotated for 24 h, during which the aqueous phase was evaporated and the catalyst was removed from the flask. Later on, the catalysts were dried at 100˚C overnight and calcined at 450 ˚C for 4 h. For Cu-modified, Pd-modified, Ni-modified and Pt-modified catalysts were prepared, using an aqueous solution of $Cu(NO_3)_2$, $Pd(NO_3)_2$, $Ni(NO_3)_2$, $Pt(NO_3)_2$ respectively as a precursor [96].	Fe-H-Beta-25-EIM **(I),** Cu-H-Beta-150-EIM **(II),** Pd-H-MCM-41-EIM **(II),** Ni-H-Beta-25-EIM **(II),** Pd-H-Y-12-EIM **(III),** Pt-H-Y-12-EIM **(III),** Pd-H-Beta-300-EIM **(III),** Cu-MCM-41-A-EIM **(III),** 1%wt.Pt-MCM-22-100-EIM **(V),** 2%wt.Pt-MCM-22-100-EIM **(V),** 5%wt.Pt-MCM-22-100-EIM **(V),** Pt-H-Y-12-IE **(V),** Pt-γ-Al_2O_3 (UOP)-EIM **(V)**
solid-state ion exchange method (SSIE)	The Fe-H-Beta-150-SSIE was prepared by the SSIE method by ball-milling the mixture of support and iron for 8 h [97]. Catalyst was dried at 100 ˚C overnight and calcined at 450 ˚C for 4 h.	Fe-H-Beta-150-SSIE **(I)**
solution ion exchange (IE)	For example, the Cu-H-Beta-25-IE catalyst was synthesized by IE method, which was carried out in a beaker using an aqueous solution of copper nitrate $Cu(NO_3)_2$ and H-Beta-25 for 24h. After ion-exchange, the catalyst was filtered and washed with two liters of distilled water and the Cu-H-Beta-25-IE catalyst was dried in an oven at 100 ˚C. The Cu-H-Beta-25-IE catalyst was calcined at 450˚C in a muffle oven for 4.5 h. The other catalysts synthesized by IE method, have similar synthesis procedures as aforementioned.	Cu-H-Beta-25-IE **(II),** Cu-H-Beta-150-IE **(II),** Cu-H-Beat-300-IE **(II),** Cu-Na-Modernite-12.8-IE **(II),** Pt-H-Y-12-IE **(V)**
deposition-precipitation (DP)	One of the most common processes of metal introduction in catalysts is the DP method, Which is a modification of the precipitation processes in liquid phase. It involves the conversion of a highly soluble metal precursor into a substance with a more limited solubility, which precipitates upon the support [98]. The Cu-H-Beta-150-DP zeolite catalyst was synthesized using the DP method. The synthesis was carried out in a beaker using aqueous copper nitrate solution $Cu(NO_3)_2$ and H-Beta-150. The pH of the aqueous solution was adjusted with NH_4OH to 10, at which the synthesis was performed. After 24 h, the Cu–H-Beta-150-DP was filtered and washed with two liters of distilled water and it was dried in oven overnight and calcined in a muffle oven at 450˚C for 4h. The Fe-SiO_2-DP catalyst was synthesized using the DP method by similar procedure.	Cu-H-Beta-150-DP **(II),** Fe-SiO_2-DP **(II)**
in-situ (IS)	The Pt and Ru modification of Pt-MCM-41-IS was carried out using the IS preparation method [98]. In-situ synthesis was performed by directly adding metal salt precursors of Pt in gel solution of MCM-41 mesoporous material.	Pt-MCM-41-IS **(III),** Ru-MCM-41-IS **(III)**

The H-Beta-25, Fe-H-Beta-25-EIM, and Fe-H-Beta-150-SSIE catalysts were applied in the presence of ozone to IBU degradation **(I)**. The Cu-H-Beta-25-IE, Cu-H-Beta-150-IE, Cu-H-Beta-300-IE, Cu-H-Beta-150-EIM, Cu-H-Beta-150-DP, Cu-Na-Mordenite-12.8-IE, Pd-H-MCM-41-EIM, Fe-SiO_2-DP, and Ni-H-Beta-25-EIM catalysts were synthesized and utilized in presence of ozone for IBU elimination **(II)**.The H-MCM-22-100, 1%wt Pt-MCM-22-100-EIM, 2%wt Pt-MCM-22-100-EIM, 5%wt Pt-MCM-22-100-EIM, Pt-H-Y-12-IE and Pt-γ-Al_2O_3 (UOP)-IMP were synthesized and utilized in the presence of ozone for the degradation of DCF **(V)**.The Cu-H-Beta-150-DP and Fe-H-Beta-25-EIM were synthesized and utilized in the presence of ozone for the degradation of SDZ **(VII)**.

2.3. Catalyst characterization

The specific surface areas and pores volume of the catalysts were determined by nitrogen adsorption using Carlo Erba Sorptomatic 1900 instrument and calculated by using the Brunauer-Emmett-Teller (B.E.T.) and Dubinin equations. Before each and every nitrogen adsorption measurement, the fresh and regenerated samples were outgassed at 150˚C and the spent catalysts at 100˚C for 3h.

The electron micrographs, metal particle size distribution and structural properties of the catalysts were investigated by transmission electron microscopy (TEM) using an electron microscope (model JEM 1400 Plus), using 120 kV accelerating voltage and a resolution of 0.38 nm provided via OSIS Quemesa 11 Mpix digital camera (rephrase/split). The average metal particle sizes and distributions were calculated by counting several particles from the transmission electron micrographs. The metal particle size (Cu, Pd, Ni) distributions were given in the form of histograms.

Scanning electron microscopy (SEM) coupled to energy disperse X-ray analysis (SEM/EDXA) was used to investigate morphology. The crystallite size and distribution of catalysts were studied by an electron microscope (SEM) Zeiss Leo 1530 Gemini equipped by ThermoNORAN vantage X-ray detector. Energy-dispersive X-ray analysis (EDXA) was carried out with the same instrument to determine the metal contents of the catalysts.

The catalyst acidities were estimated with Fourier transform infrared spectroscopy (ATI Mattson FTIR). The amounts of Brønsted and Lewis acid sites were measured by employing pyridine (≥99.5%) as the probe molecule. First, a thin pellet disc of the catalyst was pressed and placed into the FTIR cell, and heated up to 450˚C for 1h. Then, the temperature was lowered to 100˚C and background spectra of the pellet were recorded and pyridine was adsorbed on the catalyst sample for 30 min and desorbed consequently by discharge at 250, 350 and 450˚C, respectively. The pyridine desorption at 250-350˚C display weak, medium and strong sites, 350-450 ˚C display medium and strong sites while 450˚C indicate strong sites [99].

The crystallinity and structural properties of the catalysts were characterized using a powder X-ray diffraction (XRD) with PANalytical Empyrean diffractometer in Bragg-Brentano mode. The incident X-ray beam was collimated with parallel beam optics consisting of a 1/2 °

divergence slit, a 10 mm mask, a 0.04 rad Soller, a Göbel mirror and 1 ° antiscatter slit. On the diffracted side, a 7.5 mm antiscatter slit, a 0.04 rad Soller and a PIXcel^{3D} detector array by 255 × 255 pixels were applied. The Göbel mirror monochromatizes the beam into Cu-Kα_1 and Cu-Kα_2 lines giving an average wavelength of λ = 1.542 Å. The powder samples were determined on a siliceous zero background sample holder from 5 ° to 100 ° including a step size of 0.026 ° and counting for 120 s per step. The XRD data were fitted via Rietveld refinement utilizing the MAUD software [100].

X-ray photoelectron spectroscopy (XPS) was used to investigate the oxidation state of Pt. A Kratos Axis Ultra DLD electron spectrometer with monochromated Al K source was operated at 150 W. Analyser pass energy of 160 eV for acquiring wide spectra and a pass energy of 20 eV for individual photoelectron lines were used. The surface potential was stabilized with the spectrometer charge neutralization system and the binding energy (BE) scale was referenced to the C 1s line of aliphatic carbon, set at 285.0 eV. Processing of the spectra was accomplished with the Kratos software. The powder samples were gently hand-pressed into pellets directly on a sample holder using clean Ni spatula. The energy dispersive X-ray microanalyses was used to determine the chemical compositions of fresh catalytic materials.

The content of metals in the end sample after the catalytic ozonation process was determined by inductively coupled plasma optical emission spectroscopy (ICP-OES), using an Optima 5300 DV Perkin Elmer instrument to investigate the potential leaching of catalytic metals.

2.4. Kinetic ozonation experiments in a semi-batch reactor

The catalytic and non-catalytic ozonation experiments were conducted in a gas-liquid reactor system operating in semi-batch mode. In this system, a double jacket glass reactor with a capacity of 1100ml was connected to an ozone generator. The reactor system was displayed in Fig 6.

The ozone generator (Absolute Ozone, Nano model, Canada) produced approximately 60 mg/L concentration of ozone in gas when an oxygen gas flow rate of 450 mL/min combined with 50, 2.5 and 0 mL/min N_2 (super-dry feed gas dew point -60°C) gas was used. This gas flow was utilized for the IBU degradation. The concentration of dissolved ozone in water depends on several parameters such as temperature and gas flow rate. The dissolved ozone concentration at 5 ˚C, using 450 ml/min oxygen and 50 ml/min nitrogen was 4.5 mg/l and at 20˚C, using 450 ml/min oxygen and 2.5 ml/min nitrogen was 8.317 mg/l, determined with the indigo method typically used for IBU and SDZ degradation.

Due to rapid reactions of CBZ and DCF by ozone, 109.5 mL/min oxygen gas flow rate combined with 1.5 mL/min nitrogen as gas flow rate to the generator was obtained, so the total gas flow was 110 mL/min. The ozonator produced a concentration of approximately 21 mg/L of ozone in the gas phase in this gas flow rate. The dissolved ozone concentration typically used for CBZ and DCF experiments was determined to 1.668 mg/L at 5°C, 0.441 mg/L at 20 °C and 0.0921 mg/L at 50°C by indigo method.

The aqueous phase containing the pharmaceutical components was in batch mode, while a gas mixture containing ozone was continuously bubbled through the aqueous phase through a 7μm disperser at the bottom of the reactor. The reactor content was exposed to vigorous stirring having typically a stirring rate of 1070 rpm. The kinetic experiments were operating in the two phases (gas and liquid) when no catalyst was used, or in three–phase (gas, liquid, and solid) when a heterogeneous catalyst was present. The required amount (0.25-1.0 g) of catalysts was immobilized inside the Spinchem ™ rotating bed stirrer using a 200 μm mesh. The catalyst particle sizes were within 150 μm-500 μm. These particles remained inside the stirrer pretty well.

Typical operating conditions in kinetic experiment were: concentration of IBU: 10-100 mg/L, CBZ: 35 mg/L, DCF: 30 mg/L, SDZ: 10 mg/L, gas flow: 110-1100 ml/min, mixing rate: 250-1070 rpm, reactor temperature: 5-50 °C and reaction time 10-240 min.

The solutions of IBU were prepared by a stock solution of IBU in Ethanol (50 mg/ml) from which 10 ml was dissolved in 1000 ml deionized water; this was done due to the low solubility of IBU in water. The solubility of CBZ is also rather low, only 17.7 mg/L, while it is fully soluble in methanol. Therefore, the stock solution was prepared by dissolving 0.35 g CBZ in 100 ml of methanol. Thereafter, 10 ml of the stock solution was added to 1000 mL de-ionized water in the glass reactor in the beginning of each experiment. The initial concentration of pharmaceuticals were higher than the concentrations typically detected in surface waters. However, a high initial concentration allows detecting and identifying by-products of very low concentrations. In the DCF experiments, the reactor vessel was covered by aluminum foil to prevent photo-degradation.

The pH was measured by a pH-stat device (tiamo™, Metrohm), and in some experiments (when needed), it controlled the pH by addition of 1M sodium hydroxide to the liquid phase. For the measurement of the concentration of the pharmaceutical compound, pH, and dissolved ozone, samples were withdrawn from the liquid phase before, during and in the end of ozonation process for each experiment (Fig.6).

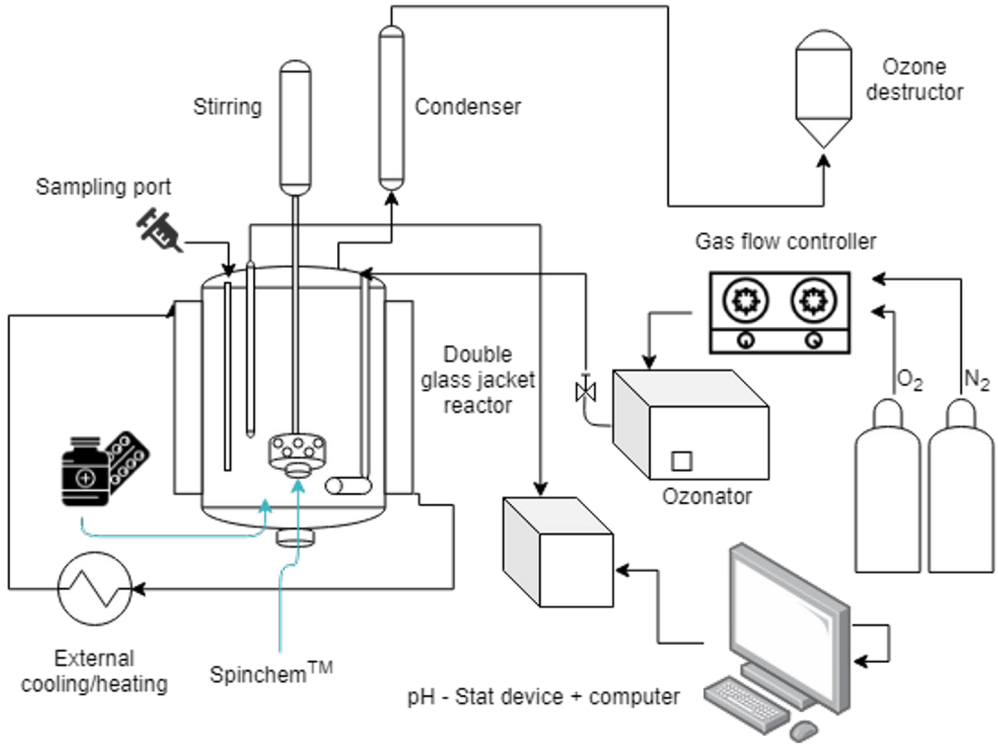

Fig. 6. Schematic view of the semi-batch reactor system for degradation of pharmaceuticals.

2.5. Chemical analysis

The concentration of dissolved ozone was determined with the indigo method. In this process, the ozone concentration in the aqueous phase can be measured by a spectrophotometer (UV–Vis) at 600 nm (pH < 4). In this method, indigo trisulfate, including alone one C=C double bond reacts with dissolved ozone; this reaction is stoichiometric and rapid. The transformation of the absorbance vs. ozone is −2.0 ± 0.1 × 104 1/M 1/cm and it is characteristic for the concentration of dissolved ozone in the range of 0.005–30 mg/L. The accuracy of the analysis is 2% or 3 µg/L for low concentrations, if a spectrophotometer or a suitable instrument is employed [101][102]. For comparative reasons, the ozone concentration in water was measured with the dipropyl-p-phenylenediamine (DPD) photometric method by using a reagent test kit to compare with the indigo method. In this method, ozone reacts with potassium iodide to produce iodine that reacts rapidly with DPD to produce a pink mixture; the intensity of the pink color is proportional to ozone concentration. The intensity was measured at 515 nm with a colorimeter or a spectrophotometer. This method is reported in mg/L of residual ozone concentration [103][104]**(I)**.

The concentration of IBU in the samples was analyzed by HPLC using an Agilent Technologies (1100 series) HPLC equipped with a UV-Vis photo diode array detector set at 214 nm, and a Quaternary pump. The column used was Ultra Techsphere ODS-5u-(C18), 250 mm × 4.6 mm.

The mobile phase consisted of 70:30 methanol and 0.5% phosphoric acid (pH: 1.8), flowing at 1 mL/min, the sample injection volume and retention time were 20 µL and 10 min, respectively (**I, II**).

For the quantification of other pharmaceuticals (CBZ, DCF, and SDZ) including identification, structure determination, quantification of the ozonation intermediates and by-products of pharmaceuticals (IBU, CBZ, DCF, and SDZ), several analyzers have been utilized by M. Kråkström.

Liquid chromatography-mass spectrometry (LC-MS/MS) and Liquid chromatography-ultraviolet (LC-UV) were utilized for the quantification of the pharmaceuticals and the ozonation by-products. The IBU, SDZ and DCF ozonation by-products were analyzed by using LC-MS/MS. For the LC-MS/MS analysis, an Agilent 6460 triple quadrupole mass spectrometer equipped with an Agilent Jet Spray electrospray ionization (ESI) source was used in a multiple reaction monitoring (MRM) modes.

DCF, CBZ, BQM, and BQD were analyzed by using the LC-UV. For LC-UV analysis, the chromatographic separation was done using an Agilent 1100 binary pump equipped with a vacuum degasser, an autosampler, a thermostatted column oven set to 30°C, a variable wavelength detector, and a Waters Atlantis T3 C18 column 2.1 × 100 mm, 3 µm.

Ion trap MS, high-resolution mass spectrometer (HRMS) and gas chromatography-mass spectrometry (GC/MS) has been employed for the structure determination of the pharmaceuticals and ozonation by-products. For Ion trap MS determination, an Agilent 1100 LC/MSD ion trap mass spectrometer equipped with an electrospray ionization (ESI) source was used in full scan and MS^n scan modes. DCF, CBZ and SDZ samples were analyzed by using the HRMS. For HRMS analysis, Bruker Daltonics micrOTOF quadrupole and time-of-flight mass spectrometer equipped with an electrospray ionization (ESI) source was used in full scan mode. The IBU samples were analyzed employing a GC/MS. For GC-MS, an Agilent Technologies 7890A gas chromatograph with a 5875C Series inert XL EI/CI MSD Triple-Axis Detector (GC–MS) was used.

The SDZ and CBZ main by-product were isolated, separated and analyzed using a 500 MHz Bruker AVANCE-III NMR-system. A detailed description of the analyses can be found in publications **(IV, VI and VII).**

3. Results and Discussion

3. Results and Discussion

3.1. Catalysts characterization results

3.1.1. Nitrogen physisorption

The specific surface areas and pore volumes of the catalysts were determined by nitrogen physisorption. The specific surface areas and pore volumes of fresh, spent and regenerated catalysts are presented in Table 2. The highest specific surface areas were obtained for the H-Beta-25 (1068 m^2/g), Cu-H-Beta-300-IE (1013 m^2/g) and Fe-H-Beta-25-EIM (953 m^2/g) catalysts and the highest pore volumes were determined for the Pt-γ-Al_2O_3 (UOP)-EIM (0.767 cm^3/g), Cu-MCM-41-A-EIM (0.765 cm^3/g) and Fe-SiO_2-DP (0.504 cm^3/g). The lowest specific surface areas were obtained for the Pt-γ-Al_2O_3 (UOP)-EIM (231 m^2/g) and Fe-SiO_2-DP (305 m^2/g) and the lowest pore volumes were determined for Cu-Na-Modernite-12.8-IE (0.158 cm^3/g) and H-MCM-22-100 (191 cm^3/g).

All the spent catalysts studied showed a decrease in the surface area and the pore volume. However, the extent to which the decrease in surface area and pore volume took place, was dependent on the catalyst structure. The reason for such a decrease in the surface area and pore volume is due to the coke formation in the pores of the catalysts. The H-Beta-25 (226 m^2/g), Fe-H-Beta-25-EIM (242 m^2/g), Fe-H-Beta-150-SSIE (486 m^2/g) Cu-H-Beta-150-EIM (548 m^2/g) and Cu-H-Beta-150-DP (470 m^2/g) spent catalysts exhibited lower surface areas and pore volumes than their fresh counterparts (Table 2). However, it is noteworthy to mention that in the case of all the spent catalysts, regeneration was possible by using a step calcination procedure and substantial surface area and pore volume were recovered: H-Beta-25-Regenerated (609 m^2/g), Fe-H-Beta-25-EIM-Regenerated (440 m^2/g, Fe-H-Beta-SSIE-Regenerated (537 m^2/g), Cu-H-Beta-150-EIM-Regenerated (640 m^2/g) and Cu-H-Beta-150-DP-Regenerated (537 m^2/g), (Table 2). The best recovery was achieved with the Fe-H-Beta-150-SSIE catalyst, whose specific surface only decreased 5 % after the regeneration. Furthermore, the presence of water in the reaction medium can lead to partial leaching of the catalytic materials.

Table 2. Specific surface area and pore volume of the fresh, spent and regenerated catalysts applied in the experiments.

Catalyst	Specific surface area (m^2/g)			Specific pore volume (cm^3/g)		
	fresh	spent	regenerated	fresh	spent	regenerated
H-Beta-25 **(I)**	1068	226	609	0.379	0.080	0.216
Fe-H-Beta-25-EIM **(I)**	953	242	440	0.222	0.085	0.156
Fe-H-Beta-150-SSIE **(I)**	567	486	537	0.216	0.172	0.190
Cu-H-Beta-25-IE **(II)**	694	_	_	0.246	_	_
Cu-H-Beta-150-IE **(II)**	542	_	_	0.192	_	_
Cu-H-Beat-300-IE **(II)**	1013	_	_	0.359	_	_
Cu-H-Beta-150-EIM **(II)**	846	470	537	0.300	0.167	0.190
Cu-H-Beta-150-DP **(II)**	731	548	640	0.259	0.194	0.227
Cu-Na-Modernite-12.8-IE **(II)**	446	_	_	0.158	_	_
Pd-H-MCM-41-EIM **(II)**	699	_	_	0.411	_	_
Fe-SiO_2-DP **(II)**	305	_	_	0.504	_	_
Ni-H-Beta-25-EIM **(II)**	567	_	_	0.201	_	_
Pt-MCM-41-IS **(III)**	429	555	_	0.409	0.552	_
Ru-MCM-41-IS **(III)**	747	677	_	0.491	0.456	_
Pd-H-Y-12-EIM **(III)**	667	732	_	0.237	0.259	_
Pt-H-Y-12-EIM **(III)**	857	344	_	0.304	0.506	_
Pd-H-Beta-300-EIM **(III)**	808	657	_	0.287	0.233	_
Cu-MCM-41-A-EIM **(III)**	612	104	_	0.765	0.314	_
H-MCM-22-100 **(V)**	538	431	_	0.191	0.153	_
1%wt.Pt-MCM-22-100-EIM **(V)**	708	493	_	0.251	0.175	_
2%wt.Pt-MCM-22-100-EIM **(V)**	631	464	_	0.224	0.165	_
5%wt.Pt-MCM-22-100-EIM **(V)**	652	468	_	0.231	0.166	_
Pt-H-Y-12-IE **(V)**	835	767	_	0.296	0.275	_
Pt-γ-Al_2O_3 (UOP)-EIM **(V)**	231	189	_	0.767	0.493	_

3.1.2. Transmission electron microscopy (TEM)

To study the metal particle size distributions and catalyst structures, TEM analyses were carried out. The transmission electron micrographs of applied catalysts are given in Publications **(I, II, III, V).** The transmission electron micrographs exhibited typical uniform porous structures of the Beta zeolite. It is significant to mention here that the methods of Fe modifications such as evaporation-impregnation (EIM) and solid state ion-exchange (SSIE) did not influence the basic porous structures of the Beta zeolites. The metal particle size distributions were determined for applied catalysts and the metal particle size distributions are given in as histograms in Publications **(I, II, III, V)**. The average metal particle sizes were measured and counted from the TEM images, which are displayed in Table 3.

The largest average copper particle size (11.49 nm) was determined for Cu-H-Beta-300-IE. It was observed that the methods of catalyst synthesis influenced the average Cu-crystal size formation. Thus, Cu-H-Beta-150-DP showed the smallest average Cu particle size (4.88 nm). For Cu-MCM-41-A-EIM, the mesoporous catalyst synthesized with the evaporation impregnation method, resulted in the average Cu particle size of 7.82 nm. It was concluded from the results of the averages particle sizes that the method of introducing Cu, Pt, Ru, Pd into the mesoporous MCM-41 influenced the sizes of the particles.

The transmission electron microscopy exhibited the largest Pt particles for the Pt-H-Y-IE catalyst (30.6 nm) and the second largest Pt particles for 1%wt.Pt-MCM-22-100-EIM (24.9 nm). The smallest average Pt particles were obtained for 5%wt.Pt-MCM-22-100-EIM (2.7 nm) catalyst. The explanation for the differences in the average Pt particles is attributed to the methods of Pt introduction in the support materials H-MCM-22, H-Y and Al_2O_3 (Table 3). Furthermore, the structure of the supports H-MCM-22, H-Y and Al_2O_3, the surface area, as well as the Brønsted and Lewis acid sites of these catalytic materials can also influence the formation of Pt particles, size and dispersion. The TEM images of the most efficient catalysts applied in removal of pharmaceuticals are given in Figure 7 (Fe-H-Beta-25-EIM, Cu-H-Beta-DP for IBU, Pd-H-Y-12-EIM for CBZ and 2%wt.Pt-MCM-22-100-EIM for DCF).

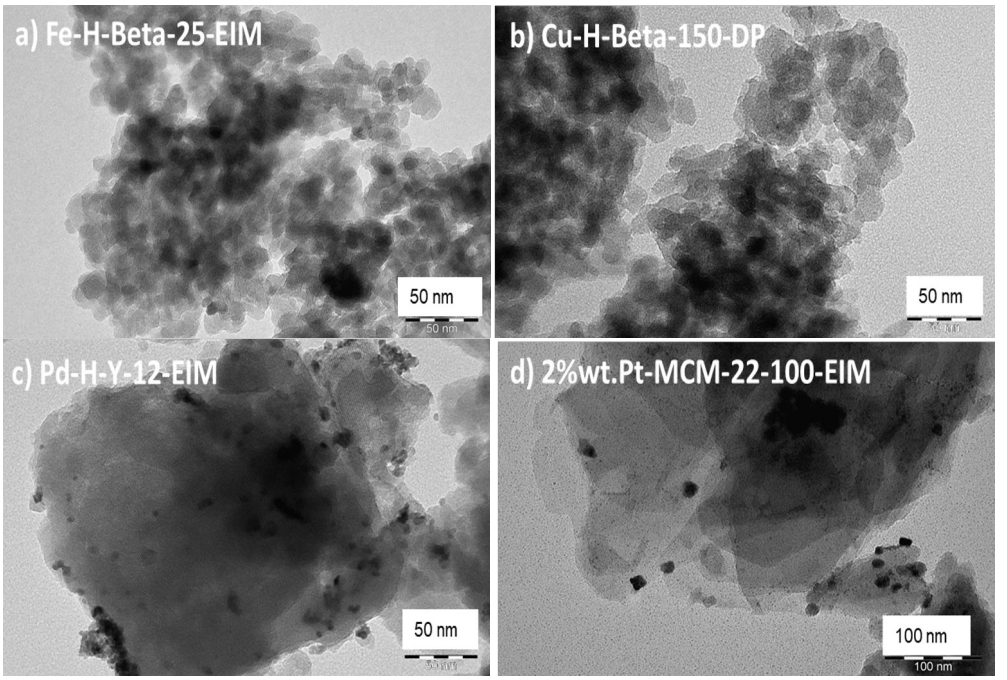

Fig.7. Transmission electron micrographs of Fe- H-Beta-25-EIM (a), Cu-H-Beta-150-DP (b), Pd-H-Y-12-EIM (c) and 2%wt-MCM-22-100-EIM (d) catalysts.

3.1.3. Scanning electron microscopy (SEM) and energy dispersive X-ray microanalyses (SEM/EDXA)

SEM was used to study the morphology, the crystal shape, size and crystal distribution of the applied catalysts. The smallest and largest crystallite sizes of H-Beta-25, Fe-H-Beta-25-EIM and Fe- H-Beta-150-SSIE were (79.83, 232.8), (71.55, 468.0), (69.89, 355.4) nm, respectively. Uniform and regular spherical particles of diverse sizes are visible in the SEM micrographs. The SEM of utilized catalysts are presented in Publications (**I, II, III, V**). The SEM images of spent and regenerated zeolites confirm that they did not undergo any morphological changes during the degradation of IBU or during the regeneration of the spent catalyst **(I).**

The average crystals sizes of most of the studied catalysts were calculated and are given in Table 3. The largest average crystal size (493 nm) was measured for the Pt-H-Y-12-IE (Table 3), while the smallest crystal size (76.08 nm) was measured for the Cu-H-Beta-25-IE catalyst.

Furthermore, the crystal size distributions for the H-MCM-22, metal modified H-Beta, H-MCM, H-Y and γ-Al_2O_3 (UOP) catalysts were determined to 100-800 nm and 300-800 nm, respectively. The explanation for the variations in the crystal sizes for the synthesized catalysts are the structures of the support e.g. H-Beta, H-Y and MCM-41 mesoporous materials. Furthermore, the methods of the Fe-, Cu-, Pt-, Ru-, Pd-, Cu- introduction and the synthesis conditions can influence the average crystal size.

It is noteworthy to mention that modifications of pristine H-MCM-22 and H-Y zeolite catalysts with Pt- did not influence the parent structures, (Figure 5 publication **V**). The SEM image of most efficient catalysts applied in the removal of pharmaceuticals are given in Figure 8 (Fe-H-Beta-25-EIM, Cu-H-Beta-150-DP for IBU, Pd-H-Y-12-EIM for CBZ and 2%wt.Pt-MCM-22-100-EIM for DCF).

The metal contents (Pt, Pd, Cu and Fe) in the metal modified catalysts were determined using energy dispersive X-ray micro-analyses (Table 3). The iron concentrations of fresh (catalyst synthesized prior to use), spent (catalyst used in the reaction) and regenerated (after calcination of spent catalyst for 2 h at 400 ˚C) Fe-H-Beta-25-EIM and Fe- H-Beta-150-SSIE were 6.05%, 4.84%, 3.11%; 2.99%, 2.5%, 1.94%, respectively. The largest amount of Cu was obtained for Cu-H-Beta-150-EIM catalyst while the lowest amount of Cu was obtained for the Cu-H-Beta-25-IE catalyst. The highest amount of Pt were found for the Pt-MCM-41-IS and Pt-γ-Al_2O_3 (UOP)-IMP catalysts around 7.13 wt% was measured. The smallest amount of Pt (0.63%wt), was measured for 1%wt Pt-H-MCM-22-100-EIM catalyst.

The differences in the loadings of metal (Pt, Pd, Cu and Fe) in H-Beta, H-MCM-22-100, H-Y-12, SiO_2, Na-Modernite and γ-Al_2O_3 catalysts were attributed to the methods of catalysts synthesis, structure of supports and SiO_2/Al_2O_3 ratios of zeolites.

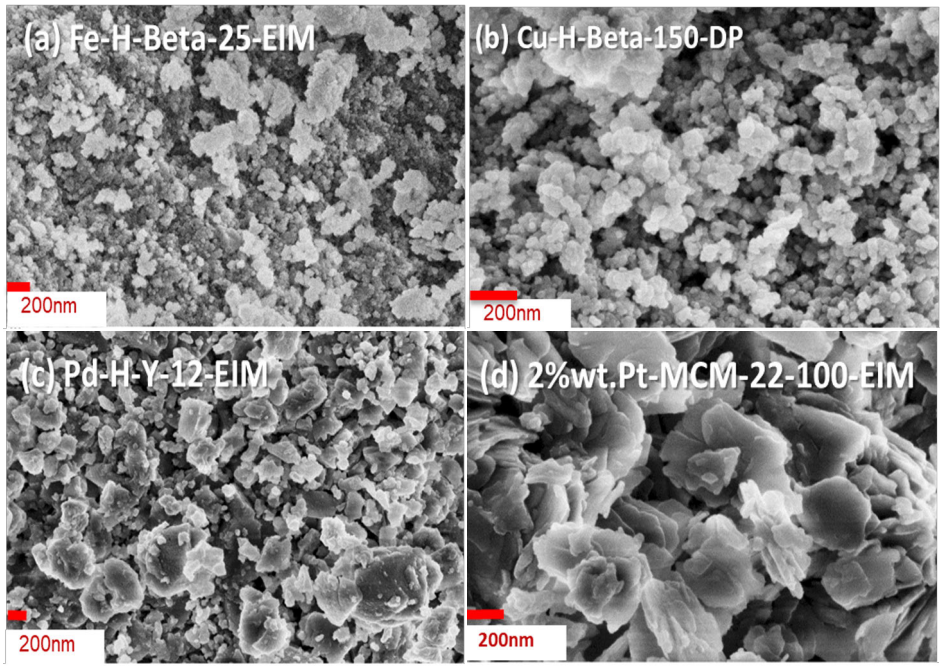

Fig.8. Scanning electron micrographs of Fe- H-Beta-25-EIM (a), Cu-H-Beta-150-DP (b), Pd-H-Y-12-EIM (c) and 2%wt-MCM-22-100-EIM (d) catalysts.

Table 3. Average metal (Fe-, Cu-, Pd-, Pt-, Ni-, Ru-) particle size, average crystal size and metal concentration of catalysts applied in the experiments.

Catalyst	Average metal particle size (nm)	Average crystal size (nm)	Metal concentration (wt %)
H-Beta-25 **(I)**	-	-	-
Fe-H-Beta-25-EIM **(I)**	21.28	-	6.05
Fe-H-Beta-150-SSIE **(I)**	16.72	-	2.99
Cu-H-Beta-25-IE **(II)**	6.42	76.08	1.13
Cu-H-Beta-150-IE **(II)**	8.13	88.142	1.34
Cu-H-Beat-300-IE **(II)**	11.49	290.42	0.53
Cu-H-Beta-150-EIM **(II)**	9.22	126.05	7.34
Cu-H-Beta-150-DP **(II)**	4.88	80.87	6.19
Cu-Na-Modernite-12.8-IE **(II)**	5.56	369.51	3.93
Pd-H-MCM-41-EIM **(II)**	6.31	155.70	2.23
Fe-SiO2-DP **(II)**	5.86	134.59	6.52
Ni-H-Beta-25-EIM **(II)**	11.61	97.07	10.31
Pt-MCM-41-IS **(III)**	13.39	219.23	7.12
Ru-MCM-41-IS **(III)**	13.29	202.39	1.55
Pd-H-Y-12-EIM **(III)**	6.47	257.12	5.34
Pt-H-Y-12-EIM **(III)**	5.72	119.62	1.67
Pd-H-Beta-300-EIM **(III)**	6.11	272.45	1.95
Cu-MCM-41-A-EIM **(III)**	7.82	88.23	3.46
H-MCM-22-100 **(V)**	-	386.20	-
1%wt.Pt-MCM-22-100-EIM **(V)**	24.9	169.67	0.63
2%wt.Pt-MCM-22-100-EIM **(V)**	8.1	193.51	1.60
5%wt.Pt-MCM-22-100-EIM **(V)**	2.7	396.79	6.81
Pt-H-Y-12-IE **(V)**	30.6	493.96	3.65
Pt-γ-Al_2O_3 (UOP)-IMP **(V)**	9.5	116.16	7.13

3.1.4. FTIR spectroscopy: pyridine adsorption-desorption

The amount of Brønsted and Lewis acid sites of the proton form and metal modified catalysts were determined by FTIR using pyridine as a probe molecule. The acidities of the catalysts used in this work are summarized in (Table 4). The concentration of Brønsted sites at 1545 cm^{-1} and Lewis sites at 1450 cm^{-1} acid sites were measured with FTIR using pyridine as a probe molecule. At 250-350˚C, pyridine desorption demonstrated weak, medium and strong sites, whereas at 350-450 ˚C it exhibited medium and strong sites and finally at 450˚C, strong sites prevail. The Brønsted acidity increases with increasing alumina content [105][106]. Following that, the data of the determination were converted into concentrations using the extinction coefficients of Emeis [107]. The large amount of Brønsted acid sites was determined for the pure H-Beta-25 zeolite catalyst. It was observed that the amount strong Brønsted and Lewis acid sites (450 ^{0}C) decreased substantially for the Fe-H-Beta-25-EIM and Fe-H-Beta-150-SSIE as compared to the pristine H-Beta-25 catalyst. [108].

The Cu- modified Cu-H-Beta-25-IE, Cu-H-Beta-150-IE and Cu-H-Beta-300-IE catalysts exhibited a decrease of the Brønsted and Lewis acid sites as compared to the pristine H-Beta-25 catalyst. The plausible explanation for the decrease in the Brønsted and Lewis acid sites in the Cu- modified H-Beta-25, Cu-H-Beta-150 and Cu-H-Beta-300 is the substitution of these sites by CuO. The largest decrease in the Brønsted and Lewis acid sites were obtained for the Cu-H-Beta-300-IE catalyst. The lowest amount of tetrahedra Al (IV) present in the H-Beta-300 is the reason for such a low amount of Bronsted and Lewis acid sites. The details of the characterization of the acid sites in H-Beta-25, H-Beta-150 and H-Beta-300 using FTIR-Pyridine and AlNMR are given in ref [109].

It was noticed that Pd-H-Y-EIM showed the presence of the largest Brønsted acidity (237 μmol/g) at 250˚C compared to other catalyst, the zeolite catalyst with the lowest SiO_2/Al_2O_3 ratio 12, the lower amount of Brønsted acid cites is attributed to the high SiO_2/Al_2O_3 ratio 100. It is noteworthy to mention that, the H-MCM-22 zeolite catalyst exhibited much lower amount of Brønsted acid sites (33 μmol/g). The Pt-modified H-MCM-22 i.e. 1%wt.Pt-MCM-22-100-EIM, 2%wt.Pt-MCM-22-100-EIM and 5%wt.Pt-MCM-22-100-EIM catalysts, exhibited an increase of the Brønsted acid sites, the enhancement is attributed to the presence of Pt in the structure of MCM-22. The Pt-γ-Al_2O_3 (UOP)-IMP catalyst exhibited the lowest amount of Brønsted acid sites, which is attributed to the lower amount of acid sites in γ-Al_2O_3 support.

Table 4. Brønsted and Lewis acidities of the proton and metal modified catalysts applied in the experiments.

Catalyst	Brønsted acidity (μmol/g)			Lewis acidity (μmol/g)		
	250°C	**350 °C**	**450 °C**	**250°C**	**350 °C**	**450 °C**
H-Beta-25 (I)	219	187	125	82	43	25
Fe-H-Beta-25-EIM (I)	216	168	17	95	36	5
Fe-H-Beta-150-SSIE (I)	193	137	45	119	41	4
Cu-H-Beta-25-IE (II)	136	211	67	180	35	3
Cu-H-Beta-150-IE (II)	153	170	113	179	46	2
Cu-H-Beat-300-IE (II)	37	41	2	74	27	2
Cu-H-Beta-150-EIM (II)	153	170	113	179	46	2
Cu-H-Beta-150-DP (II)	_	_	_	_	_	_
Cu-Na-Modernite-12.8-IE (II)	_	_	_	_	_	_
Pd-H-MCM-41-EIM (II)	_	_	_	_	_	_
Fe-SiO2-DP (II)	_	_	_	_	_	_
Ni-H-Beta-25-EIM (II)	_	_	_	_	_	_
Pt-MCM-41-IS (III)	7	2	0	1	1	0
Ru-MCM-41-IS (III)	18	0	0	9	0	0
Pd-H-Y-12-EIM (III)	237	24	0	52	6	0
Pt-H-Y-12-EIM (III)	96	28	0	3	13	0
Pd-H-Beta-300-EIM (III)	58	18	0	9	7	0
Cu-MCM-41-A-EIM (III)	44	10	0	56	9	0
H-MCM-22-100 (V)	33	67	20	13	1	0
1%wt.Pt-MCM-22-100-EIM (V)	111	4	0	3	0	0
2%wt.Pt-MCM-22-100-EIM (V)	86	3	0	5	0	0
5%wt.Pt-MCM-22-100-EIM (V)	62	0	2	10	1	1
Pt-H-Y-12-IE (V)	145	6	0	11	3	0
Pt-γ-Al_2O_3 (UOP)-IMP (V)	6	3	1	12	39	2

3.1.5. X-ray powder diffraction (XRD)

X-ray powder diffraction was utilized to determine the phase purities and structures of the H-MCM-22-100, 1%wt.Pt-MCM-22-100-EIM, 2%wt.Pt-MCM-22-100-EIM, 5%wt.Pt-MCM-22-100-EIM, Pt-H-Y-12-IE and Pt-γ-Al_2O_3 (UOP)-IMP catalysts. The measured XRD patterns of the MCM-22-100 samples are shown in Fig. 9a and 9b. The reference pattern fitted to the data is a zeolite structure with the MWW framework according to the IUPAC nomenclature [110]. The 2%wt. and 5%wt. Pt samples were phase pure. The detection limit for the impurities is around 1 vol.-% when the reference pattern fits the data well, like in this case. The 1 wt.-% Pt sample has a hint of Si phase visible. The sample without Pt has extra peaks possibly originating from a different type of framework. Estimating from the relative peak intensity, the impurity phase is about 10-20 vol.-%. The results are collected in Table 5. The lattice parameters given in the table were obtained from the Rietveld refinements and the crystal sizes were estimated from the FWHMs of the (102) peaks using the Scherrer equation after correcting the FWHMs for the instrument resolution. The agreement between the fits and the measured XRD data is good in the MCM-22-100 sample series. Thus, the phase identification and the lattice parameters can be given with a high degree of certainty. The impurities in the H-MCM-22-100 sample could have two different sources: one is a large unit cell structure visible as peaks at the low angles and the other is a small unit cell structure visible as a shoulder in the peak at 26° and as a separate peak at 49.5°. The latter peaks do not match with Al, Si or Al_2O_3.

The measured XRD pattern of the Pt-H-Y-12-IE sample is shown in Fig. 9c. The reference pattern fitted to the data is a zeolite structure with the Faujasite (FAU) framework [111]. In addition to the FAU framework, the Pt-H-Y-12-IE sample shows a Pt phase. A face centered cubic symmetry (fcc) structure was used to fit the Pt phase. The fit results are collected in Table 5. The lattice parameters given in the table were obtained from the Rietveld refinements and the crystal sizes were estimated from the FWHMs of the (331) peak for FAU and of the (111) peak for Pt phase using the Scherrer equation after correcting the FWHMs for the instrument resolution.

The measured XRD pattern of the Pt-γ-Al_2O_3 (UOP)-IMP sample is displayed in Fig. 9d. The pattern shows broad smooth features which contain multiple peaks smeared by the Scherrer broadening into a single large peak. The data were Rietveld refined using a tetragonal unit cell [112]. The fit results are collected in Table 5. The lattice parameters and the crystal sizes given in the table for the Pt-γ-Al_2O_3 (UOP)-IMP sample were obtained from the Rietveld refinements.

The majority phase in all the four types of MCM-22 zeolite catalysts were MWW. There were some impurities present in the catalysts, which were visable as SiO_2 domains in the synthesized MCM-22 zeolite. The presence of SiO_2 phase in the MCM-22 catalysts were attributed to the unreacted source of silica. It is noteworthy to mention that some of the peaks appearing, which were not identified as SiO_2, Al_2O_3 can be attributed to the PtO_2 oxide phase. The three Pt-modified catalysts 1%wt.Pt-MCM-22-100-EIM, 2%wt.Pt-MCM-22-100-EIM and 5%wt.Pt-MCM-22-100-EIM, peaks present as PtO_2 should be observed. However, due to small amount of Pt in 1%wt.Pt-MCM-22-100-EIM and 2%wt.Pt-MCM-22-100-EIM, PtO_2 phase was not

visible. A further explanation for the absence of the PtO_2 phase could be nano size of $PtO_2 < 3$ nm which are not detected by X-ray powder diffractometer.

The agreement between the fits and the measured XRD data is reasonable in both Pt-H-Y-12-IE and Pt-γ-Al_2O_3(UOP)-IMP samples. Resolving a small fraction of Pt particles from the γ-Al_2O_3 phase is very challenging because all the Pt peaks, except for a single peak at 80◦, coincide with the γ -Al_2O_3 peaks. To reliably detect small amounts of Pt in γ-Al_2O_3 it would be necessary to compare the Pt-γ-Al_2O_3(UOP)-IMP sample measurement to a clean reference sample of γ-Al_2O_3. Therefore, it was performed as reported in Figure 9d and no significant difference was detected.

Additionally, XRD was used to determine the phase purity and structure of the H-Beta-25, Fe-H-Beta-25-EIM and Fe-H-Beta-150-SSIE zeolite catalysts. The X-ray powder diffraction diagrams of the Fe-H-Beta-25-EIM, Fe-H-Beta-25-SSIE zeolite catalysts exhibited typical patterns to that of pure H-Beta zeolite, indicating that the modification of Beta zeolite with Fe by using the evaporation impregnation and solid state ion-exchange methods in the catalyst preparation did not influence the structure. The X-ray powder diffraction patterns of Fe-H-Beta-25-EIM and Fe-H-Beta-150-SSIE catalysts are displayed in publication (**I**), Fig. 3.

Table 5. The Rietveld refinement results for the H-MCM-22-100, 1% wt.Pt-MCM-22-100-EIM, 2% wt.Pt-MCM-22-100-EIM, 5% wt.Pt-MCM-22-100-EIM Pt-H-Y-12-IE and Pt-γ-Al_2O_3 (UOP)-IMP catalysts.

Sample	phase	Phase fraction (wt.-%)	α (Å)	c (Å)	Crystal size (nm)
H-MCM-22-100	MWW	80-90	14.25	25	29
1% wt.Pt-MCM-22-100-EIM	MWW	96.1	14.27	25	19
	Si	3.9	5.4		
2% wt.Pt-MCM-22-100-EIM	MWW	>99	14.25	25	20
5% wt.Pt-MCM-22-100-EIM	MWW	>99	14.23	25	22
Pt-H-Y-12-IE	FAU	98.4(3)	24.341(1)	-	66
	Pt (fcc)	1.6(3)	3.925(1)		30
Pt-γ-Al_2O_3 (UOP)-IMP	γ-Al_2O_3	-	5.678(3)	7.866(4)	4.6

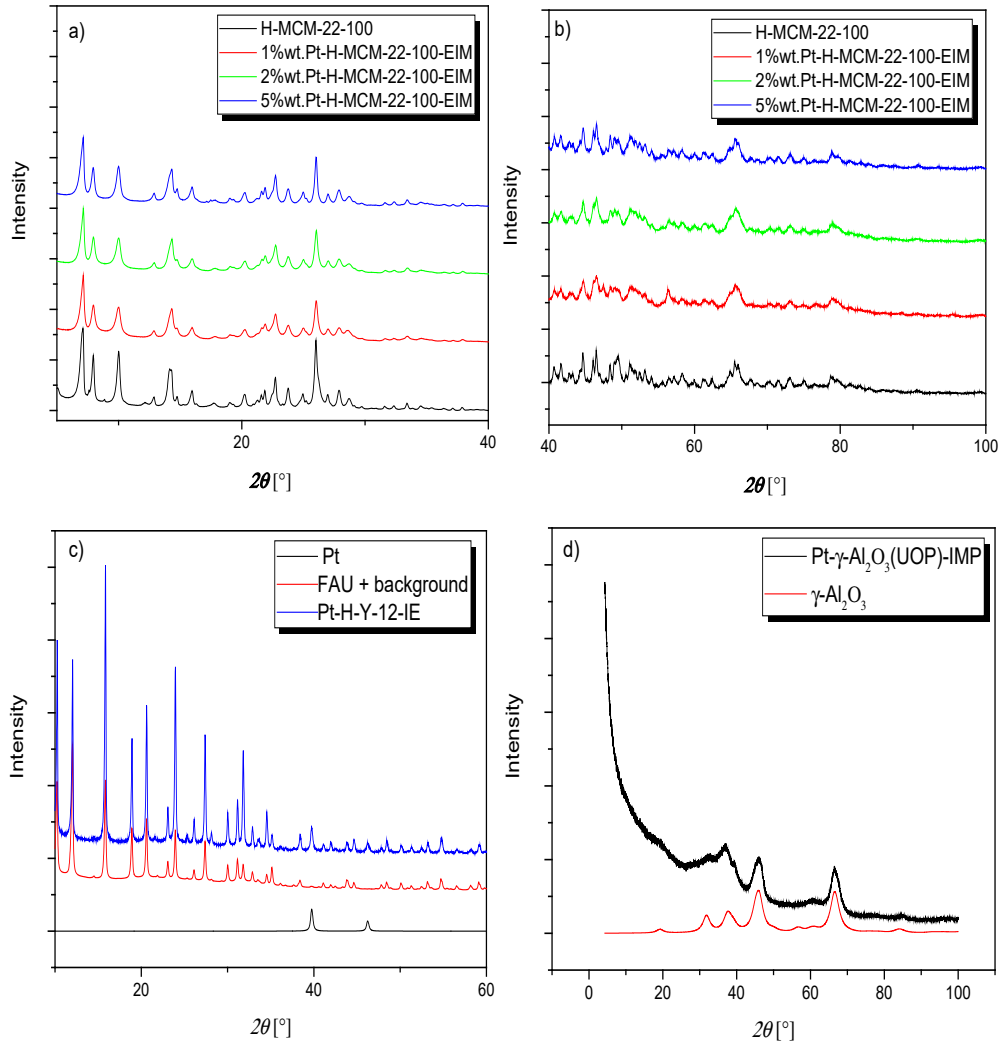

Fig.9. X-ray powder diffraction patterns of H-MCM-22-100 (a, b), 1% wt.Pt-MCM-22-100-EIM (a, b), 2% wt.Pt-MCM-22-100-EIM (a, b), 5% wt.Pt-MCM-22-100-EIM (a, b), Pt-H-Y-12-IE (c) and Pt-γ-Al_2O_3 (UOP)-IMP (d) catalysts.

3.1.6. X-ray photoelectron spectroscopy (XPS)

The surface composition and oxidation state of metals were determined by XPS. The XPS analysis indicated the oxidation states of Pt^0 and PtO on the Pt-MCM-41-IS catalyst. Similarly, the oxidation state of Pt in the Pt-H-Y-12-EIM was measured as Pt and PtO_2. The oxidation states of Ru in Ru-MCM-41-IS was determined as Ru^0 and RuO_2. The oxidation states of Pd in Pd-H-Y-12-EIM and Pd-H-Beta-300-EIM was measured to be Pd^0. The oxidation state of Cu in Cu-MCM-41-A-EIM was confirmed to be Cu^0 and CuO (publication **III**).

The oxidation states of Pt (PtO, PtO_2 and Pt^0) catalysts in 1%wt.Pt-H-MCM-22-100-EIM, 2%wt.Pt-H-MCM-22-100-EIM, 5%wt.Pt-H-MCM-22-100-EIM, Pt-H-Y-12-EIM and Pt-γ-Al_2O_3 (UOP)-EIM catalysts were determined and the presence of PtO, PtO_2 and Pt^0 were observed in all the above Pt-modified catalysts. The binding energies (eV) of the Pt^0 – 71 (eV), PtO – 72 (eV), PtO_2 – 74 (eV) were measured for all the studied Pt- modified catalysts. It was inferred from these binding energies that the Pt modified materials consisted of oxidation states of Pt^0, PtO and PtO_2, on the surface. Similar binding energies for Pt^0, PtO, PtO_2 were reported by J. Z. Shyu *et al.* [113] and R. Bouwman *et al.* [114] (publication **V**). Figure 10 shows the XPS spectrum of 2%wt.Pt-MCM-22-100-EIM catalyst.

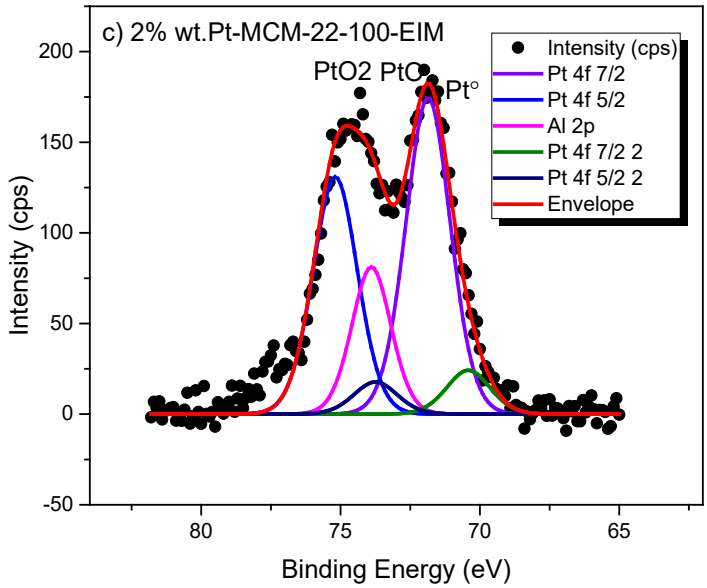

Fig. 10. XPS spectrum of 2%wt.Pt-MCM-22-100 catalyst.

3.2. Primary experiments to increase the amount of dissolved ozone in the aqueous phase

The purpose of the preliminary experiments was to find the optimal conditions to achieve the maximum ozone concentration and the best ozone mass transfer into the liquid phase. Normally, the gas flow into the ozone generator was 500 ml/min (90% oxygen, 10% nitrogen). The ozone concentration in the gas flow was calculated using the iodometric method. The ozone concentration was estimated from equation (1) as shown below [115],

$$\frac{C_{O_3}}{(g/L)} = \frac{24 * \text{volume of thiosulfate (L)} * \text{Normality of thiosulfate}}{\text{inlet volume of gas passed (L)}}$$

For example, for a gas flow of 500 ml/min and 1 minute bubbling, the concentration of ozone in the gas feed to the reactor was calculated accordingly,

$$\frac{24 * 12.5\ \text{mL} * 0.1}{500\text{mL}} = 0.06\left(\frac{\text{g}}{\text{L}}\right)$$

which equals 60 mg/L of ozone in the gas phase.

Concerning the concentration of ozone in the aqueous phase, the DPD method was found out to be inconsistent at different temperatures and values of pH. Therefore, the values obtained with the indigo method were preferred.

3.2.1. Influence of temperature and gas flow velocity on the concentration of dissolved ozone (Indigo method)

The effect of the reaction temperature (5-30˚C) on the ozone solubility was investigated without any reactants present. Figure 11a) illustrates how gas-liquid mass transfer and the solubility of ozone was influenced the different gas flows of 500, 750, 1000 ml/min, at different temperatures using a standard four-blade stirring rod. The experiment reveals that the ozone concentration decreased at higher temperatures in all of the experiments. When decreasing the temperature to 5˚C, the highest ozone concentration was observed, which ranges from approx. 3-6 mg O_3/L at 500-1000 mL/min gas flows. Figure. 11b) illustrates how the solubility of ozone changed at different temperatures (5, 10, 15˚C) and different gas flows. The results reveal that the ozone concentration is increased linearly in higher gas flow rates in all the experiments. In this work, in terms to approach economic feasibility, the gas flows were fixed to 500 ml/min in the subsequent experiments. The ozone concentration did not increase noticeable with a long period ozonation (more than 1hr) under similar conditions. Comparable results have been obtained by J. Leusink [116], who reported that a lower temperature and higher ozone concentration in the inlet gas leads to a higher dissolved ozone concentration.

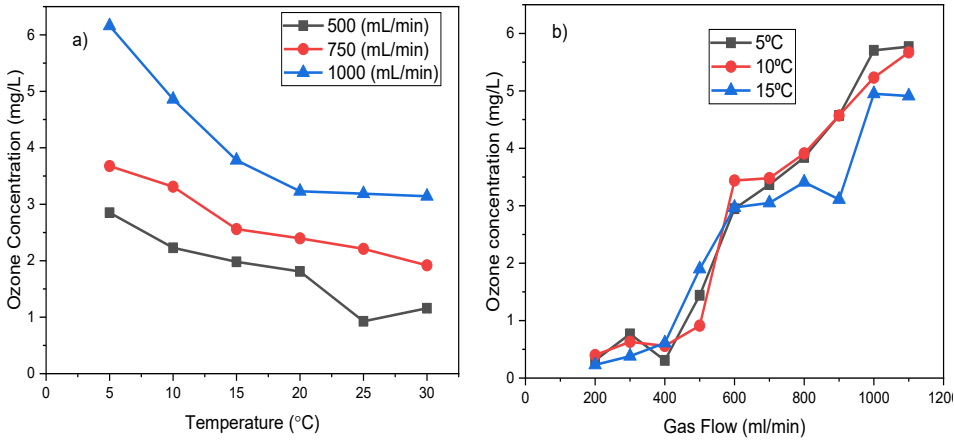

Fig. 11. a) Effect of temperature on the ozone concentration in the aqueous phase. Stirring speed= 1070 rpm, volume=1100ml, ozonation period =60min. b) Effect of the gas flow rate on the ozone concentration in the aqueous phase. Stirring speed= 1070 rpm, volume=1100 ml, ozonation period= 135 min.

3.2.2. Influence of the stirrer on the concentration of dissolved ozone

The effect of different stirrer types on the dissolved ozone concentration was investigated. A normal four-blade stirrer and Spinchem™ rotating bed stirrer were used in these experiments. The comparison in Fig. 12 illustrates that the ozone concentration was significantly higher (40 %) with the Spinchem stirrer, i.e. 4.15 mg/L at maximum 1070 rpm vs 2.95 mg/L. Therefore, the Spinchem stirrer was used in subsequent experiments. These experiments also confirmed that the stirring speed did not influence significantly the ozone concentration within the range of 450-1070 rpm. It is evident as also reported by Jenkins [117] that the stirring speed has a minor effect on the ozone decomposition in the reactor. The experiments demonstrated that only a small increase in the dissolved ozone concentration was achieved within the normal stirring speed range of 400-900 rpm.

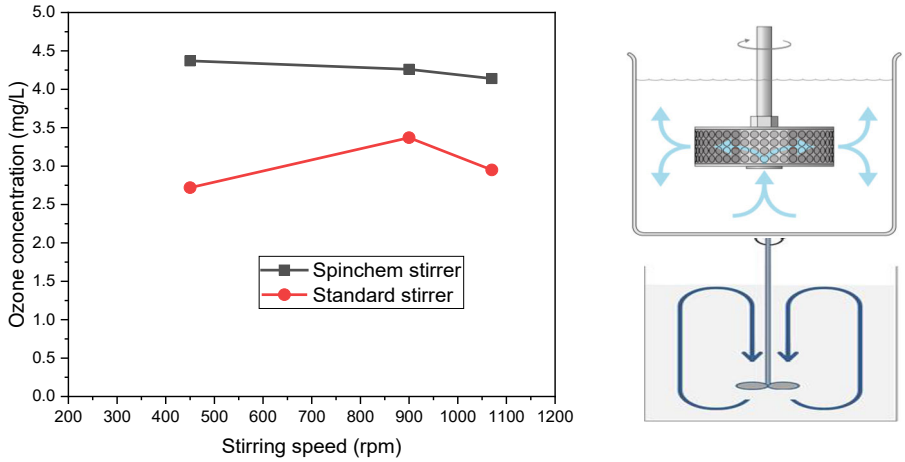

Fig. 12. Effect of stirring type and stirring speed on the ozone concentration in the aqueous phase. T=5˚C, volume=1100ml, gas flow= 500ml/min, ozonation period= 60min, stirring speeds 450, 900 and 1070 rpm.

3.2.3. Dissolved ozone model

In ozonation treatments, the amount of ozone required and the determination of optimal ozone concentration is an important subject, since wrong dosage amounts of ozone can lead to inadequate degradation, produce harmful by-products, or cause unnecessary costs [118].The dissolved ozone data were used to determine numerical values of dissolved ozone concentration in deionized water. The experimental conditions are reported in Table 6, a long with the experimental results. The obtained results are also given in the form of a surface plot in Figure 12. The experimental data were fitted with a 2-D power law, according to Eq. 1,

$$C_{O_3^*} = 6.74 - 0.044T + 7.32 \cdot 10^{-5}T^2 - 2340Q + 3.17 \cdot 10^8 Q^2 \qquad (1)$$

The result of the data fit gave a degree of explanation R^2=0.96, which is satisfactory.

Table 6. Experimental conditions imposed to conduct the ozone saturation experiments, together with the related experimental results. Q_1=8.33·10^{-6}m^3/s, Q_2=1.25·10^{-5}m^3/s, Q_3=1.67·10^{-5}m^3/s.

Experiment	T [K]	$cO_3^*(Q_1)$ [mol/m^3]	$cO_3^*(Q_2)$ [mol/m^3]	$cO_3^*(Q_3)$ [mol/m^3]
1	303.15	2.41·10^{-2}	4.00·10^{-2}	6.54·10^{-2}
2	298.15	1.93·10^{-2}	4.61·10^{-2}	6.64·10^{-2}
3	293.15	3.77·10^{-2}	4.99·10^{-2}	6.73·10^{-2}
4	288.15	4.13·10^{-2}	5.34·10^{-2}	7.88·10^{-2}
5	283.15	4.65·10^{-2}	6.90·10^{-2}	1.01·10^{-1}
6	278.15	5.94·10^{-2}	7.66·10^{-2}	1.28·10^{-1}

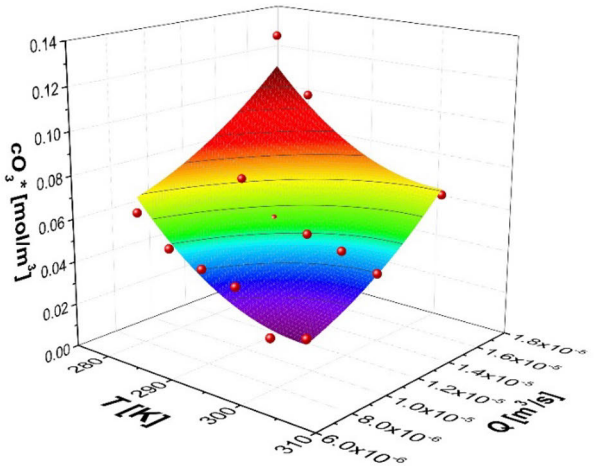

Fig. 12. Concentration of dissolved ozone as a function of temperature and gas flow-rate: experimental data and modelling results.

3.3. Removal of ibuprofen by catalytic and non-catalytic ozonation

3.3.1. Non-catalytic degradation of ibuprofen

The degradation of ibuprofen at several inlet gas flow rates, temperatures, position of the stirrer, initial IBU concentration, IBU type (native or salt), pH and nitrogen inlet gas flow was investigated. The decomposition rate of IBU increases with higher inlet gas flow rates until 500 ml/min. However, there is hardly any difference between 500 ml/min and 1000 ml/min. Probably 500 ml/min gas flow rate seems to be enough for IBU degradation. Therefore, higher flow rates were not used in later experiments, in order to avoid unnecessary consumption of oxygen (Fig. 13 a).

The formation of various kinds of radicals is highly influenced by the pH of the aqueous solution. By a constant addition of NaOH, the pH level of the reactant solution can be maintained at a desired level. Therefore, it can be concluded that ozone and NaOH react together, probably forming radicals and other components, i.e. molecular oxygen, which is indicated by the consumption of alkaline. The effect of pH on the chain reaction of ozone in the initial step is presented and herein, hydroxide ions and ozone reaction produce a superoxide anion $O_2^{\bullet -}$ and a hydroxyl radical $HO_2^{\bullet}$.

$$O_3 + OH^- \rightarrow O_2^{\bullet -} + HO_2^{\bullet} \qquad k_1 = 70\ 1/M\ 1/s \qquad [81]$$

This means that ozone decomposes by the hydroxide ion, which acts as a catalyst towards the decomposition. In the second step, ozone dissociates in the presence of $HO_2^{\bullet}$ and $O_2^{\bullet -}$. A further chain reaction produces $O_3^{\bullet -}$ and $HO_3^{\bullet}$ which results the formation of $HO^{\bullet}$. These radicals could react with organic compounds and ozone itself [81]:

$O_3 + O_2^{\bullet -} \rightarrow O_3^{\bullet -} + O_2$ $k_2 = 1.6 \times 10^9$ 1/M 1/s [81]

$HO_3^{\bullet} \leftrightarrow O_3^{\bullet -} + H^+$ $pK_a = 6.2$ [81]

$HO_3^{\bullet} \rightarrow OH^{\bullet} + O_2$ $k_3 = 1.1 \times 10^5$ 1/M 1/s [81]

Without controlling the pH, the pH level of the reaction medium tends to decrease rapidly to approximately pH=3, independent of any reactant is present or not. Figure 13b illustrates that the decomposition rate of IBU dramatically decreases at higher pH. The reason for the decrease of pH can probably be the formation of small amounts of nitric acid in the ozonation.

The formation of nitric acid is possible if the feed gas contains nitrogen and minor amounts of moisture is present in the ozonator. Nitric acid was plausibly identified (same retention time as HNO_3) as a growing peak in the standard HPLC analysis when using 10 % N_2 in the feed gas. Probably, the N_2 gas in the line contains some minor humidity, which could accumulate over a prolonged time. However, comparative experiments were carried out with either pure oxygen feed gas or including 10% nitrogen to the feed, and the results ruled out that the small amounts of nitric acid could influence the kinetics of the degradation of IBU. On the other hand, Quero-Pastor reported that the optimum IBU degradation rate by ozonation was obtained at an initial pH of 9 [119]. In that study, only the initial pH was applied, whereas in our study, the pH was kept constantly at the desired level, which could explain the differences in the results.

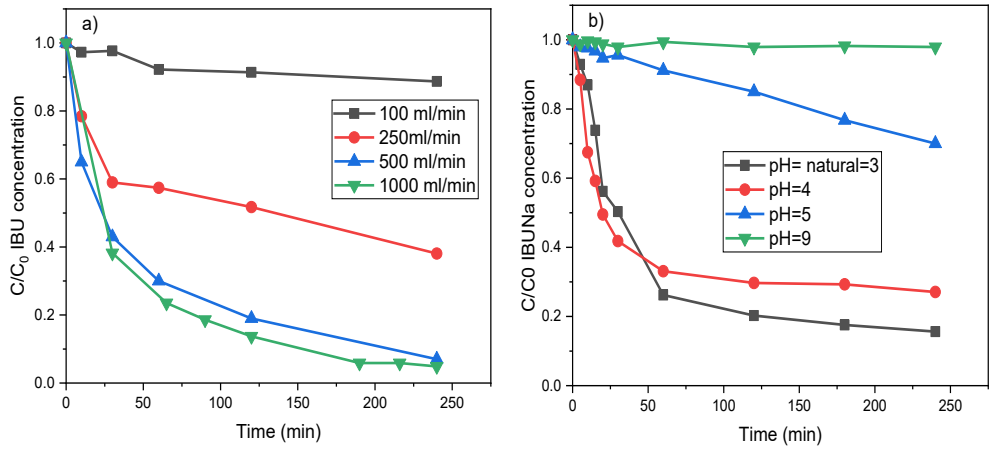

Fig. 13. a) The degradation of IBU by ozonation at different inlet gas flow rates. Initial concentration of IBU=10 mg/L, T= 25˚C, stirring speed= 1070 rpm, volume=1000ml. b) The degradation of IBUNa at different pH by ozonation. [IBU Na]=10 mg/L, gas flow rate= 500 ml/min, T= 5˚C, stirring speed= 1070 rpm, volume=1000 ml.

The decomposition rate of IBU was most prominent during the first two hours, after which there is only a minor difference in the experiments conducted at different temperatures. IBU was not degraded quantitatively in the experiments, which indicates that the reaction order is 1 or higher with respect to IBU. The Spinchem™ stirrer was placed at different vertical levels of the reactor and the IBU concentration was investigated as a function of the reaction time.

The results revealed that as the stirrer was placed at the lowest level of the reactor, IBU was decomposed at the highest rate. This is due to the fact that a better mass transfer was obtained when the stirrer was placed at as low level as possible, above the gas disperser due to fact that gas bubbles are forced through the Spinchem™ rotating bed, and further dispersed to smaller bubbles, and moreover, the residence times of the bubbles are prolonged.

The effect of the initial IBU concentration ranging between 10-30 mg/L was investigated. Normalizing experimental the data to dimensionless concentrations was helpful as it allows the experiments conducted with different initial concentrations of IBU to be compared in the same plot. The results showed that the experiments with different initial concentrations of IBU overlap, which indicates first order kinetics with respect to IBU. On the other hand, the IBU concentration tends to remain on a plateau level at higher reaction times, which indicates a somewhat higher reaction order as the reaction progresses. Aziz *et.al.* have reported similar kinetics for the degradation of IBU by direct ozonation [75]. The degradation rates of IBU and the sodium salt of IBU were measured and compared. IBU cannot be easily dissolved in water. In this research, ethanol was used for to dissolve IBU in water, but the solubility of the IBU sodium salt (IBUNa) is thousand-fold higher in water than the solubility of normal IBU, which enabled us to perform experiments with much larger initial reactant concentrations. IBUNa reacted somewhat slower than IBU. A summary of the kinetic experiments is provided in Table 7.

Table 7. Experimental conditions adopted to conduct the IBU ozonation experiments.

Experiment	$c_{IBU,0}$ **[mg/L]**	T **[°C]**	v **[rpm]**	V_L **[ml]**	Q **[ml/min]**	**Stirrer level [mm]**
1	10	5	1070	1000	500	250
2	10	15	1070	1000	500	250
3	10	20	1070	1000	500	250
4	10	25	1070	1000	500	250
5	10	30	1070	1000	500	250
6	10	5	1070	1100	500	250
7	20	5	1070	1100	500	250
8	30	5	1070	1100	500	250
9	10	5	1070	1100	500	500
10	10	5	1070	1100	500	750
11	10	25	1070	1000	100	250
12	10	25	1070	1000	250	250
13	10	25	1070	1000	1000	250

Experiment 1-8 were conducted within the kinetic regime, while experiments 9-13 were influenced by gas-liquid mass transfer. The first model was developed to determine was based on Eq (2), which was coupled to the mass balance equation (3).

$$r_{IBU} = k_{IBU} c_{O_3} c_{IBU} \tag{2}$$

$$\frac{dc_{IBU}}{dt} = -r_{IBU} \tag{3}$$

The concentration of ozone in the liquid phase was calculated assuming that ozone dissolves and diffuses in the gas-liquid film. At steady-state model for ozone is given by Eq. 4. By replacing the molar flux term and the rate equation, it is possible to obtain Eq. 5. The gas-liquid surface area was calculated from the definition, Eq. 6. The ozone concentration in the liquid phase is solved from Eq (6) giving Eq. 7.

$$N_{O_3} A + r_{O_3} V_L = 0 \tag{4}$$

$$k_L (c_{O_3 *} - c_{O_3}) A = k_{O_3} c_{O_3} V_L \tag{5}$$

$$k_L a_{sp} (c_{O_3 *} - c_{O_3}) = k_{O_3} c_{O_3} \tag{6}$$

$$c_{O_3} = \frac{c_{O_3 *}}{1 + \frac{k_{O_3}}{k_L a_{sp}}} \tag{7}$$

When kinetic regime prevails in the reaction system $k_{O3} << k_L a_{sp}$ and C_{O_3} coincides with $C_{O_3^*}$, the saturation concentration.

Experiments 1-8 were analyzed by assuming a very high value for $k_L a_{sp}$, thus it was possible to estimate the k_1 and k_{O3} values at different temperatures, assuming a modified Arrhenius law, Ea. 8.

$$k_j = k_{j,ref} \exp\left[-\frac{Ea_j}{R_g} \left(\frac{1}{T} - \frac{1}{T_{ref}} \right) \right], T_{ref} = 293K \tag{8}$$

The basic experimental data showed a double-sloped trend. The first one, that could be described by first order reaction kinetics referred to IBU, and the second one characterized by a lower slope. The experts in the analysis indicated that the data related to the second part are more uncertain, so it was decided to only use the experimental data collected at reaction times lower than 60min. Table 8 gives the parameter estimation output with statistical information.

Table 8. Parameter estimation output with statistic information.

Parameter	**Value± 95%C.I.**	***M***	$k_{IBU,ref}$	Ea_{IBU}	$k_{O3,ref}$	Ea_{O3}
$k_{IBU,ref}$ [m³/(mol·s)]	0.023±0.006	$k_{IBU,ref}$	1			
Ea_{IBU} [J/mol]	7391±125	Ea_{IBU}	0.19	1		
$k_{O3,ref}$ [1/s]	0.057±0.003	$k_{O3,ref}$	0.66	-0.51	1	
Ea_{O3} [J/mol]	2162±258	Ea_{O3}	-0.64	0.57	-0.97	1

As revealed, only the ozone reactivity parameters show a mutual correlation, for example the correlation between Ea_{o3} and K_{O3ref} is high.The confidence intervals are rather small. The experiments 9-13 were interpreted by fixing the kinetic parameters reported in Table 7, by fitting each experiment the gas-liquid mass-transfer parameter. The results are reported in Figure 14.

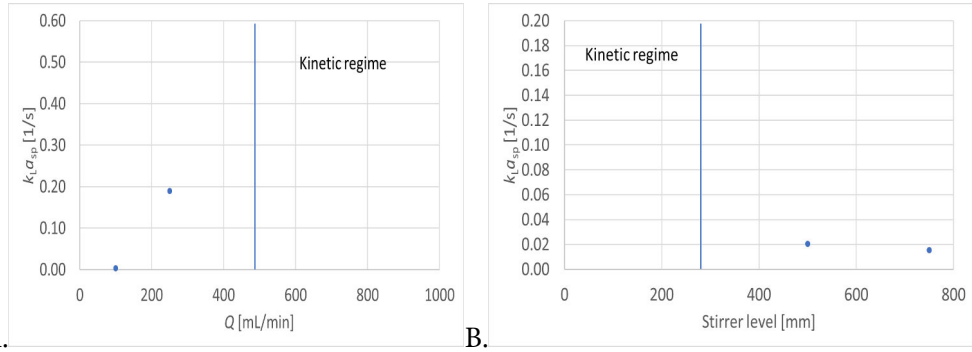

Fig. 14. The trend of the gas-liquid mass transfer coefficient trend with: A. gas flow-rate; B. stirrer level.

As revealed, Figure 14A show that the k_La_{sp} values increase with the gas flow-rate, while Figure 14B indicates that the best stirrer level is 250 mm.

3.3.2. Non-catalytic degradation of ibuprofen and by-product distribution

Fig. 15 shows the effect of the nitrogen inlet gas flow and temperature on the removal of IBU. Among these experiments, 2.5 ml/min nitrogen shows the highest decomposition rate compared to the experiments carried out without nitrogen and 50 ml/min nitrogen. A slightly higher decomposition rate was observed at 20˚C compared to 5˚C under these conditions. The dissolved ozone concentration at 20˚C, using 450 ml/min and 2.5 ml/min nitrogen was 8.32 mg/l, determined with the indigo method (in these experiments the ozonator had been repaired and therefore produced higher ozone concentration compared to aforementioned experiments).

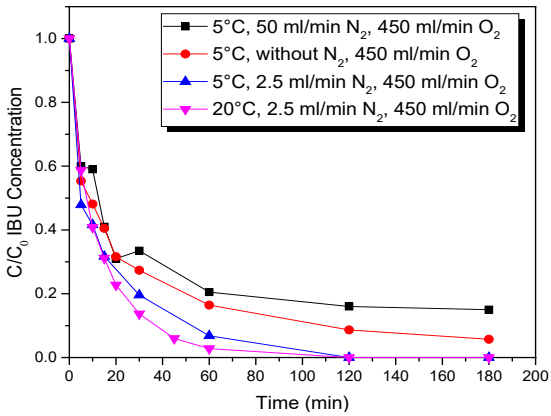

Fig. 15. The degradation of IBU by ozonation without a catalyst. [IBU]=10mg/L, gas flow rate= 450-500 ml/min, T= 20, 5˚C, stirring speed= 1070 rpm.

The degradation of IBU and diclofenac in water by ozonation alone, and in combination of photocatalysis with ozonation has been studied by H. Aziz et al [75], who suggested that ozonation alone contributes to a high energy yield, however, it gives low mineralization of pharmaceuticals. On the other hand, the combination of photocatalysis with ozonation provides a high degradation rate and mineralization for IBU.

3.3.3. Quantification of ibuprofen oxidation products

For the quantification of the transformed by-products of the ozonation and catalytic ozonation process, an analysis method was created. The commonly detected by-products in the ozonation of IBU, namely: 1-OH-IBU, 2-OH-IBU, α-OH-IBU, APMP, and 1-OXO-IBU were determined. The main by-product in all the experiments was 1-OXO-IBU, it was reached to maximum concentration (150 and 330 μg/L) at 60 minutes, after which the concentration began to decrease (Figure 16). The 1-3 % of IBU was converted into 1-OXO-IBU. The two main isomers of OH-IBU, 1-OH-IBU, and 2-OH-IBU, were transformed concurrently. Likewise, between 0.3 and 0.6 % of IBU was transformed into 1-OH-IBU, between 0.2 and 0.5 % of IBU was formed into 2-OH-IBU and up to 0.1 % of IBU is transformed into α-OH-IBU. Consequently, the total concentrations of the transformed by-products add up to only a small percentage of the original concentration of IBU. The total amount of by-product estimates for less than 5 % of the transformed IBU. A significant quantity of IBU was likely transformed to smaller, more polar compounds. Based on these results, the transformation pathway for ozonation of IBU is suggested as illustrated in Figure 17. The isomer of OH-IBU that was formed at the largest concentration was 1-OH-IBU which it was oxidized further to 1-OXO-IBU. The hydroxylated IBU products were transformed into diOH-IBU. TP 176, TP178 and TP 192 were presumably formed via carboxylation reactions while TP190 (APMP) might be formed either from TP176 or TP178. IBU was transformed through oxidation and decarboxylation. Oxidation drives to the insertion of hydroxyl groups and the oxidation of hydroxyl groups to ketone groups. Mainly, the hydroxyl groups are added to the aliphatic positions. The decarboxylation reactions drive to the

production of smaller compounds such as carboxylic acids. The analysis indicates that a significant amount of IBU is transformed into products which are not detected by LC-MS, such as small organic acids and carbon dioxide (M. Kråkström).

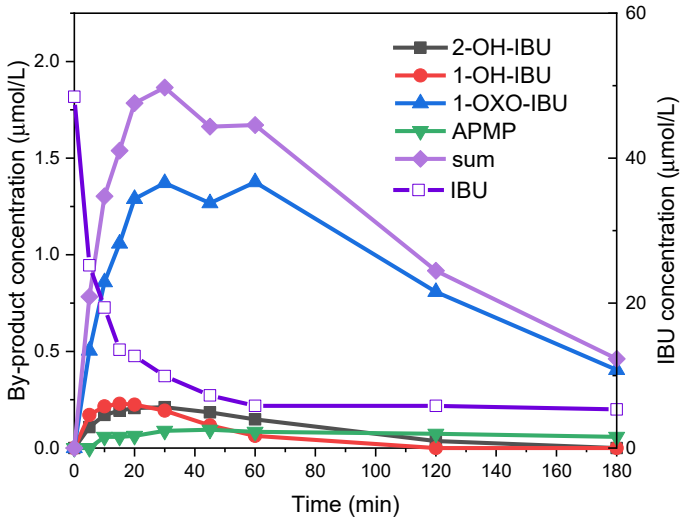

Fig. 16. The ozonation of IBU and the transformation of the main products (M. Kråkström).

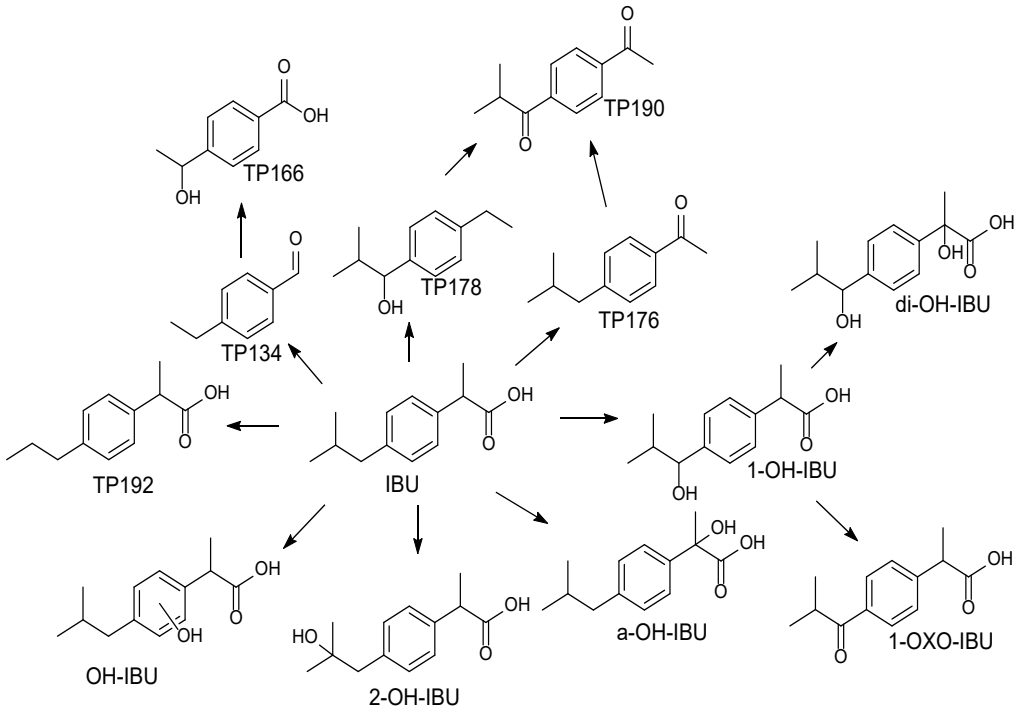

Fig 17. Proposed transformation pathway for IBU ozonation (M. Kråkström).

3.3.4. Kinetic experiments in the absence of heterogeneous catalysts with product distribution

The reaction between ozone and water leads to the formation of two hydroxyl radicals HO° and one oxygen molecule O_2 (initiation). The hydroxyl radical HO° reacts with ozone to form a hydroperoxyl radical HO_2°. The hydroperoxyl radical HO_2° can react with ozone forming a hydroxyl radical HO° (radical reaction). The hydroperoxyl radical HO_2° reacts with each other and forms oxygen and hydrogen peroxide molecule (termination).

$$O_3 + H_2O \xrightarrow{k_i} 2HO^{\circ} + O_2 \qquad \text{(Initiation)}$$

$$O_3 + HO^{\circ} \xrightarrow{k_1} O_2 + HO_2^{\circ} \qquad \text{(Radical reaction)}$$

$$O_3 + HO_2^{\circ} \xrightarrow{k_2} 2O_2 + HO^{\circ} \qquad \text{(Radical reaction)}$$

$$2HO_2^{\circ} \xrightarrow{k_T} 2O_2 + H_2O_2 \qquad \text{(Termination)}$$

From these three reaction steps, we obtain a rate expression for the ozone decomposition:

$$-rO_3 = k_1\,[O_3]\,[HO^{\circ}] + k_2[O_3][HO_2^{\circ}] \tag{9}$$

By assuming a quasi- steady state for the hydroperoxyl radical and the hydroxyl radical concentration, eq. 10 and eq.11 are obtained:

$$\frac{d[HO_2^{\circ}]}{dt} = k_1\,[O_3][HO^{\circ}] - k_2[O_3][HO_2^{\circ}] - k_T[HO_2^{\circ}]^2 \tag{10}$$

$$\frac{d[HO^{\circ}]}{dt} = k_i\,[O_3]\,[H_2O] - k_1[O_3][OH^{\circ}] + k_2[O_3][HO_2^{\circ}] = 0 \tag{11}$$

Because the concentration of water is high and can be approximated constant the Eq.11 is transformed to Eq.13, and the hydroxyl radical concentration can be transformed to Eq.14,

$$k_i' = k_i[H_2O] \tag{12}$$

The quasi-steady state by hypothesis for $[OH^{\circ}]$ gives,

$$k_i'[O_3] + k_2[O_3][HO_2^{\circ}] = k_1[O_3][OH^{\circ}] \tag{13}$$

$$[OH^{\circ}] = (\frac{k_i'}{k_1} + \frac{k_2}{k_1}[HO_2^{\circ}])/[O_3] \tag{14}$$

By applying eq.14 in eq.10, eq.15 is obtained and after some arrangement it is transformed to eqs.16 and 17,

$$k_1\,[O_3]\frac{k_i'}{k_1} - k_1[O_3]\frac{k_2}{k_1}[O_2^{\circ}] - k_2[O_3][HO_2^{\circ}] - k_T[HO_2^{\circ}]^2 = 0 \tag{15}$$

$$k_i'[O_3] + k_2[O_3][HO_2^{\circ}] - k_2[O_3][HO_2^{\circ}] - k_T[HO_2^{\circ}]^2 = 0 \tag{16}$$

$$k_i'[O_3] = k_T[HO_2^{\circ}]^2 \tag{17}$$

From Eq.17, the hydroperoxyl radical concentration is easily obtained,

$$[HO_2^{\circ}] = \left\{\frac{k_i'}{k_T}[O_3]\right\}^{0.5} \tag{18}$$

Combining Eq.18 and Eq.14 gives the concentration of the hydroxyl radicals,

$$[OH^{\circ}] = \frac{k_i'}{k_1} + \frac{k_2}{k_1}\left\{\frac{k_i'}{k_T}[O_3]\right\}^{0.5} \tag{19}$$

Equation 18 and 19 are integrated in Eq.9 giving,

$$-rO_3 = [O_3]\left[\left\{k_1\left(\frac{k_i'}{k_1} + \frac{k_2}{k_1}\left\{\frac{k_i'}{k_T}[O_3]\right\}^{0.5}\right)\right\} + k_2\left\{\frac{k_i'}{k_T}[O_3]\right\}^{0.5}\right] \tag{20}$$

$$= [O_3]\left[k_i' + k_2\left\{\frac{k_i'}{k_T}[O_3]\right\}^{0.5} + k_2\left\{\frac{k_i'}{k_T}[O_3]\right\}^{0.5}\right] \tag{21}$$

$$= [O_3]\left[k_i' + 2k_2\left\{\frac{k_i'}{k_T}[O_3]\right\}^{0.5}\right] \tag{22}$$

which is combined with the mass transfer Eq.6, giving

$$k_l a_{sp}\left(C_{O_3^*} - [O_3]\right) = k_1[O_3]\left[\frac{k_i'}{k_1} + \frac{2k_2}{k_1}\left\{\frac{k_i'}{k_T}[O_3]\right\}^{0.5}\right] \tag{23}$$

The kinetic expressions for the IBU by-products of IBU are given by Eq.24-27

$$IBU + OH^{\circ} \xrightarrow{k_{c1}} 2 - OH - IBU + H^{\circ}$$

$$+r_{2-OH-IBU} = k_{c1}[IBU][OH^{\circ}] = k_{c1}[IBU]\left[\frac{k_i'}{k_1} + \frac{k_2}{k_1}\left\{\frac{k_i'}{k_T}[O_3]\right\}^{0.5}\right] \tag{24}$$

$$IBU + OH^{\circ} \xrightarrow{k_{c2}} 1 - OH - IBU + H^{\circ}$$

$$+r_{1-OH-IBU} = k_{c2}[IBU][OH^{\circ}] = k_{c2}[IBU]\left[\frac{k_i'}{k_1} + \frac{k_2}{k_1}\left\{\frac{k_i'}{k_T}[O_3]\right\}^{0.5}\right] \quad (25)$$

$$1 - OH - IBU \xrightarrow{k_{c3}} 1 - OXO - IBU + H_2$$

$$+r_{1-OXO-IBU} = k_{c3}[1 - OH - IBU] \quad (26)$$

$$IBU \xrightarrow{k_{c4}} APMP$$

$$+r_{APMP} = k_{c4}[IBU] \quad (27)$$

$$K_A = \frac{k_i'}{k_1}$$

$$K_B = \frac{k_2}{k_1}$$

$$K_C = \frac{k_i'}{k_T}$$

These kinetics expressions leads to the expressions for R.

$$R = K_A + K_B(K_C . c_{O_3})^{\frac{1}{2}}$$

IBU and the by-products undergo further decomposition which is included in model (d1, d2, d3, d4). The rate equation are summarized below,

$r_{2-OH-IBU} = k_{c1} . C_{IBU} . R$

$r_{1-OH-IBU} = k_{c2} . C_{IBU} . R$

$r_{OXO} = k_{c3} . C_{1-OH-IBU}$

$r_{APMP} = k_{c4} . C_{IBU}$

$r_{d1} = k_{cd1} . C_{2-OH-IBU}$

$r_{d2} = k_{d2} . C_{1-OH-IBU}$

$r_{d3} = k_{d3} . C_{1-OXO-IBU}$

$r_{d4} = k_{d4} . C_{APMP}$

$r_{d0} = k_{d0} . C_{IBU}$

For IBU and its by-products, the mass balances are written as

$$\frac{dc_{IBU}}{dt} = -r_{2-OH-IBU} - r_{1-OH-IBU} - r_{PMP} - r_{d0}$$

$$\frac{dc_{2-OH-IBU}}{dt} = +r_{2-OH-IBU} - r_{d1}$$

$$\frac{dc_{1-OH-IBU}}{dt} = +r_{1-OH-IBU} - r_{1-OXO-IBU} - r_{d2}$$

$$\frac{dc_{1-OXO-IBU}}{dt} = +r_{1-OXO-IBU} - r_{d3}$$

$$\frac{dc_{APMP}}{dt} = +r_{APMP} - r_{d4}$$

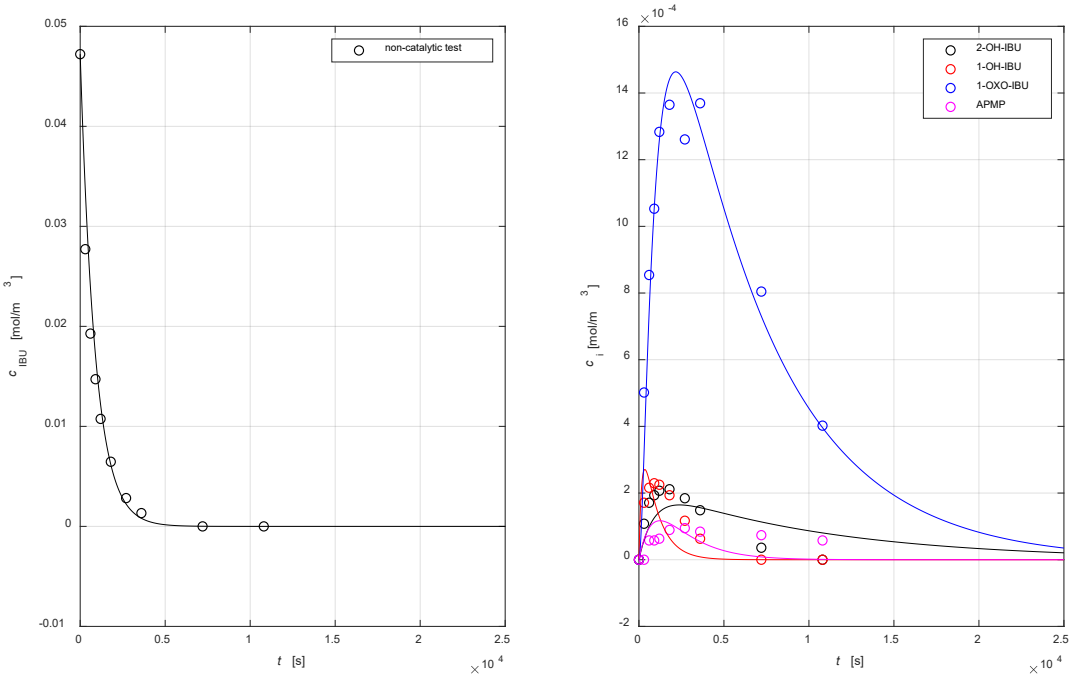

Fig. 19. Kinetics of an IBU ozonation experiment conducted in the absence of heterogeneous catalyst and the by-product concentrations during the decomposition of IBU. The symbols represent the experimental data, while lines give the model prediction.

As revealed in Figure 19, a relatively good fit among the results of experiments and the proposed model was obtained for the IBU and the by-product concentrations during the ozonation experiment.

Table. 9. Parameter estimation in the absence of heterogeneous catalyst.

Parameters	***Value***
$k_1\,[(m^3/mol).s^{-1}]$	$2.35 \cdot 10^{-3}$
$K_A\,(mol/m^3)$	$99.25 \cdot 10^{-3}$
K_B	$54.06 \cdot 10^{-6}$
$K_C\ (mol/m^3)$	$48.26 \cdot 10^{-6}$
$k_{c1}\,[(m^3/mol).s^{-1}]$	$49.80 \cdot 10^{-6}$
$k_{c2}\,[(m^3/mol).s^{-1}]$	$499.11 \cdot 10^{-6}$
$k_{c3}\,(s^{-1})$	$5.75 \cdot 10^{-3}$
$k_{c4}\,(s^{-1})$	$5.54 \cdot 10^{-6}$
$k_{d1}\,(s^{-1})$	$95.47 \cdot 10^{-6}$
$k_{d2}\,(s^{-1})$	$41.67 \cdot 10^{-6}$
$k_{d3}\,(s^{-1})$	$170.31 \cdot 10^{-6}$
$k_{d4}\,(s^{-1})$	$550.26 \cdot 10^{-6}$
$k_{d0}\,(s^{-1})$	$1.07 \cdot 10^{-3}$

3.3.5. Catalytic degradation of ibuprofen

In the following experiments, the combination of ozone with a solid catalyst was used for the degradation of IBU. The desired amount of the solid catalyst was inserted into the Spinchem™ compartment. After the experiments, the spent catalyst was carefully removed for further analysis. Otherwise, the experiments followed the same procedures as in the non-catalytic case. The main results are summarized in this reaction. Heterogeneous catalysts with a sufficient stability and low loss improve the efficiency of the ozonation process. The performance of the catalytic ozonation mainly depends on the type of catalyst, its surface characteristics and pH of the solution, which influence the properties of the active sites. Therefore, the crucial step is to select an appropriate catalyst [120]. The degradation rates of IBU in the presence of using Cu- modified Beta zeolite catalysts were higher than in the non-catalytic experiments (Figure 5). The explanation for the higher degradation rate of IBU is attributed to the presence of catalytic active site Cu sites, as well as the presence of Brønsted and Lewis acid sites. Furthermore, the amount of Cu present in the Beta zeolite, the Cu particle size and acid sites were associated to the high activity in degradation of IBU. Cu-H-Beta-150-EIM and Cu-H-Beat-150-DP catalysts showed the highest catalytic activity (Figure 20) in the degradation of ibuprofen.

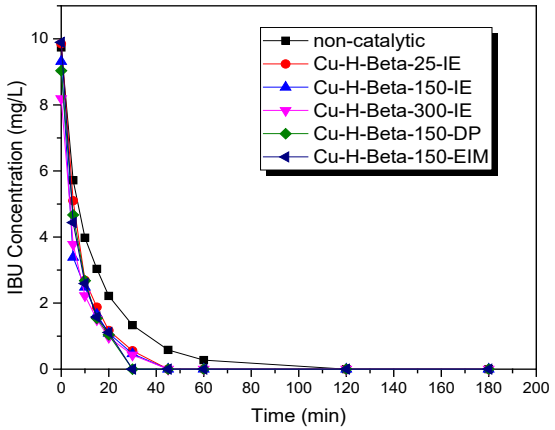

Fig. 20. The degradation of IBU by ozonation with and without catalyst in the presence of 2.5 ml/min nitrogen. [IBU]=10 mg/L, gas flow rate= 452.5 ml/min, T= 5˚C, stirring speed= 1070 rpm.

Ikhlaq et al. studied the ozonation of ibuprofen with ZSM-5 zeolites, and revealed the formation of carboxylic acids by-products, which was not formed by using ozonation alone. It can be concluded that during the catalytic ozonation in contrast to plain ozonation, an effective oxidative process took place [90].

Fig. 21 shows the by-product concentrations during the decomposition of IBU. The effect of the catalyst synthesis method on the formation and removal of the by-products can be seen in these figures. The Cu-H-Beta-150-DP catalysts synthesized by deposition-precipitation illustrate the highest degradation activity of by-products (Figure 21a). The catalytic activity using Cu-H-Beta-150-DP was better in the degradation of 1-OXO-IBU, 1-OH-IBU, 1-OH-IBU and APMP compared to the other Cu zeolite catalysts and non-catalytic experiments (Figure 21a-d). The highest catalytic activity achieved with Cu-H-Beta-150-DP is attributed to the smallest Cu nanoparticles (4.88 nm).

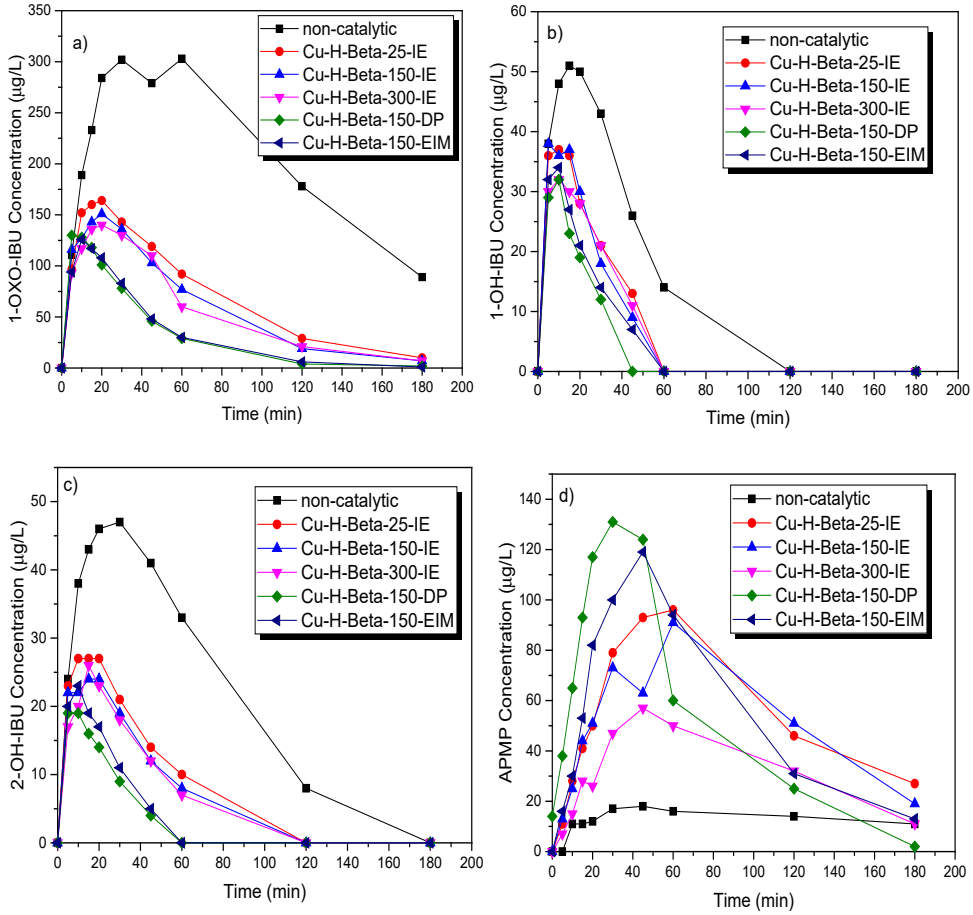

Fig. 21. a) 1-OXO-IBU, b) 1-OH-IBU, c) 2-OH-IBU, d) APMP concentration during the decomposition of IBU in the presence of 2.5 ml/min nitrogen. [IBU]=10 mg/L, gas flow rate= 450 ml/min, T= 20˚C, stirring speed= 1070 rpm.

Fig. 22 illustrates the decomposition of IBU in the presence of fresh and regenerated catalysts. As revealed by the figure, the regenerated catalysts give similar decomposition rates for IBU compared to the fresh ones. The regeneration of the Cu-H-Beta-150-DP and Cu-H-Beta-150-EIM spent catalysts were carried out at 400 ^{0}C for 120 min. It was observed that Cu-H-Beta-150-DP-Regenerated and Cu-H-Beta-150-EIM-Regenerated catalysts, exhibited a similar catalytic activity in the degradation of ibuprofen to that of the fresh counterparts. The regeneration and reuse of these catalysts is important from the long-term point of view of the catalyst stability and cost efficiency.

Although the regenerated catalysts exhibited an activity in the removal of by-products similar to the fresh catalysts (Fig. 23 a-d) it should be mentioned that the degradation of 1-OXO-IBU was much higher for the Cu-H-Beta-150-DP, Cu-H-Beta-EIM fresh, Cu-H-Beta-150-DP-Regenerated and Cu-H-Beta-150-EIM catalysts than the non-catalytic degradation (Figure 23 a-d).

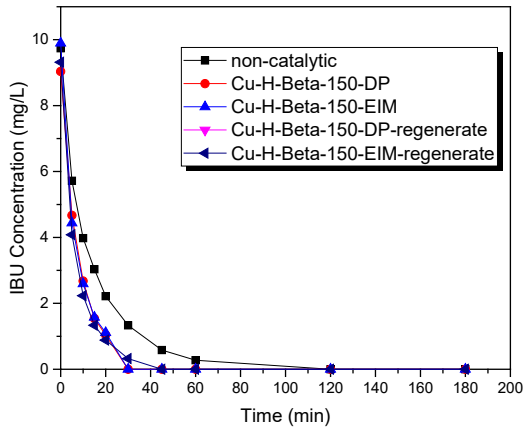

Fig. 22. The degradation of IBU by ozonation with and without the catalyst in the presence of 2.5 ml/min nitrogen. [IBU]=10 mg/L, gas flow rate= 452.5 ml/min, T= 5˚C, stirring speed= 1070 rpm.

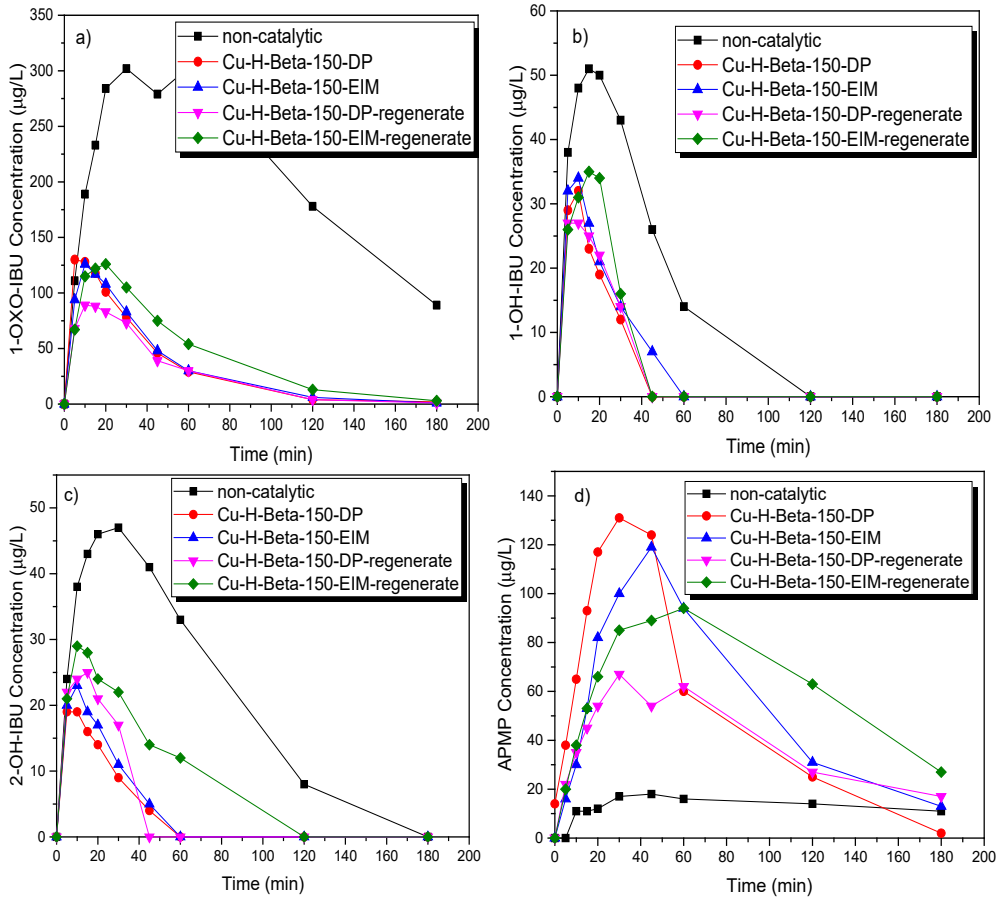

Fig. 23. a) 1-OXO-IBU, b) 1-OH-IBU, c) 2-OH-IBU, d) APMP concentration during the decomposition of IBU in the presence of 2.5 ml/min nitrogen. [IBU]=10mg/L, gas flow rate= 450 ml/min, T= 20˚C, stirring speed= 1070 rpm.

The degradation of IBU was studied in the presence of different metal catalysts as well as several support structures (Fig. 24). These experiments showed that the degradation rate of IBU was higher with Cu-H-Beta-150-DP, Cu-Na-Mordenite 12.8-IE, Fe-SiO_2-DP, Pd-MCM-41-EIM catalysts than the non-catalytic. However, the Cu-H-Beta-150-DP showed the highest degradation rate of all the studied catalysts.

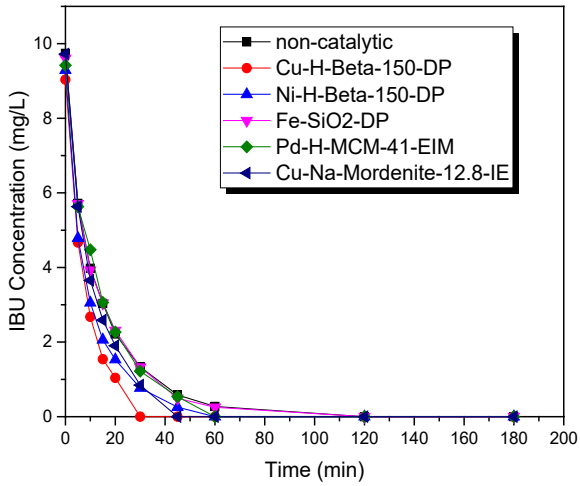

Fig. 24. The degradation of IBU by ozonation with and without the catalyst in the presence of 2.5 ml/min nitrogen. [IBU]=10 mg/L, gas flow rate= 452.5 ml/min, T= 5˚C, stirring speed= 1070 rpm.

As illustrated by Fig. 25, the effect of different catalysts on the appearance and degradation of by-products is significant. Cu-H-Beta-150-DP, Cu-Na-Mordenite-12.8-IE, Ni-H-Beta-25-EIM, and Pd-H-MCM-41-EIM showed a higher decomposition rate of 1-OXO-IBU compared to the non-catalytic experiments. Cu-H-Beta-150-DP, Cu-Na-Mordenite-12.8-IE, Ni-H-Beta-25-EIM showed a higher decomposition rate of 1-OH-IBU compared to non-catalytic experiments. Cu-H-Beta-150-DP, Cu-Na-Mordenite-12.8-IE, Ni-H-Beta-25-EIM, and Pd-H-MCM-41-EIM show higher decomposition rate of 2-OH-IBU compared to the non-catalytic experiment.

The formation of transformation products is dependent on structure of support, type of metal, oxidation state of metal, amount of Brønsted and Lewis acid sites of the catalysts (Figure 25a-d). Copper-catalyzed reactions produce less of the transformation products than the non-catalytic process. Using other catalysts in some cases led to a reduction in the amount of products formed but in some cases to an increase in the amount of products formed. The amount of products that are formed correlated with the rate of the IBU transformation reaction so that in the experiments with a faster reaction rate a lower amount of intermediate products was created.

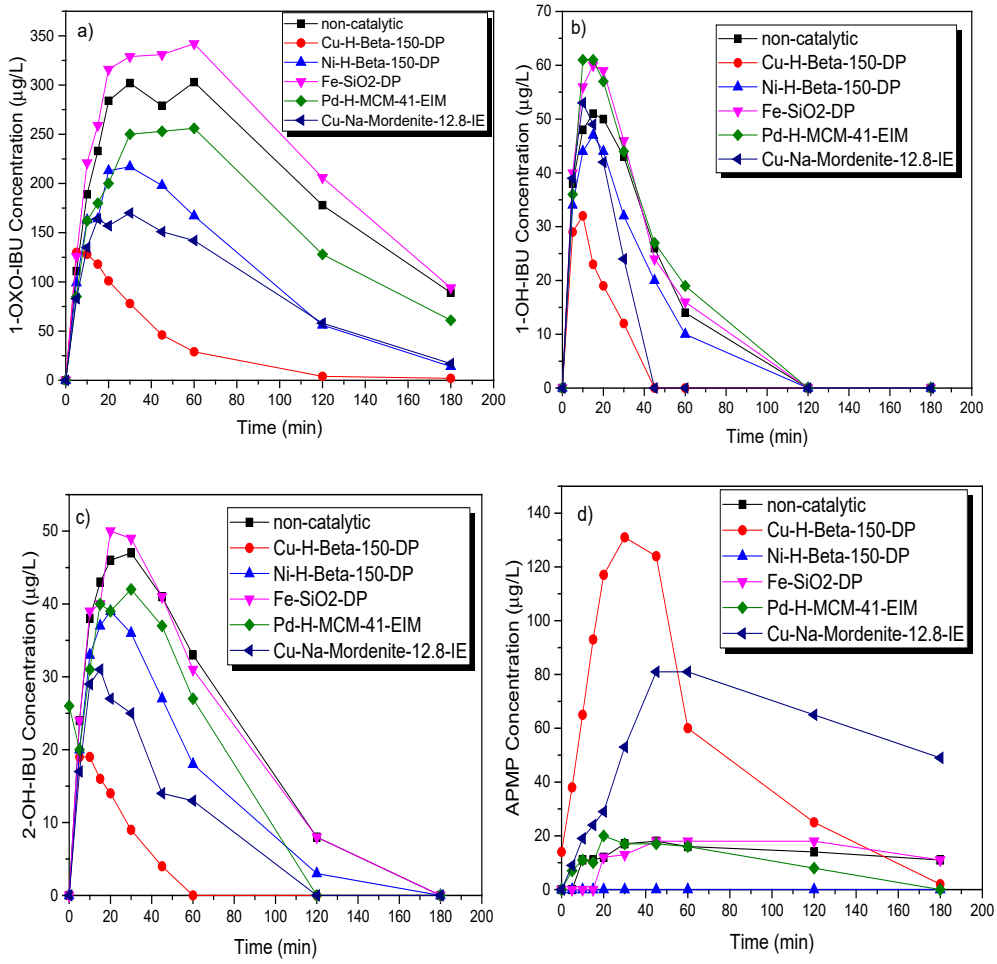

Fig. 25. a) 1-OXO-IBU, b) 1-OH-IBU, c) 2-OH-IBU concentration during the decomposition of IBU in the presence of 2.5 ml/min nitrogen. [IBU]=10mg/L, gas flow rate= 450 ml/min, T= 20˚C, stirring speed= 1070 rpm.

3.4. Removal of carbamazepine by catalytic and non-catalytic ozonation

3.4.1. Non-catalytic degradation of carbamazepine

The influence of different temperatures (5°C, 20˚C and 50˚C) on the decomposition rate of CBZ was evaluated using ozone in the absence of any catalyst. The results are displayed in Figure 26. These experiments illustrate that the transformation of CBZ was rapid and approximately equal at different temperatures. After 5 min of ozonation, a complete conversion of CBZ was observed. Somathilake *et al.* obtained similar results when ozonating CBZ [121]. Evidently, ozone alone is a powerful oxidant for the conversion of this pharmaceutical, but by-products were formed. The use of the catalyst could reduce the formed by-products, and therefore several catalysts were tested, see section 3.4.3.

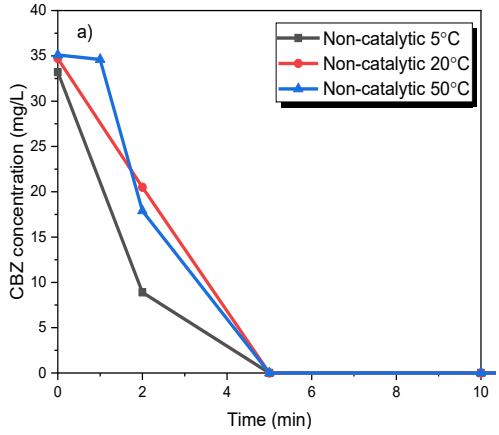

Fig. 26. CBZ degradation by ozonation at different temperatures (5°C, 10°C, 20˚C and 50˚C). b) CBZ degradation by catalysis in the presence and absence of ozone at temperature 20˚C. (Stirring speed= 900 rpm, $C_{O3,\,g}$=21 mg/L, C_{CBZ}≈35 mg/L, gas flow rate= 110 mL/min).

3.4.2. Quantification of oxidation products

Han *et al.* studied [49] cytotoxicity and genotoxicity of the removal of CBZ through chlorination, chloro- amination and ozonation processes. The CBZ alone induces chromosomal damage, and on the other hand, the genotoxicity of the CBZ residues after each treatment was found to be higher. However, it was demonstrated that the most efficient way for the degradation of CBZ was by ozonation among the all these treatments. Still, the by-products formed during the ozonation exhibited the highest cytotoxicity and an elevated genotoxicity. They suspected that the by-products BQM and BQD might cause chromosomal damage effects. The main ozonation pathway of CBZ is a rapid, almost instantaneous reaction leading to BQM (Fig. 27), which is slowly transformed further to BQD [122]. In order to investigate the effect of heterogeneous catalysis on the formation and transformation of BQM

and BQD, the products were isolated from the kinetic experiments and a quantification method was developed.

Figure 27 shows the molar concentrations of CBZ, BQM, and BQD during non-catalytic ozonation. The initial concentration of CBZ was 139 µmol/L and the maximum concentration of BQM was 103 µmol/L, hence 74 % of CBZ was transformed into BQM in this reaction. BQM was more resistant compared to CBZ and the concentration of CBZ was under the detection limit within 5 minutes, whereas 3 µmol/L of BQM remained still 240 minutes of ozonation. Furthermore, BQD is likewise BQM is more resistant than CBZ during ozonation. After 240 minutes ozonation of pure BQD 16 % of the initial concentration was still present.

CBZ can react with ozone generating two aldehyde groups which lead to the formation of BQM, and the BQM could react further with ozone generating BQD. The TP225 by-product is presumably transformed by a radical reaction from the intermediate product N,N-bis (2-formylphenyl)urea. Since the TP225 is generated, carbamic acid is probably formed besides. Moreover, the hydroxyl radicals could react TP225 and generate TP241. Since the pH of the solution during the ozonation is acidic there is the potential that this product transforms to TP223, and reacts further with hydroxyl radicals into TP239. Either the ozone or the hydroxyl radicals could attack the aldehydes of both BQM and BQD and generate BaQM and BaQD, sequentially. The TP146 and TP162 could be generated from the splite of a nitrogen-carbon bond. The TP300 and TP238 is generated from BaQD. The entire ozonation pathway of CBZ is displayed in Figure 28.

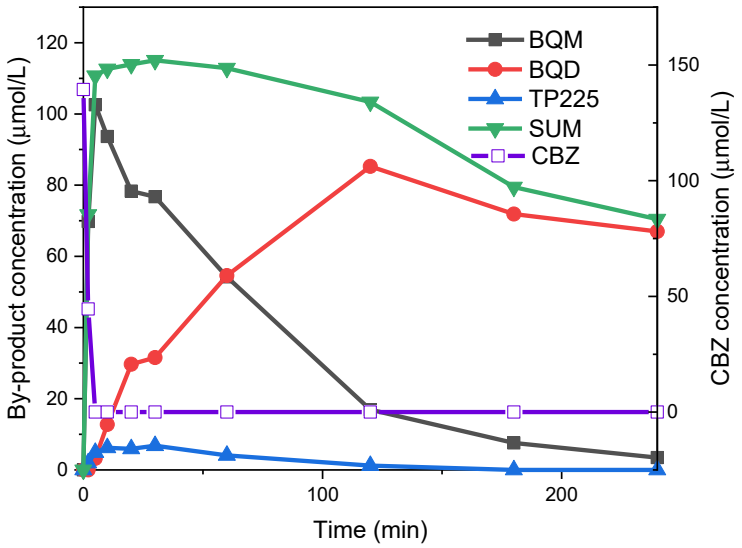

Fig. 27. Molar concentrations of CBZ, BQM and BQD (M. Kråkström).

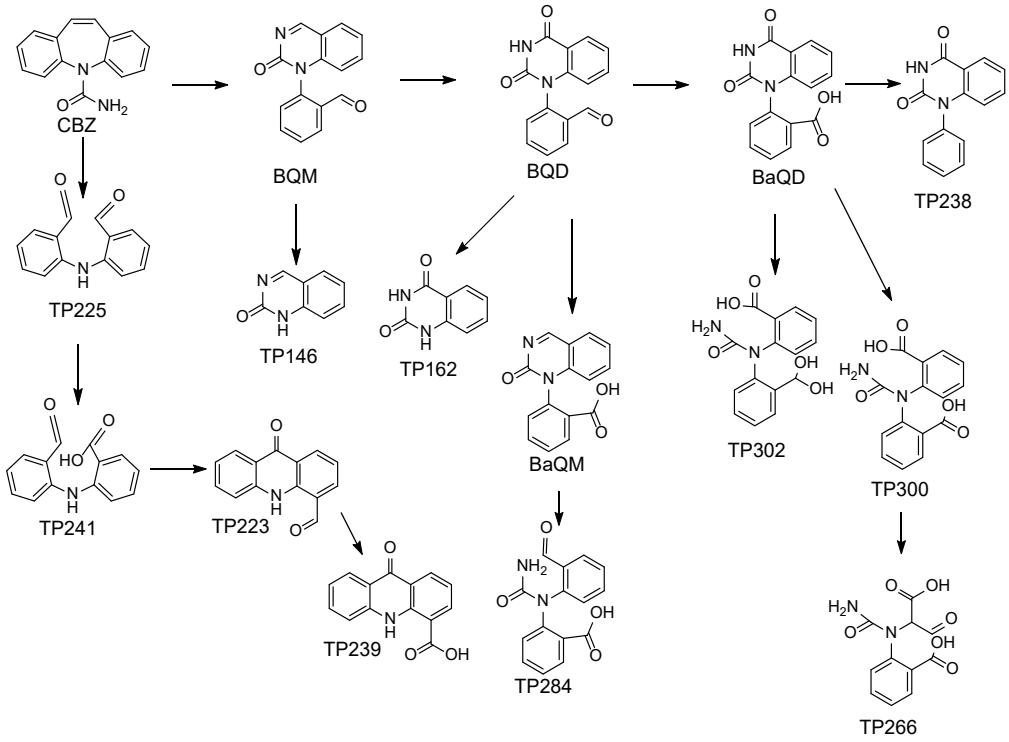

Fig. 28. CBZ ozonation pathways (M. Kråkström).

At the reaction time of 120 min the concentration of BQD was 85 μmol/L, so at least 83 % of BQM was transformed into BQD. Also BQD is more resistant than CBZ during ozonation. When pure BQD was ozonated, 16 % of the initial concentration of BQD still remained after 240 minutes. The sum of the concentrations of all the major products decreased with 16.5 % in the first two minutes. The concentration of CBZ decreased below the detection limit in five minutes, while the concentration of BQM and BQD were much more stable.

The formation of by-products was studied using no catalysts at three different temperatures. The influence of the reaction temperature on the ozonation of CBZ into BQM and BQD is illustrated in Fig. 29. It can be noticed that at higher temperature (50˚C), the concentration of BQM remained at a high level and after 4 h it had only decreased to 19.5 mg/l from the highest value of 28 mg/ml. At lower temperatures (20˚C and 5˚C), the reaction proceeds more rapidly, and almost all of BQM was removed or transformed to secondary products after four hours. The concentration of the secondary by-product BQD increased simultaneously to 20-24 mg/l when performing the experiments at low temperature (5-20˚C), but it remained low at the higher temperature (50˚C). Due to a slow transformation of BQM, BQD was formed more slowly at higher temperatures. If the experiment at 50˚C had been continued, the concentration of BQD might have been the same as for the experiments at lower temperatures. It can be concluded that by lowering the temperature due to the higher concentration of dissolved ozone, CBZ rapidly converts to BQM, and later on it transforms to BQD faster than at the higher temperature (50˚C).

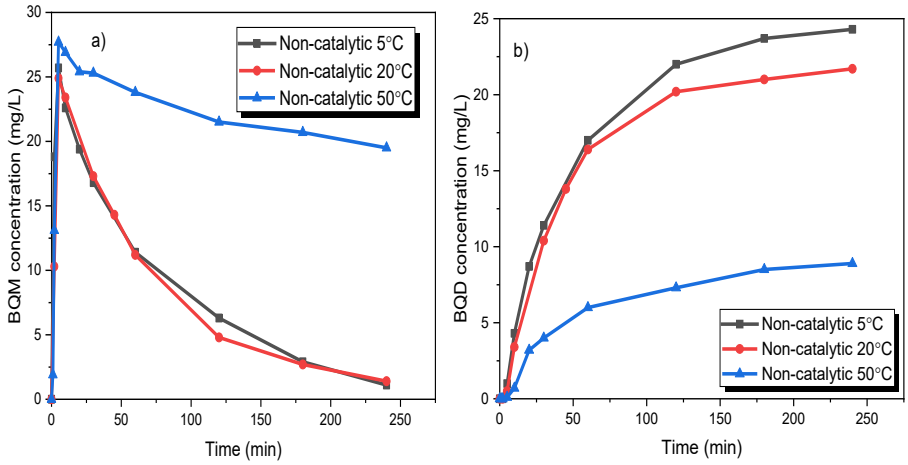

Fig. 29. a) BQM and b) BQD concentration during the ozonation of CBZ. C_{CBZ}≈35 mg/L, gas flow rate= 110 mL/min, T= 5°C, 10°C, 20˚C and 50˚C, stirring speed= 900 rpm, $C_{O3,g}$=21mg/L.

3.4.3. Catalytic degradation of Carbamazepine

A series of catalytic ozonation experiments were conducted at 20˚C in order to evaluate the effect of different heterogeneous catalysts on the degradation rate of CBZ as well as the kinetics of the by-products. Even though the degradation was rapid without any catalyst, there were some catalysts which improving the degradation rate, such as Cu-MCM-41-A-EIM and Ru-MCM-41-IS (see Figure 30a). The conversion of CBZ was complete already after two minutes for the Cu-catalyst, and the Ru-catalyst was almost equally active.

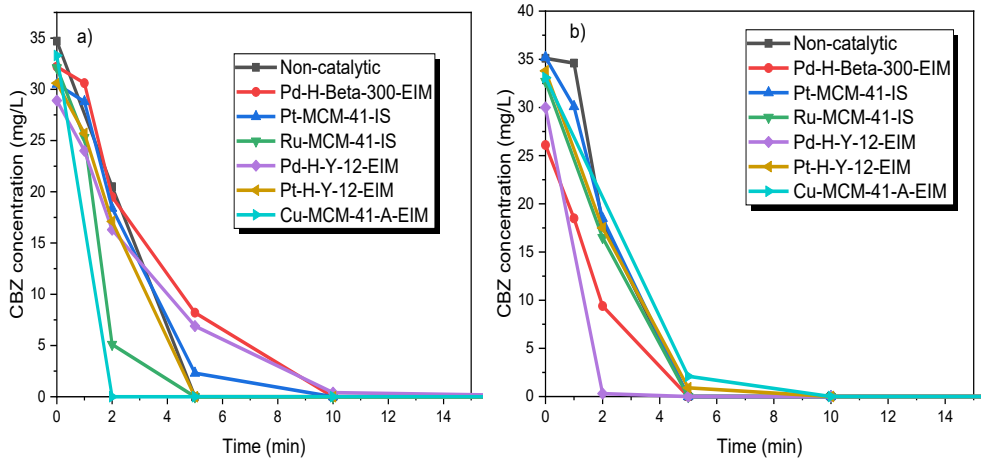

Fig. 30. CBZ degradation by ozonation and ozonation combined with catalysis. C_{CBZ}≈35 mg/L, gas flow rate= 110 mL/min, stirring speed= 900 rpm, $C_{O3,g}$=21mg/L, $C_{catalysts}$=0.5 g/L. **a)** T= 20˚C, **b)** T= 50˚C.

A similar series of catalytic ozonation experiments were conducted with a significantly higher temperature, at 50˚C, to evaluate the effect of increased temperature on the catalyst activity

while ozonating CBZ (Figure 30b). As was revealed in our previous experiments, the concentration of dissolved ozone decreases at higher temperature but, on the other hand, the activity of the catalysts increases at higher temperature [96][123]. Here, the Pd-H-Y-12-EIM and Pd-H-Beta-300-EIM illustrate the highest decomposition rate compared to other catalysts as well as the non-catalytic experiment. Due to the rapid reaction, it is a challenge to evaluate the temperature effect on the decomposition rate of CBZ.

3.4.4. Quantification of catalytic ozonation products

After the non-catalytic studies, several solid catalysts were synthesized and characterized by our group, and thereafter employed to reveal the catalytic effect on the ozonation of CBZ. The formation kinetics of BQM and BQD are displayed in Figs. 31 and 32. It was observed that during the first minutes of experiments performed at 20˚C, the BQM concentration increased to a maximum 25.7 mg/L (Cu-MCM-41-A-EIM) and later on, after 2 hours it had decreased to only 4 mg/L. However, for non-catalytic ozonation at same temperature 20˚C, the BQM concentration increased to 25.7 mg/L but after 2 h it had decreased to 4.8 mg/L. The catalysts Pt-H-Y-12-EIM and Ru-MCM-41-IS showed a slightly higher transformation rate of BQM compared to the corresponding non-catalytic experiment. As revealed by Figure 31, BQD was slightly formed within 2h. The maximum concentration of BQD was 20.2 mg/L for the non-catalytic experiment. The catalyst Pd-H-Y-12-EIM showed the lowest BQD concentration (1.7 mg/L).Three mechanisms could be possible in these experiments: 1) ozone adsorption on the catalyst surface and generation of active radical species that reacts with BQM and BQD; 2) BQM and BQD sorption on the catalyst surface followed via the reaction by dissolved ozone in the water; 3) sorption of all three species ozone, BQM and BQD on the catalyst surface followed by a direct or indirect reaction [81].

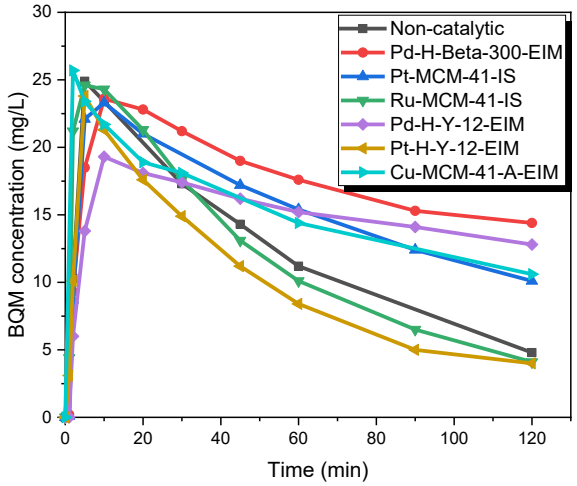

Fig.31. BQM concentration during the catalytic and non-catalytic ozonation of CBZ. C_{CBZ}≈35 mg/L, gas flow rate= 110 mL/min, T= 20˚C, stirring speed= 900 rpm, $C_{O3,g}$=21mg/L, $C_{catalysts}$=0.5 g/L.

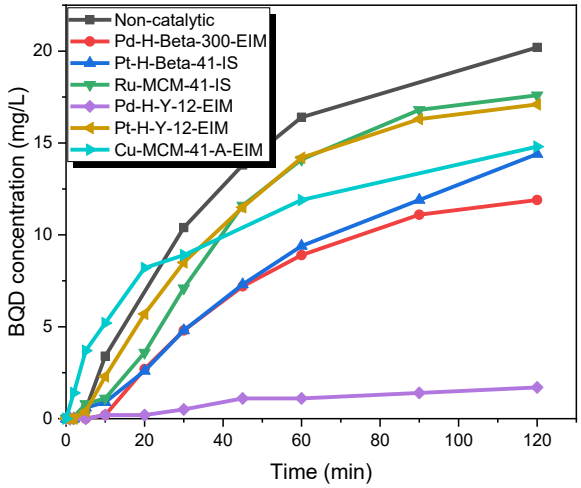

Fig.32. BQD concentration during the catalytic and non-catalytic ozonation of CBZ. C_{CBZ}≈35 mg/L, gas flow rate= 110 mL/min, T= 20˚C, stirring speed= 900 rpm, $C_{O3,g}$=21mg/L, $C_{catalysts}$=0.5 g/L.

The catalytic experiments were carried out using several temperatures. Figure 33 shows that in the first minutes, 27.7 mg/L of BQM was formed (almost equal to non-catalytic ozonation), but later on, the BQM concentration slightly decreased to 9 mg/L when using the Pd-H-Y-12-EIM catalyst. For non-catalytic ozonation at 50˚C, the BQM concentration increased to 27.7 mg/L, after which it decreased to 21.4 after 2 h, and after 4 h it had decreased to 19 mg/L. It can be noticed from the results that the activity of catalysts increased with higher temperature, because the dissolved ozone concentration is very low at 50˚C (approximately five times lower than at 20˚C). For example, after 2 h of ozonation combined with Pd-H-Y-12-EIM catalyst, the BQM and BQD concentration were 11.2 mg/l and 0.9 mg/l at 50˚C which were lower compared to 20˚C (BQM concentration was 12.8 mg/l and BQD concentration was 1.7 mg/l) using the same catalyst (Figure 34). An explanation for the increased catalytic efficiency at higher temperature could be due to that instead of ozonation, catalytic oxidation is observed, where dissolved oxygen is adsorbed on metal oxides and they further generate active atomic oxygen species as well as lattice oxygen atoms, present on the metal oxides of the catalysts [124].

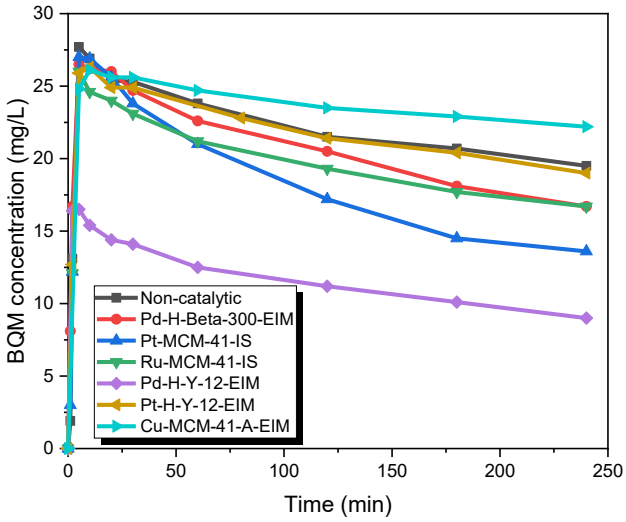

Fig. 33. BQM concentration during the catalytic and non-catalytic ozonation of CBZ. C_{CBZ}≈35 mg/L, gas flow rate= 110 mL/min, T= 50˚C, stirring speed= 900 rpm, $C_{O3,g}$=21mg/L, $C_{catalysts}$=0.5 g/L.

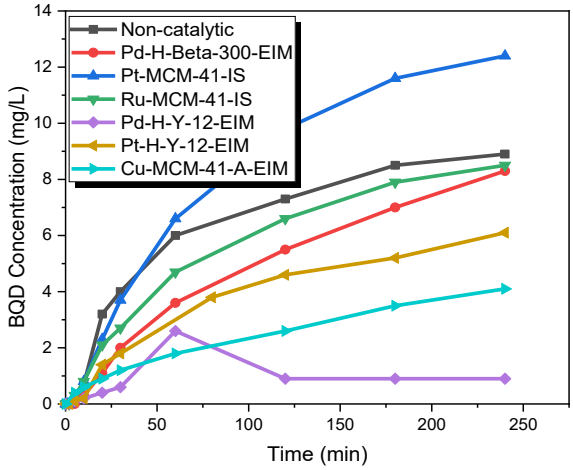

Fig. 34. BQD concentration during the catalytic and non-catalytic ozonation of CBZ. C_{CBZ}≈35 mg/L, gas flow rate= 110 mL/min, T= 50˚C, stirring speed= 900 rpm, $C_{O3,g}$=21mg/L, $C_{catalysts}$=0.5 g/L.

These results were in line with a previous work of Rosal *et al.* who investigated catalytic ozonation of CBZ. Their ozonation results revealed that utilizing a titanium dioxide catalyst combined with ozonation provides a significant benefit where the ozone decomposition as well as ozonation reactions were improved, as well as an increase of the formation of hydroxyl radicals and the rate of mineralization, compared to non-catalytic ozonation [125].

3.5. Removal of diclofenac by catalytic and non-catalytic ozonation

3.5.1. Concentration of diclofenac in catalytic and non-catalytic ozonation

The degradation of DCF was investigated by non-catalytic as well as catalytic experiments using ozone as the oxidant. The catalysts chosen here were H-MCM-22-100 with different Pt-modified concentrations (Fig. 35). The experiments revealed that the degradation rate of DCF was higher in the presence of heterogeneous catalysts compared to non-catalytic experiments. The 2%wt.Pt-MCM-22-100–EIM showed the highest decomposition rate, since 95 % of DCF had transformed at already after 4 min, whereas there was still 65% of DCF left at that moment when no catalyst was used. This catalyst also showed higher decomposition rate for DCF compared to proton form, 1% Pt and 5% Pt modified of MCM-22-100 catalysts. In addition, ozonation of DCF was investigated with 0, 0.25, 0.50 and 1.00 g of 2%wt.Pt-MCM-22-100-EIM catalyst. The results reveal that using 0.25 g of 2%wt.Pt-MCM-22-100-EIM catalyst increased the degradation rate compared to non-catalytic experiments. Moreover, 0.5 g and 1 g of 2%wt.Pt-MCM-22-100-EIM catalyst showed a maximun degradation rate of DCF. After 4 min of ozonation, 65% of DCF was still left in case of non-catalytic experiments whereas in case of catalytic reactions, 40% remained when 0.25 g catalyst was added 8.3% when 0.5g was added and 13% when 1g of 2%wt.Pt-MCM-22-100-EIM catalyst was added (Fig. 36 a). Moreover, the normalized figure of these three amounts of catalyst illustrates an overlap revealing that the degradation rate is not dependent on the catalyst concentration (Fig. 36b). A comprehensive study on the ozonation of DCF using different Pt-modified catalyst structures was conducted to evaluate their effect on the transformation of DCF. Two catalysts, Pt-H-Y-IE and Pt-γ-Al_2O_3 (UOP)-IMP were used and compared with the 2%wt.Pt-MCM-22-100-EIM. Figure 37 shows that the transformation of DCF was relatively similar for these three catalysts.

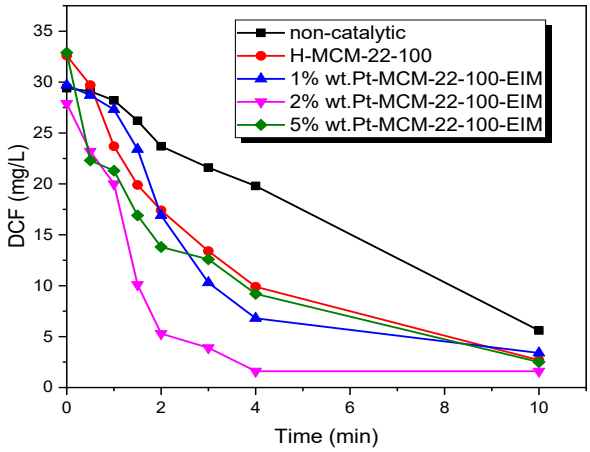

Fig. 35. DCF degradation by ozonation and H-MCM-22-100, 1%wt.Pt-MCM-22-100-EIM, 2%wt.Pt-MCM-22-100-EIM and 5%wt.Pt-MCM-22-100-EIM catalysts. C_{DCF}=30 mg/L, gas flow rate= 110 ml/min, T= 20˚C, stirring speed= 900 rpm, $C_{O3,g}$=21mg/L, $C_{catalysts}$=0.5 g/L.

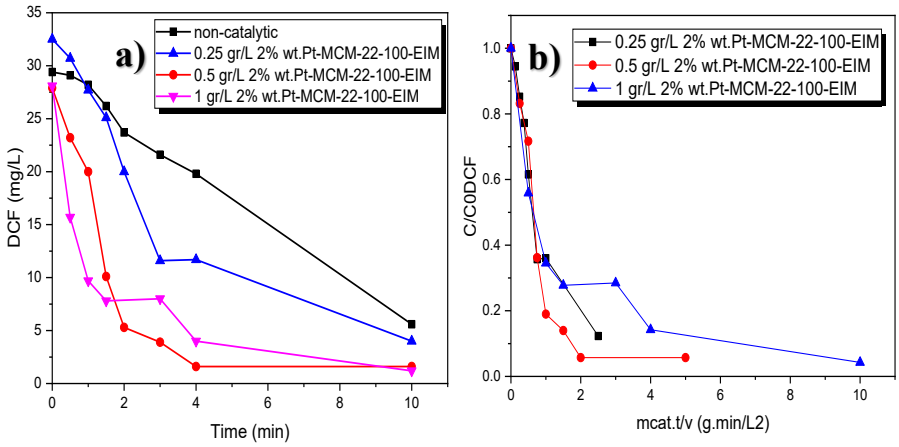

Fig. 36. DCF degradation by ozonation with 0, 0.25, 0.50 and 1.00 g of 2%wt.Pt-MCM-22-100 catalyst. C_{DCF}=30 mg/L, gas flow rate= 110 ml/min, T= 20˚C, stirring speed= 900 rpm, $C_{O3,g}$=21mg/L.

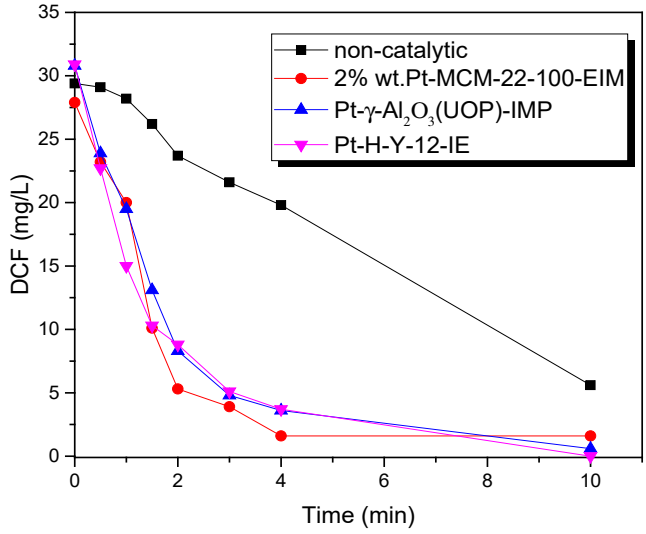

Fig. 37. DCF degradation by ozonation and 2%wt.Pt-MCM-22-100-EIM, Pt-γ-Al_2O_3 (UOP)-IMP and Pt-H-Y-12-IE catalysts. C_{DCF}=30 mg/L, gas flow rate= 110 ml/min, T= 20˚C, stirring speed= 900 rpm, $C_{O3,g}$=21mg/L, $C_{catalysts}$=0.5 g/L.

3.5.2. Quantification of catalytic and non-catalytic ozonation products of DCF

Three of the main by-products of the ozonation of DCF were quantified, see Figure 38. Here, the concentrations were converted from w% to molar concentration, So that 30 mg/L of initial DCF corresponded to 99 µmol/L. After 10 minutes, 80 % of DCF had transformed into by-products. The first observed, product formed was NO_2-DCF. This compound had a maximum concentration after one minute, and it was 3.5 % of the initial DCF concentration.

The first of the OH-DCF isomers formed was 4'-OH-DCF and a maximum concentration was observed after 4 minutes, and following that, the concentration has remained stable. The highest concentration of 4'-OH-DCF was 8.5 % of the initial concentration of DCF. The second OH-DCF isomer, 5-OH-DCF was generated slowly compared to 4'-OH-DCF. The sum of the concentrations of the DCF by-products accounts only to 20 % of the transformed DCF, which confirms that a significant quantity of DCF is transformed into other products, such as QI-DCF and small carboxylic acids.

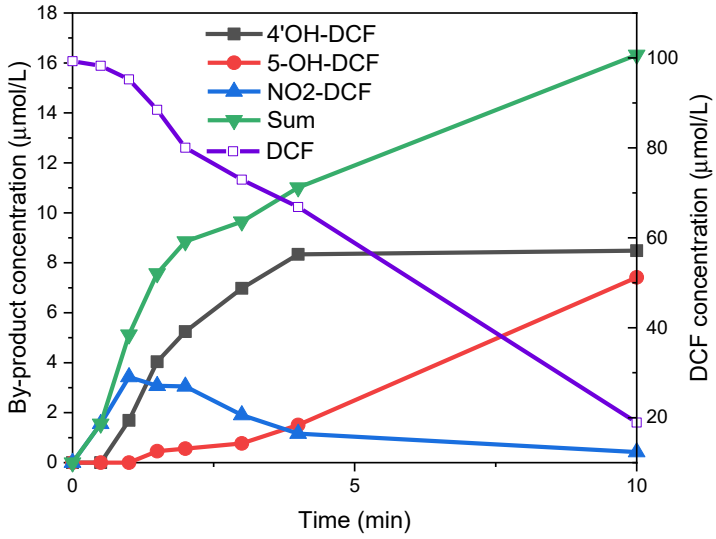

Fig.38. The ozonation of DCF and the transformation of the main products (M. Kråkström).

Based on the results, a reation pathway of the ozonation DCF is proposed in Figure 39. DCF is transformed by the addition of hydroxyl groups and further oxidized to quinone imine. Additionally, DCF was decarboxylated and the aromatic bond was broken. Furthermore, the bond between nitrogen and the aromatic ring was broken as well.

According to literature, the advanced oxidation process of DCF leads to the formation of one or more hydroxylated products [126][85]. Two of the hydroxylated products (4'-OH-DCF and 5-OH-DCF) were purchased and a multiple reaction monitoring (MRM) method was developed to quantify them in order to investigate the effect of heterogeneous catalysis on the formation and transformation of hydroxylated DCF products. The presence of the

hydroxylated internal standard of the 4'-OH-DCF isomer further helped to distinguish between the isomers. Chen *et al.* studied the mineralization of DCF by ozonation combined with Fe-MCM-41 and Fe-MCM-48 catalysts. Their research results illustrated that mineralization of DCF using these catalysts is higher compared to non-catalytic ozonation [127][128]. For this reason, the MCM-structured catalyst was applied in our experiments to study the degradation of by-products and the MCM catalyst was compared with other structures.

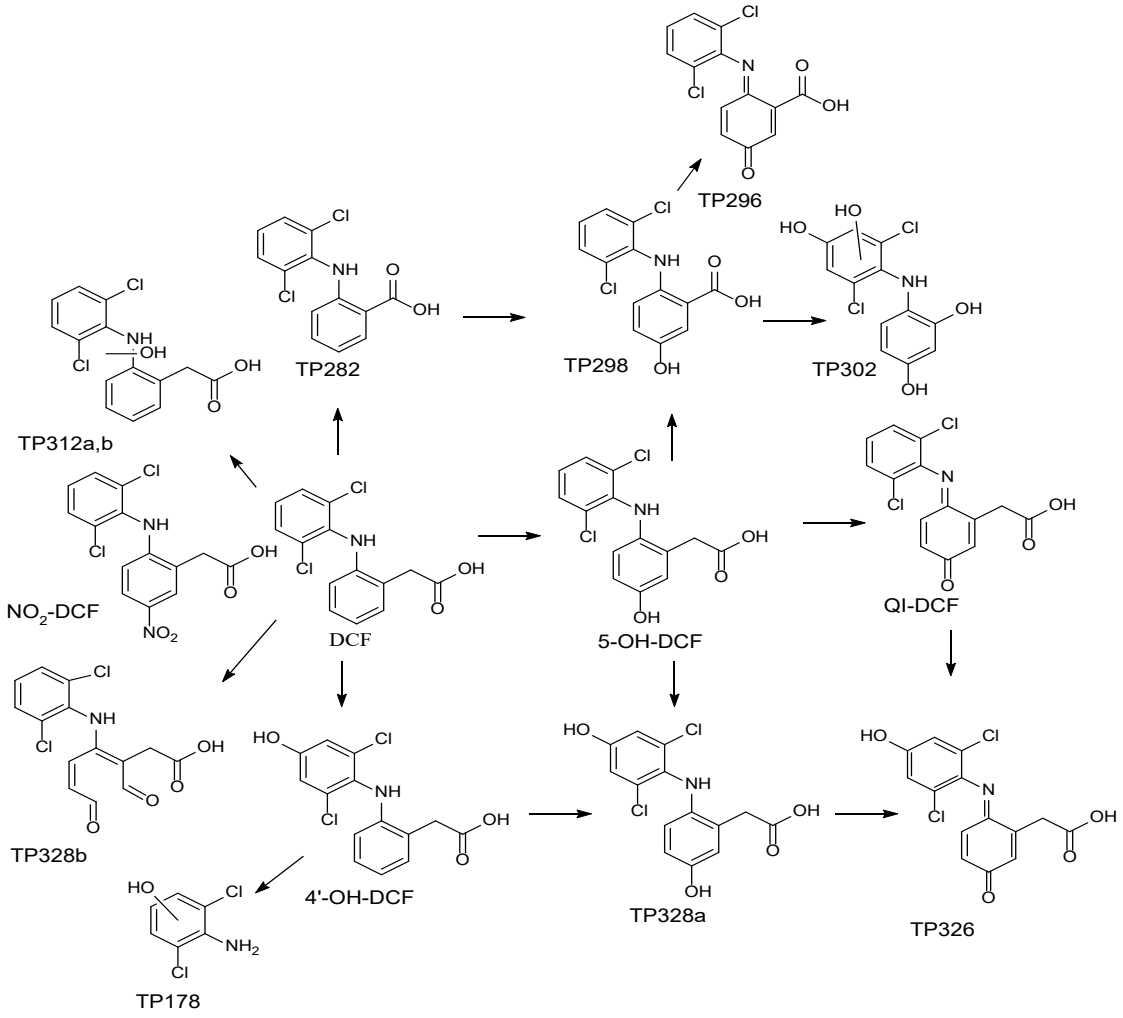

Fig. 39. Proposed DCF ozonation pathway (M. Kråkström).

Figure 40 illustrates the growth of the by-products 5-OH-DCF during the catalytic and non-catalytic ozonation experiments. In these experiments, using a heterogeneous catalyst resulted in a lower maximum concentration of 5-OH-DCF compared to non-catalytic experiments. The lowest maximum concentration of 5-OH-DCF was observed for the 2%wt.Pt-MCM-22-100

modified catalyst. The presence of heterogeneous catalysts affected the formation of 5-OH-DCF. When only the H-MCM-22-100 catalyst was used, the concentration of 5-OH-DCF increased more rapidly than in the metal-catalyzed experiments. The presence of a heterogeneous catalyst also resulted in a decrease of the maximum concentration of 5-OH-DCF. In all the experiments, except the one catalyzed by H-MCM-22-100, 5-OH-DCF were detected towards the end of the experiment. The 5-OH-DCF isomer was always formed after the 4'-OH-DCF isomers. Three different catalyst amounts 0.25, 0.5, 1 g of 2%wt.Pt-MCM-22-100-EIM were studied (Fig. 41). The concentration of 5-OH-DCF which was formed during ozonation decreased as the higher amount of catalyst was used. When 1 g of catalyst was used, 5-OH-DCF could not be detected at all, which implies that the catalyst inhibits the formation of 5-OH-DCF. The transformation of 5-OH-DCF with three different catalyst structures in the ozonation of DCF are illustrated in Figure 42. The decrease of 5-OH-DCF was strongly influenced by different kinds of catalysts, especially with 2%wt.Pt-MCM-22-100-EIM and the use of this catalyst resulted in the lowest amount of 5-OH-DCF (0.085 mg/L). Moreover, the concentration of 5-OH-DCF started to decline from 4 min in the presence of the Pt-H-Y-12-IE catalyst.

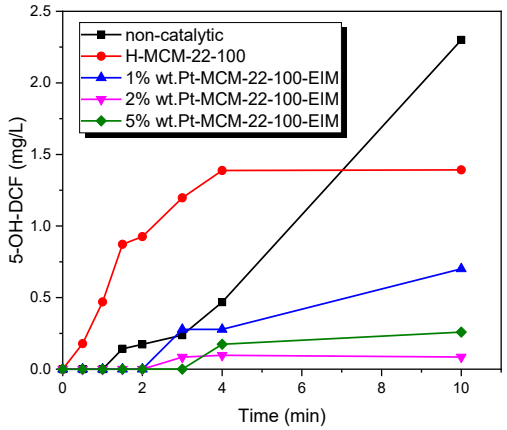

Fig. 40. The concentration of 5-OH-DCF during the decomposition of DCF by catalytic and non-catalytic ozonation. C_{DCF}=30 mg/L, gas flow rate= 110 ml/min, T= 20˚C, stirring speed= 900 rpm, $C_{O3,g}$=21mg/L, $C_{catalysts}$=0.5 g/L.

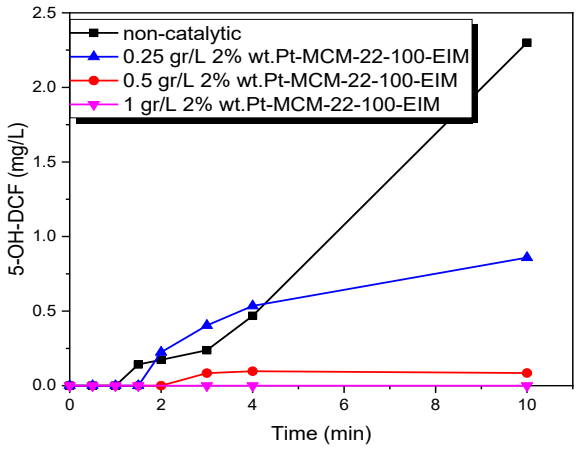

Fig. 41. The concentration of 5-OH-DCF during the ozonation of DCF using different amount of 2%wt.Pt-MCM-22-100-EIM catalyst (0.25, 0.50 and 1.00 g/L). C_{DCF}=30 mg/L, gas flow rate= 110 ml/min, T= 20˚C, stirring speed= 900 rpm, $C_{O3,g}$=21mg/L.

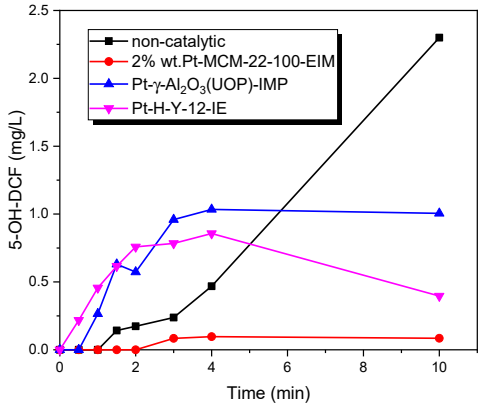

Fig. 42. The concentration of 5-OH-DCF during the decomposition of DCF by catalytic and non-catalytic ozonation. C_{DCF}=30 mg/L, gas flow rate= 110 ml/min, T= 20˚C, stirring speed= 900 rpm, $C_{O3,g}$=21mg/L, $C_{catalysts}$=0.5 g/L.

Figure 43 illustrates the formation of the second isomer, 4'-OH-DCF during ozonation. During non-catalytic experiments, the concentration of 4'-OH-DCF increased to a maximum of 2 % after 4 minutes and remained stable until the end of the experiment (Fig. 43). As MCM-22-100 was used, the maximum concentration of 4'-OH-DCF was lower than in the non-catalytic experiment, and it started to decrease towards the end of the experiment. The lowest final concentration was observed as 2%wt.Pt-MCM-22-100 was used. Three different catalyst amounts (0.25, 0.5, 1g) of 2%wt.Pt-MCM-22-100-EIM were studied (Fig. 44). The maximum concentration of 4'-OH-DCF which diminished when a higher amount of catalyst was used. After 10 minutes of ozonation, it was only 0.06 mg/L when 1 g of 2%wt.Pt-MCM-22-100-EIM was used, compared to 2.63 mg/L when no catalyst was present. This implies that the catalyst inhibits the formation of 4'-OH-DCF and/or enhances the transformation of it forwards other

by-products. The effects of the different structures of Pt-modified catalysts on the transformation of 4'-OH-DCF are displayed in Figure 45. 4'-OH-DCF increased to appr. 1 mg/L at 2 min and later on, it declined to zero after 10 minutes. All these three catalysts turned to be efficient upon transformation of 4'-OH-DCF compared to the non-catalytic process.

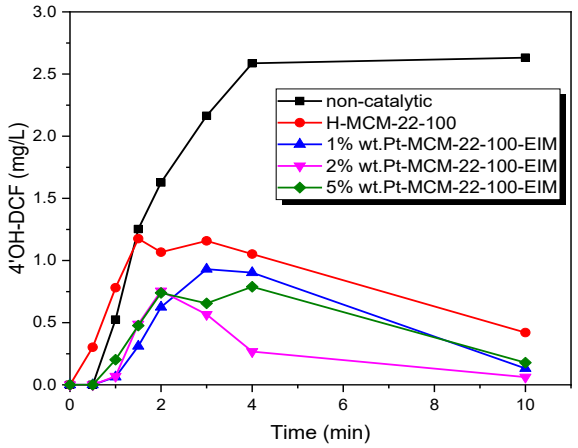

Fig. 43. The concentration of 4´OH-DCF during the decomposition of DCF by catalytic and non-catalytic ozonation. C_{DCF}=30 mg/L, gas flow rate= 110 ml/min, T= 20˚C, stirring speed= 900 rpm, $C_{O3,g}$=21mg/L, $C_{catalysts}$=0.5 g/L.

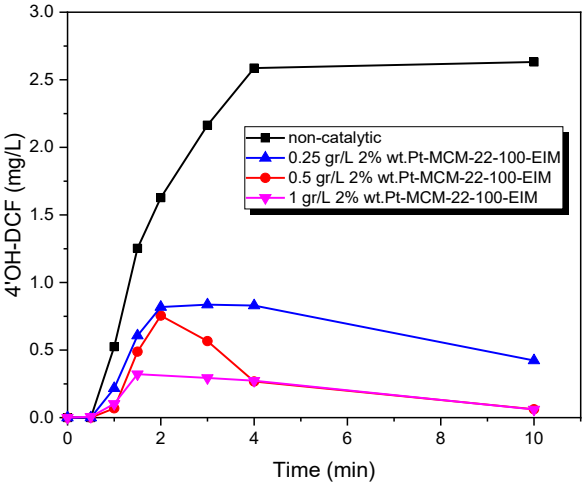

Fig. 44. The concentration of 4´OH-DCF during the ozonation of DCF using different amount of 2%wt.Pt-MCM-22-100 catalyst (0.25, 0.50 and 1.00 g). C_{DCF}=30 mg/L, gas flow rate= 110 ml/min, T= 20˚C, stirring speed= 900 rpm, $C_{O3,g}$=21mg/L.

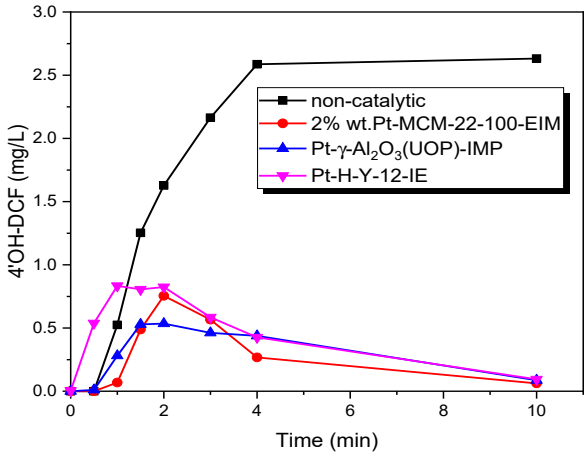

Fig. 45. The concentration of 4´OH-DCF during the decomposition of DCF by catalytic and non-catalytic ozonation. C_{DCF}=30 mg/L, gas flow rate= 110 ml/min, T= 20˚C, stirring speed= 900 rpm, $C_{O3,g}$=21mg/L, $C_{catalysts}$=0.5 g/L.

3.6. Removal of sulfadiazine by catalytic and non-catalytic ozonation

3.6.1. Non-catalytic degradation of sulfadiazine

The influence of the gas flow mixture (oxygen and nitrogen) on the reaction rate of SDZ was evaluated and the results are displayed in Figure 46a. These experiments revealed that the gas mixture composition plays a difference. The transformation rate of SDZ was rapid with 2.5 ml/min nitrogen gas flow (lower than 1% of total flow). With a nitrogen flow rate of 50 mL/min and 0 mL/min, SDZ was entirely transformed after 10 minutes, while with a nitrogen flow rate of 2.5 mL/min. SDZ was completely transformed within one minuet (The ozonator manufacturer suggested the use of a small amount of N_2 in the gas feed in order to enhance the performance of the generator). Hence, a nitrogen flow rate of 2.5 mL/min is optimal for SDZ degradation. Thereafter, the influence of the oxygen gas flow was studied. The transformation of SDZ was significantly slower when the oxygen gas flow was decreased (Figure 46b), which indicates that less ozone was produced at lower oxygen gas flow.

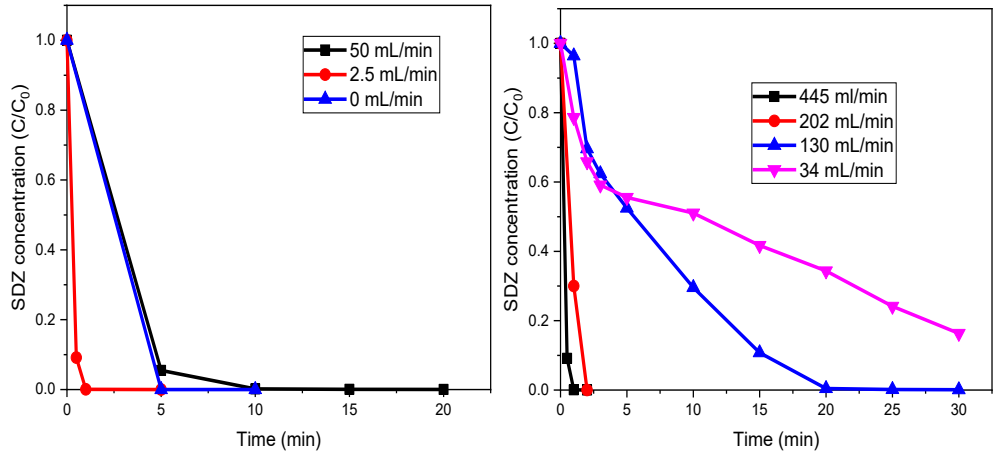

Fig 46. Transformation of SDZ with **a)** different nitrogen flow rates and **b)** different oxygen flow rates. The numbers in the legend represent the gas flow rate. C_{SDZ}=10 mg/L, T= 25˚C.

3.6.2. Quantification of oxidation products

Several by-products where found when ozonating SDZ. In the following section, proposed reaction mechanisms and by-producs are discussed (see Fig.47). Two isomers of SDZ-P1 were detected, where an OH group had been added to the aniline ring. Two isomers of SDZ-P2 were generated by the addition of three hydroxyl groups on SDZ. The formation of SDZ-P4 is proposed to occur by oxidation of the amine to a nitro group and attaching of an OH group to the aromatic ring. SDZ-P5 is presumably generated via a radical reaction of SDZ.

The SDZ-P6 product could be generated via hydroxylation of SDZ-P5 (where the NH_2 group had been replaced by an OH group). SDZ was transformed via the attachment of hydroxyl groups, the oxidation of the amine group to a nitro group, the break of the S-N bond and the

removal of the amine group replaced by a hydroxyl group. The main by-product of this pathway detected was 2-aminopyrimidine (2-AP). Furthermore, during the ozonation of SDZ, the product underwent a rearrangement reaction Figure 47 (b). From the rearrangement reactions, SDZ-15 had the largest concentration at the end of the experiments.

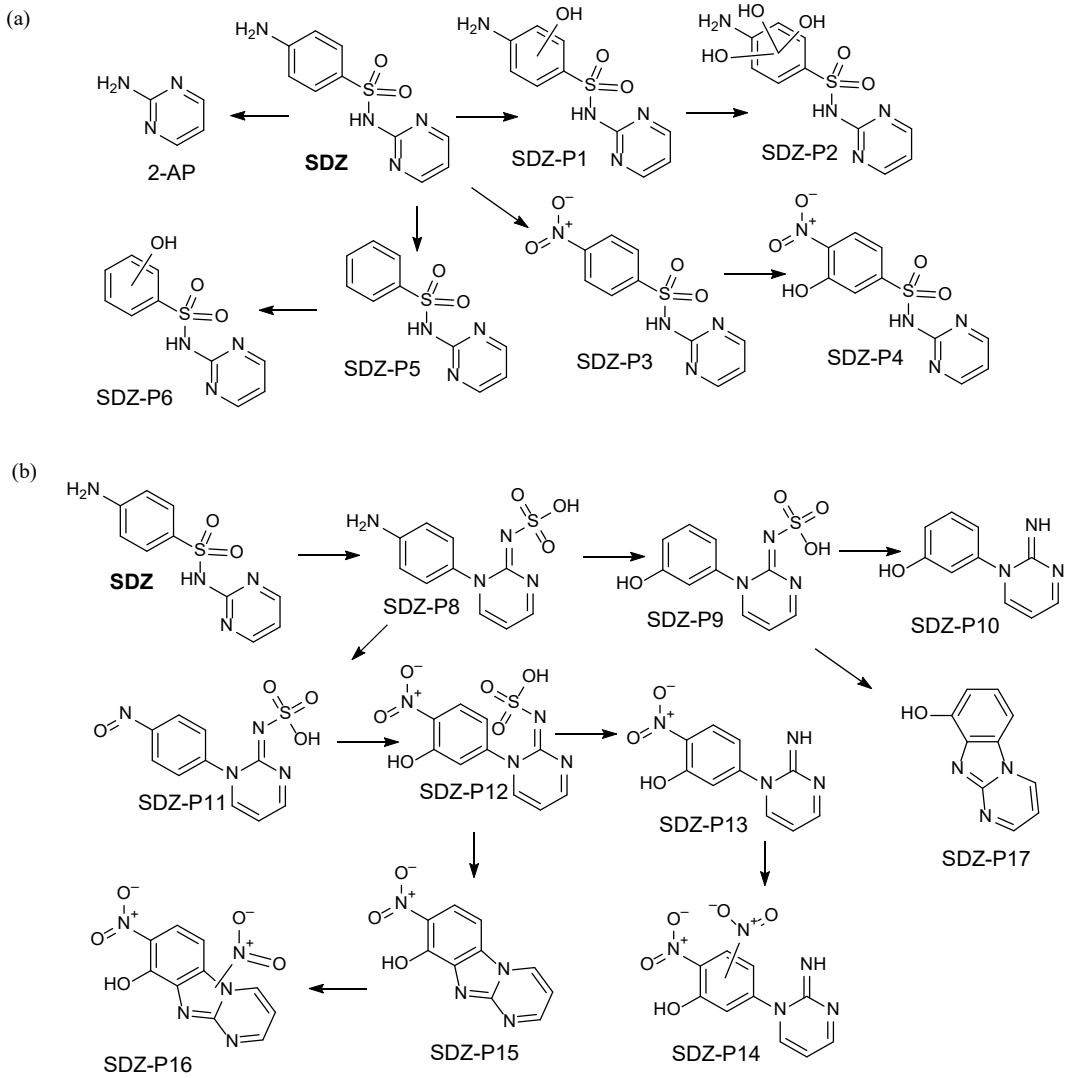

Fig 47. SDZ ozonation pathways (a) the N-(pyrimidin-2-yl) benzenesulfonamide pathway and (b) the rearrangement pathway (M. Kråkström).

The concentrations of SDZ-P15 and 2-AP during the ozonation experiment can be seen in Figure 48. Approximately 0.2 mg/L (or 2 μM) of 2-AP was generated during the SDZ ozonation, which corresponds to 6 % of the entire amount of SDZ. The transformation velocity of 2-AP was slower compared to SDZ, wherein after 240 min, 0.04 mg/L of 2-AP was detected.

The SDZ-P15 concentration increased to a maximum after 60 minutes and after which the concentration started to decrease. In total, 28% of SDZ was transformed into SDZ-P15 in ozonation process.

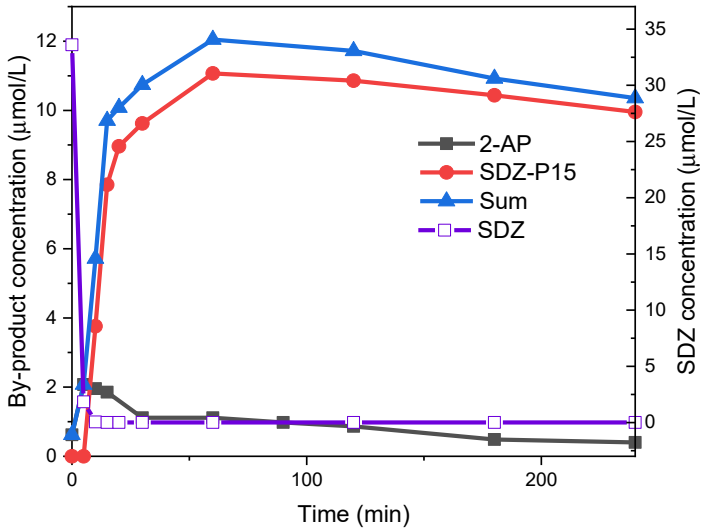

Fig 48. Molar concentration of SDZ, and products 2-AP and SDZ-P15 (M. Kråkström).

3.6.3. Catalytic degradation of sulfadiazine

The Fe-H-Beta-25-EIM and Cu-H-Beta-150-DP catalysts were employed for the SDZ degradation, because these catalysts had earlier shown an improvement in the elimination of the IBU ozonation. However, Figure 49 demonstrates that the SDZ transformation was slower in the presence of catalysts. The different efficiencies of these catalysts on the ozonation between IBU and SDZ could be due to the different molecular structures of these components. The IBU molecule holds a carboxylic acid group, but in contrast, the SDZ molecule contains an amine group and a sulfonyl group.

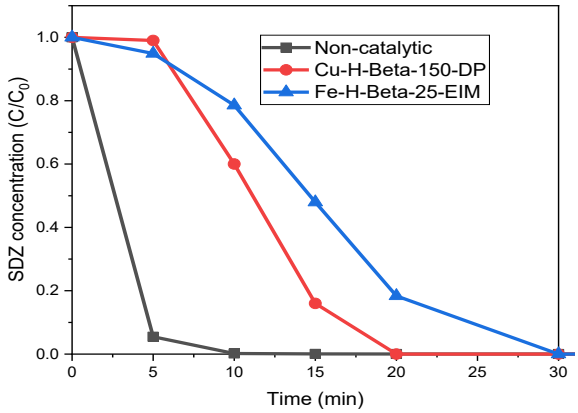

Fig 49. Catalytic and non-catalytic transformation of SDZ. C_{SDZ}=10 mg/L, T= 25˚C.

The experiments were still carried out for a longer time, even if all SDZ was transformed, since the behavior of the by-products was studied as well. The formation of 2-AP was lower when Fe-H-Beta-25-EIM catalyst was employed compared to Cu-H-Beta-25-EIM and non-catalytic ozonation (Figure 50a). Additionally, Figure 50b shows that the generation of SDZ-P15 was significantly smaller in the presence of Fe-H-Beta-25-EIM during the ozonation. Evidently Fe-H-Beta-25-EIM enhances the transformation of these by-products compared to non-catalytic ozonation. This was advantageous considering SDZ-P15 that is more resistant than SDZ. It can be concluded that the presence of the catalyst did not improve the transformation of SDZ, but, it improved the removal of the major by-product formed during the ozonation process. Catalysts have previously been demonstrated to enhance the elimination of by-products in pharmaceutical transformations while the same catalyst did not have efficiency in the transformation of the parent compound (Gomes et al. 2017). Hence, a combination of catalysts and ozone is required for the complete elimination of SDZ from wastewater.

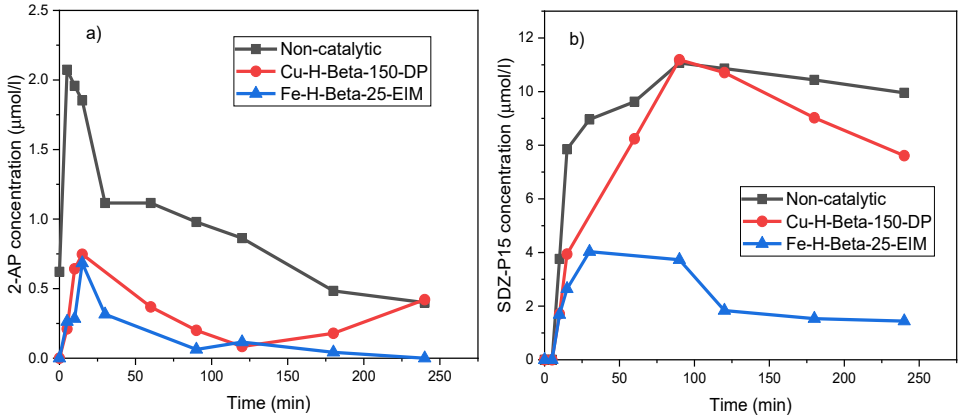

Fig 50. (a) Concentration of 2-AP formed during catalytic and non-catalytic transformation of SDZ (b) Concentration of SDZ-P15 formed during catalytic and non-catalytic transformation of SDZ. C_{SDZ}=10 mg/L, T= 25˚C

4. Conclusions

4. Conclusions

Ozonation and heterogeneously catalyzed ozonation of pharmaceuticals (IBU, CBZ, DCF, SDZ) were studied in a semi-batch reactor system. Dissolved ozone concentration in the solution depends on many parameters (pH, temperature, stirrer type, stirrer position, stirrer speed, gas flow, and nitrogen inlet gas flow), wherein, several experiments were conducted to obtain the optimum condition to reach the maximum concentration of ozone dissolved into the aqueous solution. The data from these experiments were employed for further non-catalytic and catalytic ozonation of pharmaceuticals, and intermediate by-product species were identified and concentrations were analyzed during the course of reaction. Advanced liquid chromatography-mass spectrometry was used to quantify by-products at low concentration levels.

The Fe-H-Beta-25-EIM and Fe-H-Beta-150-SSIE, Cu-H-Beta-25-IE, Cu-H-Beta-150-IE, Cu-H-Beta-300-IE, Cu-Na-Mordenite, Ni-H-Beta-25-EIM, Fe-SiO2-DP, Pd-H-MCM-41 catalysts were successfully synthesized and used for the degradation of IBU in the presence of ozone. The results showed that IBU was successfully decomposed by ozone in the absence of any heterogeneous catalyst at, 20˚C, 450 ml/min oxygen, 2.5 ml/min nitrogen within one hour. The presence of most of the catalysts improved the IBU decomposition rate significantly in the aqueous environment. In catalytic experiments, Cu-H-Beta-150-EIM and Cu-H-Beta-150-DP showed the highest degradation rates, and IBU degraded entirely within 30 min. Most of the catalysts were active in the elimination of by-products. The Cu catalysts were most effective in the removal of the by-products, especially Cu-H-Beta-150-DP. The regenerated Cu catalysts were usable for the degradation of IBU (**I, II**).

The Pt-MCM-41-IS, Ru-MCM-41-IS, Pd-H-Y-12-EIM, Pt-H-Y-12-EIM, Pd-H-Beta-300-EIM and Cu-MCM-41-A-EIM catalysts were synthesized and applied in combination with ozone for the removal of CBZ and its transformed ozonation products using two reaction temperatures (20˚C and 50˚C). Several experiments were carried out in order to evaluate the influence of temperature on the catalytic activity. By increasing the reactor temperature to 50˚C, the catalyst activities increased, even though the dissolved ozone concentration decreased dramatically at 50 ˚C compared to 20˚C. The formation of the products BQM and BQD were kinetically displayed. CBZ was rapidly transformed into BQM and later into BQD. The by-product analysis illustrated that the degradation of BQM and BQD was higher when using a catalyst combined with ozonation. In addition, Pd-H-Y-12-EIM prepared by evaporation impregnation method revealed the highest degradation rate of BQM and BQD compared to other catalysts at 50˚C. The catalyst Pd-H-Y-12-EIM has highest Brønsted acidity 237 μmol/g at 250˚C and a moderately high Lewis acidity 52 μmol/g at 250˚C. This indicates that the acidity of the catalyst has a big role in the transformation of CBZ. Moreover, this catalyst has a high average crystal size, 257.11 nm, compared to the other catalysts, and the Pd concentration is relatively large, 5.34 wt%. Metal leaching was relatively low for Pd and Al for these catalysts, which makes it a promising alternative for the ozonation of pharmaceuticals of this kind (**III**).

The 1%wt.Pt-MCM-22-100-EIM, 2%wt.Pt-MCM-22-100-EIM and 5%wt.Pt-MCM-22-100-EIM, Pt-γ-Al_2O_3 (UOP)-IMP and Pt-H-Y-12-IE catalysts were synthesized and applied with combination of ozone for the removal of DCF and its transformed ozonation products. These catalysts were observed to be active in the degradation of DCF. Furthermore, the by-products of diclofenac such as 5-hydroxydiclofenac, 4-hydroxydiclofenac were removed from the aqueous phase using these catalysts. The concentration of Pt on the MCM-22-100 catalyst, concentration of catalysts in ozonation process and different type of Pt-modified catalysts were studied for degradation of DCF. The highest degradation rate of DCF, the by-products 5-OH-DCF and 4'OH-DCF was obtained using 2%wt.Pt-MCM-22-100-EIM catalyst **(V)**.

Cu-H-Beta-150-DP and Fe-H-Beta-25-EIM catalysts were used for the ozonation of SDZ. However, the catalysts did not improve the transformation of SDZ during the ozonation process. Nevertheless, these catalysts affected the transformation of two dominating by-products of the SDZ ozonation process. The major by-product of SDZ ozonation was SDZ-P-15: around 28 % of SDZ was transformed into SDZ-P15 during ozonation. Moreover, SDZ-P15 was more resistant compared to SDZ in the ozonation experiments. The concentration of SDZ-P15 was significantly lower by utilizing the Fe-H-Beta-24-EIM catalyst. These results illustrated that catalytic ozonation was beneficial for the elimination of the transformation by-products **(VII**).

The method of introduction of metals (Fe, Cu, Pd, Pt) in catalysts, particle size of metals and acid sites was observed to influence the degradation of the pharmaceutical compounds (IBU, CBZ, DCF, SDZ). Furthermore, the type and structure of the supports used for the catalysts synthesis of catalysts H-Beta, H-Y-12, H-MCM-22 zeolites, H-MCM-41 structured mesoporous material and SiO_2 , Al_2O_3 mesoporous, were of immense importance for the catalytic activity in the degradation of the pharmaceutical compounds. The catalysts displayed leaching in the solution in the range 0-80%. The physico-chemical characterization of catalytic materials was carried out using several techniques such as XRD, SEM, EDX, TEM, XPS and N_2-physisorption. It was possible to regenerate the spent catalysts by calcination after the degradation of the pharmaceuticals (IBU, CBZ, DCF, SDZ).

References

[1] K. Kummerer, The presence of pharmaceuticals in the environment due to human use – present knowledge and future challenges, 90 (2009) 2354–2366.

[2] Pharmaceutical products, World Heal. Organ. (2019).

[3] C. Gómez-Canela, V. Pueyo, C. Barata, S. Lacorte, R.M. Marcé, Development of predicted environmental concentrations to prioritize the occurrence of pharmaceuticals in rivers from Catalonia, Sci. Total Environ. 666 (2019) 57–67.

[4] D. White, D.J. Lapworth, W. Civil, P. Williams, Tracking changes in the occurrence and source of pharmaceuticals within the River Thames, UK; from source to sea, Environ. Pollut. 249 (2019) 257–266.

[5] H.Q. Liu, J.C.W. Lam, W.W. Li, H.Q. Yu, P.K.S. Lam, Spatial distribution and removal performance of pharmaceuticals in municipal wastewater treatment plants in China, Sci. Total Environ. 586 (2017) 1162–1169.

[6] M.S.U. Rehman, N. Rashid, M. Ashfaq, A. Saif, N. Ahmad, J.I. Han, Global risk of pharmaceutical contamination from highly populated developing countries, Chemosphere. 138 (2015) 1045–1055.

[7] G. Wen, Y. Xu, Z. Xu, Z. Tian, Direct conversion of cellulose into hydrogen by aqueous-phase reforming process, Catal. Commun. 11 (2010) 522–526.

[8] S. Ortiz, D. García, P.A. García-encina, R. Irusta-mata, The potential ecotoxicological impact of pharmaceutical and personal care products on humans and freshwater , based on USEtox ™ characterization factors . A Spanish case study of toxicity impact scores, Sci. Total Environ. 609 (2017) 429–445.

[9] J.L. Liu, M.H. Wong, Pharmaceuticals and personal care products (PPCPs): A review on environmental contamination in China, Environ. Int. 59 (2013) 208–224.

[10] J. Wang, S. Wang, Removal of pharmaceuticals and personal care products (PPCPs) from wastewater : A review, J. Environ. Manage. 182 (2016) 620–640.

[11] S. Sukiman, F.A.M. Nasir, Z. Hanafi, A.Z. Aris, S.N.M. Shaifuddin, N. Kamarudin, S.M. Praveena, T.H.T. Ismail, Pharmaceuticals residues in selected tropical surface water bodies from Selangor (Malaysia): Occurrence and potential risk assessments, Sci. Total Environ. 642 (2018) 230–240.

[12] A.J. Ebele, M. Abou-Elwafa Abdallah, S. Harrad, Pharmaceuticals and personal care products (PPCPs) in the freshwater aquatic environment, Emerg. Contam. 3 (2017) 1–16.

[13] E. Fattore, E. Zuccato, S. Castiglioni, E. Davoli, F. Riva, Risk assessment of a mixture of emerging contaminants in surface water in a highly urbanized area in Italy, J. Hazard. Mater. 361 (2018) 103–110.

[14] M.G. Cantwell, D.R. Katz, J.C. Sullivan, D. Shapley, J. Lipscomb, J. Epstein, A.R. Juhl, C. Knudson, G.D. O'Mullan, Spatial patterns of pharmaceuticals and wastewater tracers in the Hudson River Estuary, Water Res. 137 (2018) 335–343.

[15] P. Lindholm-Lehto, Occurrence of pharmaceuticals in municipal wastewater treatment plants and receiving surface waters in central and southen Finland, University of Jyväskylä, Finland, 2016.

[16] N. Vieno, P. Hallgren, P. Wallberg, M. Pyhälä, S. Zandaryaa, Pharmaceuticals in the aquatic environment of the Baltic Sea region – A status report, UNESCO and HELCOM. UNESCO Emerging Pollutants in Water Series – No. 1, UNESCO Publishing, Paris., 2017.

[17] Gary, S Browne, C. Nelson, T. Nguyen, A.E. Bronwyn, O.D. Richard, M.W. Kenneth, Stereoselective and substrate-dependent inhibition of hepatic mitochondrial β-oxidation and oxidative phosphorylation by the non-steroidal anti-inflammatory drugs ibuprofen, flurbiprofen, and ketorolac, Biochem. Pharmacol. 57 (1999) 837–844.

[18] R.M. Nanau, M.G. Neuman, Ibuprofen-induced hypersensitivity syndrome, Transl. Res. 155 (2010) 275–293.

[19] M.J. Quero-Pastor, M.C. Garrido-Perez, A. Acevedo, J.M. Quiroga, Ozonation of ibuprofen: A degradation and toxicity study, Sci. Total Environ. 466–467 (2014) 957–964.

[20] F.T. Mathias, D.H. Fockink, G.R. Disner, V. Prodocimo, J.L.C. Ribas, L.P. Ramos, M.M. Cestari, H.C. Silva de Assis, Effects of low concentrations of ibuprofen on freshwater fish Rhamdia quelen, Environ. Toxicol. Pharmacol. 59 (2018) 105–113.

[21] A. Garrard, Encyclopedia of Toxicology (Third Edition), Ibuprofen, Elsevier, 2014.

[22] Q. Sui, X. Cao, S. Lu, W. Zhao, Z. Qiu, G. Yu, Occurrence, sources and fate of pharmaceuticals and personal care products in the groundwater: A review, Emerg. Contam. 1 (2015) 14–24.

[23] N. Lindqvist, T. Tuhkanen, L. Kronberg, Occurrence of acidic pharmaceuticals in raw and treated sewages and in receiving waters, Water Res. 39 (2005) 2219–2228.

[24] S. Bertinetti, M. Minella, K. Hanna, C. Minero, D. Vione, Degradation of ibuprofen with a Fenton-like process triggered by zero-valent iron (ZVI-Fenton), Environ. Res. Submitted (2019) 108750.

[25] P. Kay, S.R. Hughes, J.R. Ault, A.E. Ashcroft, L.E. Brown, Widespread, routine occurrence of pharmaceuticals in sewage effluent, combined sewer overflows and receiving waters, Environ. Pollut. 220 (2017) 1447–1455.

[26] A. Meierjohann, J.M. Brozinski, L. Kronberg, Seasonal variation of pharmaceutical concentrations in a river/lake system in Eastern Finland, Environ. Sci. Process. Impacts. 18 (2016) 342–349.

[27] N.M. Vieno, T. Tuhkanen, L. Kronberg, Seasonal variation in the occurrence of pharmaceuticals in effluents from a sewage treatment plant and in the recipient water, Environ. Sci. Technol. 39 (2005) 8220–8226.

[28] S. Han, K. Choi, J. Kim, K. Ji, S. Kim, B. Ahn, J. Yun, K. Choi, J.S. Khim, X. Zhang, J.P. Giesy, Endocrine disruption and consequences of chronic exposure to ibuprofen in Japanese medaka (Oryzias latipes) and freshwater cladocerans Daphnia magna and Moina macrocopa, Aquat. Toxicol. 98 (2010) 256–264.

[29] L. Xia, L. Zheng, J.L. Zhou, Effects of ibuprofen, diclofenac and paracetamol on hatch and motor behavior in developing zebrafish (Danio rerio), Chemosphere. 182 (2017) 416–425.

[30] A.B.A. Boxall, V.D.J. Keller, J.O. Straub, S.C. Monteiro, R. Fussell, R.J. Williams, Exploiting monitoring data in environmental exposure modelling and risk assessment of pharmaceuticals, Environ. Int. 73 (2014) 176–185.

[31] Y. Jin, S.P. Sun, X. Yang, X.D. Chen, Degradation of ibuprofen in water by FeII-NTA complex-activated persulfate with hydroxylamine at neutral pH, Chem. Eng. J. 337 (2018) 152–160.

[32] Y. Xiang, J. Fang, C. Shang, Kinetics and pathways of ibuprofen degradation by the UV/chlorine advanced oxidation process, Water Res. 90 (2016) 301–308.

[33] K. Fent, A.A. Weston, D. Caminada, Ecotoxicology of human pharmaceuticals, Aquat. Toxicol. 76 (2006) 122–159.

[34] Q. Fu, Y. Han, Y. fei Xie, N. bo Gong, F. Guo, Carbamazepine cocrystals with several aromatic carboxylic acids in different stoichiometries: Structures and solid state characterization, J. Mol. Struct. 1168 (2018) 145–152.

[35] WHO model list of essential medicines, 20th edition, March 2017, Http://Www.Who.Int/Medicines/Publications/Essentialmedicines/En/. (2017) 1–58.

[36] Y. Zhang, S.U. Geißen, C. Gal, Carbamazepine and diclofenac: Removal in wastewater treatment plants and occurrence in water bodies, Chemosphere. 73 (2008) 1151–1161.

[37] K.I. Ekpeghere, W.J. Sim, H.J. Lee, J.E. Oh, Occurrence and distribution of carbamazepine, nicotine, estrogenic compounds, and their transformation products in wastewater from various treatment plants and the aquatic environment, Sci. Total Environ. 640–641 (2018) 1015–1023.

[38] H.L. Teo, L. Wong, Q. Liu, T.L. Teo, T.K. Lee, H.K. Lee, Simple and accurate measurement of carbamazepine in surface water by use of porous membrane-protected micro-solid-phase extraction coupled with isotope dilution mass spectrometry, Anal. Chim. Acta. 912 (2016) 49–57.

[39] B. Björlenius, M. Ripszám, P. Haglund, R.H. Lindberg, M. Tysklind, J. Fick, Pharmaceutical residues are widespread in Baltic Sea coastal and offshore waters – Screening for pharmaceuticals and modelling of environmental concentrations of carbamazepine, Sci. Total Environ. 633 (2018) 1496–1509.

[40] T. Radović, S. Grujić, A. Petković, M. Dimkić, M. Laušević, Determination of pharmaceuticals and pesticides in river sediments and corresponding surface and ground water in the Danube River and tributaries in Serbia, Environ. Monit. Assess. 187 (2015).

[41] A. Bahlmann, W. Brack, R.J. Schneider, M. Krauss, Carbamazepine and its metabolites in wastewater: Analytical pitfalls and occurrence in Germany and Portugal, Water Res. 57 (2014) 104–114.

[42] A. Jurado, R. López-Serna, E. Vázquez-Suné, J. Carrera, E. Pujades, M. Petrovic, D. Barceló, Occurrence of carbamazepine and five metabolites in an urban aquifer, Chemosphere. 115 (2014) 47–53.

[43] E. Brezina, C. Prasse, J. Meyer, H. Mückter, T.A. Ternes, Investigation and risk evaluation of the occurrence of carbamazepine, oxcarbazepine, their human metabolites and transformation products in the urban water cycle, Environ. Pollut. 225 (2017) 261–269.

[44] Â. Almeida, V. Calisto, V.I. Esteves, R.J. Schneider, A.M.V.M. Soares, E. Figueira, R. Freitas, Presence of the pharmaceutical drug carbamazepine in coastal systems: Effects on bivalves, Aquat. Toxicol. 156 (2014) 74–87.

[45] P. Tsiaka, V. Tsarpali, I. Ntaikou, M.N. Kostopoulou, G. Lyberatos, S. Dailianis, Carbamazepine-mediated pro-oxidant effects on the unicellular marine algal species Dunaliella tertiolecta and the hemocytes of mussel Mytilus galloprovincialis, Ecotoxicology. 22 (2013) 1208–1220.

[46] K. Rajendran, S. Sen, Adsorptive removal of carbamazepine using biosynthesized hematite nanoparticles, Environ. Nanotechnology, Monit. Manag. 9 (2018) 122–127.

[47] M. Chtourou, M. Mallek, M. Dalmau, J. Mamo, E. Santos-Clotas, A. Ben Salah, K. Walha, V. Salvadó, H. Monclús, Triclosan, carbamazepine and caffeine removal by activated sludge system focusing on membrane bioreactor, Process Saf. Environ. Prot. 118 (2018) 1–9.

[48] S. Wang, J. Wang, Degradation of carbamazepine by radiation-induced activation of peroxymonosulfate, Chem. Eng. J. 336 (2018) 595–601.

[49] Y. Han, M. Ma, N. Li, R. Hou, C. Huang, Y. Oda, Z. Wang, Chlorination, chloramination and ozonation of carbamazepine enhance cytotoxicity and genotoxicity: Multi-endpoint evaluation and identification of its genotoxic transformation products, J. Hazard. Mater. 342 (2018) 679–688.

[50] N. Vieno, M. Sillanpää, Fate of diclofenac in municipal wastewater treatment plant - A review, Environ. Int. 69 (2014) 28–39.

[51] D. Cheikh, F. García-Villén, H. Majdoub, C. Viseras, M.B. Zayani, Chitosan/beidellite nanocomposite as diclofenac carrier, Int. J. Biol. Macromol. 126 (2019) 44–53.

[52] R. Zhuan, J. Wang, Degradation of diclofenac in aqueous solution by ionizing radiation in the presence of humic acid, Sep. Purif. Technol. 234 (2020) 116079.

[53] V. Acuña, A. Ginebreda, J.R. Mor, M. Petrovic, S. Sabater, J. Sumpter, D. Barceló, Balancing the health benefits and environmental risks of pharmaceuticals: Diclofenac as an example, Environ. Int. 85 (2015) 327–333.

[54] L.P. Arias-Marín, C. Boix, R.J. Rincón, R. Torres-Palma, D. Martínez-Pachón, L. Manrique-Losada, A.M. Botero-Coy, N. Castillo, F. Hernández, A. Moncayo-Lasso, 'An investigation into the occurrence and removal of pharmaceuticals in Colombian wastewater,' Sci. Total Environ. 642 (2018) 842–853.

[55] B. Hoeger, B. Köllne, D.R. Dietrich, B. Hitzfeld, Water-borne diclofenac affects kidney and gill integrity and selected immune parameters in brown trout (Salmo trutta f. fario), Aquat. Toxicol. 75 (2005) 53–64.

[56] B. Bonnefille, E. Gomez, F. Courant, A. Escande, H. Fenet, Diclofenac in the marine environment: A review of its occurrence and effects, Mar. Pollut. Bull. 131 (2018) 496–506.

[57] J. Lee, K. Ji, Y. Lim Kho, P. Kim, K. Choi, Chronic exposure to diclofenac on two freshwater cladocerans and Japanese medaka, Ecotoxicol. Environ. Saf. 74 (2011) 1216–1225.

[58] L. Lonappan, S.K. Brar, R.K. Das, M. Verma, R.Y. Surampalli, Diclofenac and its transformation products: Environmental occurrence and toxicity - A review, Environ. Int. 96 (2016) 127–138.

[59] S.J. Facey, B.A. Nebel, L. Kontny, M. Allgaier, B. Hauer, Rapid and complete degradation of diclofenac by native soil microorganisms, Environ. Technol. Innov. 10 (2018) 55–61.

[60] R. Ghemit, A. Makhloufi, N. Djebri, A. Flilissa, L. Zerroual, M. Boutahala, Adsorptive removal of diclofenac and ibuprofen from aqueous solution by organobentonites: Study in single and binary systems, Groundw. Sustain. Dev. 8 (2019) 520–529.

[61] W. Li, R. Yu, M. Li, N. Guo, H. Yu, Y. Yu, Photocatalytical degradation of diclofenac by Ag-BiOI-rGO: Kinetics, mechanisms and pathways, Chemosphere. 218 (2019) 966–973.

[62] S.R. Hill, WHO model formulary published, Pharm. J. 269 (2002) 312.

[63] Wikipedia contributors, Sulfadiazine, Wikipedia,The Free Encycl. (2019) 917669742.

[64] I. Varó, J.C. Navarro, G. Rigos, J. Del Ramo, J.A. Calduch-Giner, A. Hernández, J. Pertusa, A. Torreblanca, Proteomic evaluation of potentiated sulfa treatment on gilthead sea bream (Sparus aurata L.) liver, Aquaculture. 376–379 (2013) 36–44.

[65] T. Shi, L. Tan, H. Fu, J. Wang, Application of molecular imprinting polymer anchored on CdTe quantum dots for the detection of sulfadiazine in seawater, Mar. Pollut. Bull. 146 (2019) 591–597.

[66] F. Hayati, A. Akbar Isari, B. Anvaripour, M. Fattahi, B. Kakavandi, Ultrasound-assisted photocatalytic degradation of sulfadiazine using MgO@CNT heterojunction composite: Effective factors, pathway and biodegradability studies, Chem. Eng. J. 381 (2019) 122636.

[67] M. Conde-Cid, J.C. Nóvoa-Muñoz, M.J. Fernández-Sanjurjo, A. Núñez-Delgado, E. Álvarez-Rodríguez, M. Arias-Estévez, Pedotransfer functions to estimate the adsorption and desorption of sulfadiazine in agricultural soils, Sci. Total Environ. 691 (2019) 933–942.

[68] R. Ma, B. Wang, L. Yin, Y. Zhang, S. Deng, J. Huang, Y. Wang, G. Yu, Characterization of pharmaceutically active compounds in Beijing, China: Occurrence pattern, spatiotemporal distribution and its environmental implication, J. Hazard. Mater. 323 (2017) 147–155.

[69] V. Burke, D. Richter, J. Greskowiak, A. Mehrtens, L. Schulz, G. Massmann, Occurrence of Antibiotics in Surface and Groundwater of a Drinking Water Catchment Area in Germany, Water Environ. Res. 88 (2016) 652–659.

[70] H. Wang, S. Wang, J.Q. Jiang, J. Shu, Removal of sulfadiazine by ferrate(VI) oxidation and montmorillonite adsorption - Synergistic effect and degradation pathways, J. Environ. Chem. Eng. 7 (2019) 103225.

[71] J. Sun, Q. Wang, J. Zhang, Z. Wang, Z. Wu, Degradation of sulfadiazine in drinking water by a cathodic electrochemical membrane filtration process, Electrochim. Acta. 277 (2018) 77–87.

[72] J.F. Yang, M. He, T.F. Wu, A.P. Hao, S.B. Zhang, Y.D. Chen, S.B. Zhou, L.Y. Zhen, R. Wang, Z.L. Yuan, L. Deng, Sulfadiazine oxidation by permanganate: Kinetics, mechanistic investigation and toxicity evaluation, Chem. Eng. J. 349 (2018) 56–65.

[73] D. Kanakaraju, B.D. Glass, M. Oelgem, Advanced oxidation process-mediated removal of pharmaceuticals from water : A review, J. Environ. Manage. 219 (2018) 189–207.

[74] B.M. Peake, R. Braund, A.Y.C. Tong, L.A. Tremblay, Degradation of pharmaceuticals in wastewater, Elsevier Ltd., 2016.

[75] H.A. kosar Hikmat, H. Miessner, S. Mueller, D. Kalass, D. Moeller, I. Khorshid, M.A.M. Rashid, Degradation of pharmaceutical diclofenac and ibuprofen in aqueous solution, a direct comparison of ozonation, photocatalysis, and non-thermal plasma, Chem. Eng. J. 313 (2017) 1033–1041.

[76] J.C. Lancheros, C.A. Madera-Parra, A. Caselles-Osorio, W.A. Torres-López, X.M. Vargas-Ramírez, Ibuprofen and Naproxen removal from domestic wastewater using a Horizontal Subsurface Flow Constructed Wetland coupled to Ozonation, Ecol. Eng. 135 (2019) 89–97.

[77] J.D. García-Espinoza, P.M. Nacheva, Degradation of pharmaceutical compounds in water by oxygenated electrochemical oxidation: Parametric optimization, kinetic studies and toxicity assessment, Sci. Total Environ. 691 (2019) 417–429.

[78] S.K. Ray, Y.K. Kshetri, D. Dhakal, C. Regmi, S.W. Lee, Photocatalytic degradation of Rhodamine B and Ibuprofen with upconversion luminescence in Ag-BaMoO4: Er3+/Yb3+/K+ microcrystals, J. Photochem. Photobiol. A Chem. 339 (2017) 36–48.

[79] J. Gomes, R. Costa, R.M. Quinta-Ferreira, R.C. Martins, Application of ozonation for pharmaceuticals and personal care products removal from water, Sci. Total Environ. 586 (2017) 265–283.

[80] M.E. Lovato, C.A. Martín, A.E. Cassano, A reaction-reactor model for O3 and UVC radiation degradation of dichloroacetic acid: The kinetics of three parallel reactions, Chem. Eng. J. 171 (2011) 474–489.

[81] C. Gottschalk, J.A. Libra, A. Saupe, Ozonation of water and waste water, WILEY-VCH, 2010.

[82] K.M.S. Hansen, A. Spiliotopoulou, R.K. Chhetri, M. Escolà Casas, K. Bester, H.R. Andersen, Ozonation for source treatment of pharmaceuticals in hospital wastewater - Ozone lifetime and required ozone dose, Chem. Eng. J. 290 (2016) 507–514.

[83] N.F.F. Moreira, C.A. Orge, A.R. Ribeiro, J.L. Faria, O.C. Nunes, M.F.R. Pereira, A.M.T. Silva, Fast mineralization and detoxification of amoxicillin and diclofenac by photocatalytic ozonation and application to an urban wastewater, Water Res. 87 (2015) 87–96.

[84] K. Tang, A. Spiliotopoulou, R. K.Chhetri, G.T.H. Ooi, K.M.S. Kaarsholm, K. Sundmark, B. Florian, C. Kragelund, K. Bester, H.R. Andersen, Removal of pharmaceuticals, toxicity and natural fluorescence through the ozonation of biologically-treated hospital wastewater, with further polishing via a suspended biofilm, Chem. Eng. J. 359 (2018) 321–330.

[85] A.D. Coelho, C. Sans, A. Agüera, M.J. Gómez, S. Esplugas, M. Dezotti, Effects of ozone pre-treatment on diclofenac: Intermediates, biodegradability and toxicity assessment, Sci. Total Environ. 407 (2009) 3572–3578.

[86] C. Wei, F. Zhang, Y. Hu, C. Feng, H. Wu, Ozonation in water treatment: the generation, basic properties of ozone and its practical application, Rev. Chem. Eng. 33 (2016).

[87] N.C. Shang, Y.H. Yu, H.W. Ma, C.H. Chang, M.L. Liou, Toxicity measurements in aqueous solution during ozonation of mono-chlorophenols, J. Environ. Manage. 78 (2006) 216–222.

[88] J. Wang, Z. Bai, Fe-based catalysts for heterogeneous catalytic ozonation of emerging contaminants in water and wastewater, Chem. Eng. J. 312 (2017) 79–98.

[89] A. Aghaeinejad-Meybodi, A. Ebadi, S. Shafiei, A. Khataee, A.D. Kiadehi, Degradation of Fluoxetine using catalytic ozonation in aqueous media in the presence of nano-Γ-alumina

catalyst: Experimental, modeling and optimization study, Sep. Purif. Technol. 211 (2019) 551–563.

[90] A. Ikhlaq, D. R. Brown, B. Kasprzyk-Hordern, Catalytic ozonation for the removal of organic contaminants in water on ZSM-5 zeolites, Appl. Catal. B Environ. 154–155 (2014) 110–122.

[91] B. Kasprzyk-Hordern, M. Ziółek, J. Nawrocki, Catalytic ozonation and methods of enhancing molecular ozone reactions in water treatment, Appl. Catal. B Environ. 46 (2003) 639–669.

[92] O. Chedeville, A. Di Giusto, S. Delpeux, B. Cagnon, Oxidation of pharmaceutical compounds by ozonation and ozone/activated carbon coupling: a kinetic approach, Desalin. Water Treat. 57 (2016) 18956–18963.

[93] C.A. Orge, J.J.M. Órfão, M.F.R. Pereira, Catalytic ozonation of organic pollutants in the presence of cerium oxide-carbon composites, Appl. Catal. B Environ. 102 (2011) 539–546.

[94] J. Vittenet, J. Rodriguez, E. Petit, D. Cot, J. Mendret, A. Galarneau, S. Brosillon, Removal of 2,4-dimethylphenol pollutant in water by ozonation catalyzed by SOD, LTA, FAU-X zeolites particles obtained by pseudomorphic transformation (binderless), Microporous Mesoporous Mater. 189 (2014) 200–209.

[95] M. Stekrova, N. Kumar, S.F. Díaz, P. Mäki-Arvela, D.Y. Murzin, H- and Fe-modified zeolite beta catalysts for preparation of trans-carveol from α-pinene oxide, Catal. Today. 241 (2015) 237–245.

[96] S. Saeid, P. Tolvanen, N. Kumar, K. Eränen, J. Peltonen, M. Peurla, J.P. Mikkola, A. Franz, T. Salmi, Advanced oxidation process for the removal of ibuprofen from aqueous solution: A non-catalytic and catalytic ozonation study in a semi-batch reactor, Appl. Catal. B Environ. 230 (2018) 77–90.

[97] M. Stekrova, N. Kumar, A. Aho, I. Sinev, W. Grünert, J. Dahl, J. Roine, S.S. Arzumanov, P. Mäki-arvela, D. Yu, Applied Catalysis A : General Isomerization of α-pinene oxide using Fe-supported catalysts : Selective synthesis of campholenic aldehyde, Appl. Catal. A Gen. J. 470 (2014) 162–176.

[98] J. Regalbuto, Catalyst Preparation: Science and Engineering By John R. Regalbuto, 2006.

[99] E. Behravesh, N. Kumar, Q. Balme, J. Roine, J. Salonen, A. Schukarev, J.P. Mikkola, M. Peurla, A. Aho, K. Eränen, D.Y. Murzin, T. Salmi, Synthesis and characterization of Au nano particles supported catalysts for partial oxidation of ethanol: Influence of solution pH, Au nanoparticle size, support structure and acidity, J. Catal. 353 (2017) 223–238.

[100] L. Lutterotti, S. Matthies, H.R. Wenk, A.S. Schultz, J.W. Richardson, Combined texture and structure analysis of deformed limestone from time-of-flight neutron diffraction spectra, J. Appl. Phys. 81 (1997) 594–600.

[101] A. Ziylan, N.H. Ince, Catalytic ozonation of ibuprofen with ultrasound and Fe-based catalysts, Catal. Today. 240 (2015) 2–8.

[102] H. Bader, J. Hoigné, Determination of ozone in water by the indigo method, Water Res. 15 (1981) 449–456.

[103] K.A.H. Buchan, D.J. Martin-Robichaud, T.J. Benfey, Measurement of dissolved ozone in sea water: A comparison of methods, Aquac. Eng. 33 (2005) 225–231.

[104] O. Meunpol, K. Lopinyosiri, P. Menasveta, The effects of ozone and probiotics on the survival of black tiger shrimp (Penaeus monodon), Aquaculture. 220 (2003) 437–448.

[105] P. Mäki-Arvela, J. Zhu, N. Kumar, K. Eränen, A. Aho, J. Linden, J. Salonen, M. Peurla, A. Mazur, V. Matveev, D.Y. Murzin, Solvent-free "green" amidation of stearic acid for synthesis of biologically active alkylamides over iron supported heterogeneous catalysts, Appl. Catal. A Gen. 542 (2017) 350–358.

[106] A. Aho, N. Kumar, K. Eränen, T. Salmi, M. Hupa, D.Y. Murzin, Catalytic pyrolysis of biomass in a fluidized bed reactor: Influence of the acidity of h-beta zeolite, Process Saf. Environ. Prot. 85 (2007) 473–480.

[107] A. Aho, T. Salmi, D.Y. Murzin, Catalytic Pyrolysis of Lignocellulosic Biomass, Role Catal. Sustain. Prod. Bio-Fuels Bio-Chemicals. (2013) 137–159.

[108] K. Maduna, N. Kumar, D.Y. Murzin, Influence of SI/AL ratios on the properties of copper bearing zeolites with different framework types, Tech. J. 6168 (2017) 96–100.

[109] K. Yu, N. Kumar, A. Aho, J. Roine, I. Heinmaa, D.Y. Murzin, A. Ivaska, Determination of acid sites in porous aluminosilicate solid catalysts for aqueous phase reactions using potentiometric titration method, J. Catal. 335 (2016) 117–124.

[110] M.A. Camblor, A. Corma, M.-J. Díaz-Cabañas, C. Baerlocher, Synthesis and Structural Characterization of MWW Type Zeolite ITQ-1, the Pure Silica Analog of MCM-22 and SSZ-25, J. Phys. Chem. B. 102 (2002) 44–51.

[111] M. Colligan, P.M. Forster, A.K. Cheetham, Y. Lee, T. Vogt, J.A. Hriljac, N. York, Synchrotron X-ray powder diffraction and computational investigation of purely siliceous zeolite Y under pressure, J. Am. Chem. Soc. (2004) 12015–12022.

[112] G. Paglia, C.E. Buckley, A.L. Rohl, B.A. Hunter, R.D. Hart, J. V Hanna, L.T. Byrne, Tetragonal structure model for boehmite-derived γ-alumina, Am. Phys. Soc. 68 (2003) 144110.

[113] J.Z. Shyu, K. OTTO, Identification of platinum phases on γ-alumina by XPS, Appl. Surf. Sci. 32 (1988) 246–252.

[114] R. Bouwman, P. Biloen, Valence state and interaction of platinum and germanium on investigated by X-ray photoelectron spectroscopy, J. Catal. 48 (1977) 209–216.

[115] INTERNATIONAL OZONE ASSOCIATION, Quality Assurance Committee, Revised Standardized Procedure 001/96., 1987.

[116] J. Leusink, Dissolved Ozone vs Temperature, Ozone J. (2011).

[117] S.H. Jenkins, water pollution Research, Eighth International Conference on Water Pollution Research: Proceedings of the 8th International Conference, Sydney, Australia, 1976, pergamon press, 2013.

[118] M. Sik, D. Cha, K. Lee, H. Lee, T. Kim, C. Lee, Modeling of ozone decomposition , oxidant exposures , and the abatement of micropollutants during ozonation processes, Water Res. 169 (2020) 115230.

[119] J.M. Quero-Pastor, M.J., Garrido-Perez, M.C., Acevedo, A., Quiroga, Science of the Total Environment Ozonation of ibuprofen : A degradation and toxicity study, Sci. Total Environ. 466–467 (2014) 957–964.

[120] Y. Guo, L. Yang, X. Wang, The application and reaction mechanism of catalytic ozonation in water treatment, J. Environ. Anal. Toxicol. 02 (2012).

[121] P. Somathilake, J.A. Dominic, G. Achari, H. Cooper, Degradation of Carbamazepine by Photo-assisted Ozonation : Influence of Wavelength and Intensity of Radiation Degradation of Carbamazepine by Photo-assisted Ozonation : Influence of Wavelength and Intensity of Radiation, Ozone Sci. Eng. 40 (2018) 1–9.

[122] D.C. Mcdowell, M.M. Huber, M. Wagner, U. Von Gunten, T.A. Ternes, Ozonation of carbamazepine in drinking water: Identification and kinetic study of major oxidation products, Environ. Sci. Technol. 39 (2005) 8014–8022.

[123] T. Cai, Y. Gao, J. Yan, Y. Wu, J. Di, Visual detection of glucose using triangular silver nanoplates and gold nanoparticles, RSC Adv. 7 (2017) 29122–29128.

[124] H. Einaga, N. Maeda, Y. Nagai, Comparison of catalytic properties of supported metal oxides for benzene oxidation using ozone, Catal. Sci. Technol. 5 (2015) 3147–3158.

[125] R. Rosal, A. Rodríguez., M.S. Gonzalo, E. García-Calvo, Catalytic ozonation of naproxen and carbamazepine on titanium dioxide, Appl. Catal. B Environ. 84 (2008) 48–57.

[126] J.M. Monteagudo, H. El-taliawy, A. Durán, G. Caro, K. Bester, Sono-activated persulfate oxidation of diclofenac: Degradation, kinetics, pathway and contribution of the different radicals involved, J. Hazard. Mater. 357 (2018) 457–465.

[127] X. Li, W. Chen, Y. Tang, L. Li, Relationship between the structure of Fe-MCM-48 and its activity in catalytic ozonation for diclofenac mineralization, Chemosphere. 206 (2018) 615–621.

[128] W. Chen, X. Li, Z. Pan, S. Ma, L. Li, Effective mineralization of Diclofenac by catalytic ozonation using Fe-MCM-41 catalyst, Chem. Eng. J. 304 (2016) 594–601.

ISBN 978-952-12-3911-3 (printed version)
ISBN 978-952-12-3912-0 (electronic version)
ISSN 2669-8315 2670-0638 (*Acta technologiae chemicae Aboensia* 2020 A/1)
Painosalama Oy Turku/Åbo 2020